

https://dspace.org/

Effect of heat treatment on the microstructure and mechanical properties of high-speed selective laser melted Ti6Al4V Alloy

Lekoadi, Paul Masekuru

2021

https://hdl.handle.net/10539/31908

Downloaded from a DSpace repository. https://dspace.org/



EFFECT OF HEAT TREATMENT ON THE MICROSTRUCTURE AND MECHANICAL PROPERTIES OF HIGH-SPEED SELECTIVE LASER MELTED TI6AL4V ALLOY

Paul Masekuru Lekoadi (1355576)

A dissertation submitted to the School of Chemical and Metallurgical Engineering, Faculty of Engineering and the Built Environment, University of the Witwatersrand, Johannesburg, in fulfillment of the requirements for the degree of Masters of Science in Engineering.

April 2021

Declaration

I declare that the content in this dissertation is my own unaided work. It is being submitted for the degree of Masters of Science in Engineering to the University of the Witwatersrand, Johannesburg. I also confirm that it has not been submitted before for any degree or examination to any other university and that all sources are acknowledged by means of referencing.

Student signature:  Date: 26/04/2021 .

Abstract

Selective laser melting (SLM) technique is a promising 3D printing technique used in the aerospace application, amongst other additive manufacturing (AM) techniques. Parallel to SLM, Ti6Al4V is a suitable alloy in the aerospace industry because of the advantages it offers which include superior combination of strength and reduced weight. The advantages of producing Ti6Al4V by SLM manufacturing process results in an increasing demand of SLM Ti6Al4V parts in the industry. The Aeroswift^{TM} SLM machine, available at Council for Scientific and Industrial Research (CSIR), is capable of producing components using high speed and high-power laser of up to 5 kW.

The ability of Aeroswift^{TM} machine to print components using high speed and power, result in accelerated production of high precision parts, which leads to reduced production times. However, because of high cooling rates together with large thermal gradients that accompany the SLM technique, the produced components exhibit an acicular martensitic α'-phase. The martensitic α'-phase (which leads to low ductility) formed during the production of SLM produced Ti6Al4V components make their components not to achieve the same mechanical properties compared to their wrought counter parts.

This study is aimed at using post heat treatment to overcome challenges presented by SLM process by improving the microstructure and mechanical properties of Ti6Al4V coupons. Ti6Al4V samples were produced on a high-speed powder bed Aeroswift^{TM} machine and then heat treated under different conditions. Microstructural and phase analyses were performed by using optical microscope (OM) and the scanning electron microscope (SEM). Mechanical properties of the samples were evaluated by performing Vickers micro-hardness and tensile tests.

The as-built microstructure was characterized by large columnar prior β grains. Sharp acicular martensite α'-phase was found inside the prior β grains. Heat treatment was applied to the as-produced samples to transform the metastable martensitic α' structure into stable phases, thereby improving the microstructure.

It was found that heat treating at 700°C does not transform the martensitic α'-phase. Heat treating at 950°C and 1000°C transformed the martensite α'-phase into fully lamella α + β. Moreover, 1000°C changed the columnar β grains to equiaxed morphology. The hardness was found to decrease with increasing heat treatment temperature. Furthermore, heat treatment at 1000°C followed by water quenching (WQ) and air cooling (AC) initiated formation of a finer martensite α'-phase which resulted in increased hardness. Heat treating at 1000°C for 2 hrs, cooling by furnace cooling (FC) improved the ductility to at least 13%. Furthermore, yield strength (YS) and ultimate tensile strength (UTS) were found to have decreased after heat treatment.

Acknowledgements

I would first like to thank my supervisors, Dr Nthabiseng Maledi from the School of Chemical and Metallurgical Engineering at the University of the Witwatersrand, Dr Bathusile Masina and Dr Monnamme Tlotleng both from the Council of Scientific and Industrial Research (CSIR), for their valuable guidance and support throughout my studies. I express my deep appreciation for their constructive comments, advice, patience, love, kindness and guidance throughout. They were always accessible and always willing to help and share their scientific knowledge which played an important role in shaping my career.

I also give thanks to my CSIR National Laser Centre (NLC) colleagues, Prof Sisa Pityana, Nana Arthur, Ipfi Mathoho, Thabo Lengopeng, Khoro Malabi, Mfanufikile Shange, Samuel Skhosana, Londiwe Motibane, and Washington Makoana for their support especially with the laboratory work. Their support made my laboratory work very simple. I got a chance to meet Mr Mandy Seerane and Mr Pierre Rossouw from the Manufacturing Cluster within the CSIR, and Dr Kofi Annan and Dirk from the University of Pretoria (Mineral Science Department), who assisted me with heat treatment facilities.

I appreciate the support I received from my parents Mr William and Mrs Grace Lekoadi, and family Dinah Lekoadi, Moshibudi Mabote, Tebogo Mabote, Erens Kgomo and Kgotso Radingoana. Their moral support played an important role in my journey towards completing my studies. Mr Abram Luphondo, Adv Papi Mosima, Mr Sam Nkadimeng and Miss Tsebego Maripane, whom are my friends, are recognised for their encouragement and support during my studies.

I thank the Department of Science and Innovation (DSI) for their financial support and the CSIR for availing their laboratories for me to conduct my research work. Lastly, I thank God of Mount Zion, for through him, the completion of my MSc project was successful.

List of contributions

Lekoadi, P., Tlotleng, M., Kofi, A., Maledi, N., Masina, B. (2021), Evaluation of heat treatment parameters of microstructure and hardness properties of high-speed selective laser melted Ti6Al4V, *Metals*, vol, 11,pp.1-15.

Lekoadi, P., Maledi, N., Tlotleng, M., Masina, B. (2020), Investigation of martensite α'-phase transformation during heat treatment of high-speed selective laser melted Ti6Al4V components, *149th annual TMS conference*, San Diego, USA, 21-27 February 2020.

Lekoadi, P., Maledi, N., Tlotleng, M., Masina, B. (2019), Improving the microstructure of high-speed selective laser melted Ti6Al4V components by varying residence time during heat treatment, *20th annual RAPDASA conference*, Bloemfontein, South Africa, 06-08 November 2019.

Lekoadi, P., Maledi, N., Tlotleng, M., Masina, B. (2018), Investigation of microstructural characteristics of heat-treated high-speed selective laser melted Ti6Al4V components, *19th annual international RAPDASA conference*, Johannesburg, South Africa, 06-09 November 2018.

Table of Contents

Declaration ..... **i**

Abstract ..... **ii**

Acknowledgements ..... **iv**

List of contributions ..... **v**

List of Figures ..... **x**

List of Tables ..... **xiii**

List of Abbreviations ..... **xiv**

Chapter 1 : Introduction **1**

1.1 Background 1

1.1.1 Metal additive manufacturing 1

1.1.2 Selective laser melting 1

1.1.3 Titanium and titanium alloys 2

1.1.4 Selective laser melting produced Ti6Al4V 2

1.1.5 Heat treatment of SLM Ti6Al4V components 3

1.2 Gaps and significance of the research 4

1.3 Problem statement 4

1.4 Research objectives 6

1.5 Hypothesis 6

1.6 Delineations and limitations 6

1.7 Structure of dissertation 7

Chapter 2 : Literature Review **8**

2.1 Metallurgy of titanium and titanium alloys 8

2.1.1 Titanium alloying 9

2.1.2 Classification of titanium alloys 9

2.1.3 Ti6Al4V alloy 10

2.1.4 Phase diagram of Ti6Al4V 12
2.2 Manufacturing of Ti6Al4V alloy 12
2.2.1 Traditional methods 12
2.2.2 Additive manufacturing techniques 13
2.2.3 Processing parameters 20
2.2.4 Challenges associated with SLM technique 21
2.3 Microstructure of SLM Ti6Al4V produced components 22
2.4 Mechanical properties 24
2.5 Heat treatment 24
2.5.1 Phase transformations 25
2.5.2 β-transus temperature 26
2.5.3 Effect of heat treatment temperature 27
2.5.4 Effect of cooling rate 29
2.5.5 Effect of residence time 32
2.5.6 Stress relieving 35
2.5.7 Hot isostatic pressing 35
2.6 Possible microstructure after heat treatment 36
2.6.1 Fully martensitic α' microstructure 37
2.6.2 Fully Lamella microstructure 37
2.6.3 Equiaxed microstructure 38
2.6.4 Bimodal microstructure 39
2.7 Summary of Chapter 2 42
Chapter 3 : Experimental Procedure 43
3.1. Materials 43
3.2. Powder Characterization 43
3.2.1. Powder analysis 43
3.3. Sample production 45

3.4. Heat treatment design 46
3.5. Heat treatment 48
3.5.1. Optimizing heat treatment temperature 48
3.5.2. Optimizing cooling method 48
3.5.3. Optimizing residence time 48
3.6. Characterization of samples 49
3.6.1. Metallographic sample preparation 49
3.6.2. Microstructural analyses 49
3.6.3. Hardness measurements 50
3.6.4. X-ray micro-computer tomography scan (micro-CT-scan) 50
3.6.5. Tensile testing 51
3.7. Summary of Chapter 3 51
Chapter 4 : Heat treatment for process development 53
4.1. Process development for heat treatment optimisation 53
4.1.1. Microstructures of the samples after heat treatment 54
4.1.2. Hardness 57
4.1.3. Selection of heat treatment temperature 59
4.2. Optimisation of cooling method 60
4.2.1. Microstructures 60
4.2.2. Hardness 62
4.3. Optimisation of residence time 63
4.3.1. Microstructures 64
4.3.2. Hardness 66
4.4. Discussion of Chapter 4 68
4.5. Summary of Chapter 4 69
Chapter 5 : Heat treatment using optimized conditions 70
5.1. Porosity analysis 70

5.2. Optimized heat treatment process 73
5.2.1. Microstructures 73
5.2.2. Hardness 74
5.2.3. Tensile properties 75
5.3. Discussion of Chapter 5 78
5.4. Summary of Chapter 5 79
Chapter 6 : Conclusions 80
6.1. Summary of findings 80
6.2. Main conclusions 82
6.3. Recommendations 83
References 84
Appendix A: Metals Journal article 2021 95
Appendix B: 149th annual TMS conference paper 2020: 112
Appendix C: 20th annual RAPDASA conference paper 2019: 121
Appendix D: 19th annual RAPDASA conference paper 2018: 128

List of Figures

Figure 1.1: Microstructures of Ti6Al4V (a) Wrought, (b) SLM (Kasperovich et al., 2015).....3
Figure 1.2: Microstructure of SLM produced Ti6Al4V (Vrancken et al., 2012). 5
Figure 2.1: Crystal structures of titanium (a) hcp and (b) bcc (Pederson, 2002).....8
Figure 2.2: Illustration of alloying elements transformation temperatures (Leyens and Peters, 2003). 9
Figure 2.3: Phase diagram for Ti6Al4V (Majumdar et al, 2019). 12
Figure 2.4: EBM process (Biamo et al., 2010). 14
Figure 2.5: Microstructures of Ti6Al4V produced by (a) EBM and (b) Casting (Murr et al., 2009). 15
Figure 2.6: Schematic representation of LENS process (Zhai et al., 2016).....17
Figure 2.7: Microstructures of Ti6Al4V samples produced by (a) LENS technique (b) Wrought (Zhai et al., 2016).....17
Figure 2.8: Schematic representation of SLM process. 19
Figure 2.9: Relationship between energy density and relative density (Han et al., 2017).....20
Figure 2.10: Illustration of the effect of energy density on porosity (a) 58 J/mm^3, (b) 117 J/mm^3 and (d) 292 J/mm^3 (Kasperovich et al., 2016) 22
Figure 2.11: SLM produced Ti6Al4V microstructure at different magnifications (Lekoadi et al., 2019). 23
Figure 2.12: Elongation of Ti6Al4V components produced by different AM techniques (Yan and Yu, 2015).....24
Figure 2.13: Illustration of phase fractions at elevated temperatures calculated by Thermo-Calc software (Zhao et al., 2018).....27
Figure 2.14: Relationship of heat treatment temperature and ductility (Shipley et al., 2018). 28
Figure 2.15: CCT diagram of Ti6Al4V (Seniawski et al., 2013). 30
Figure 2.16: Ti6Al4V microstructures after heat treatment at 800°C (a) FC (b) WQ (Layens and Peters., 2003).....31
Figure 2.17: Ti6Al4V microstructures after heat treatment at 940°C for (a) 2 hrs, (b) 20 hrs (Vrancken et al., 2012).....33
Figure 2.18: Relationship of hardness and yield strength of Ti6Al4V (Keist and Palmer, 2017). 34
Figure 2.19: Ti6Al4V microstructures (a) As-built (b) HIPed (Eklund et al., 2018). 36

Figure 2.20: Ti6Al4V microstructures after heat treatment for 2 hrs followed by WQ (a) 800°C (b) 840°C (c) 875°C and 900°C (Wu et al., 2016). 37
Figure 2.21: Ti6Al4V lamella microstructures (a) schematic diagram (Chraponiski and Szkliniarz, 2001), (b) Optical image (Nalla et al., 2002)....38
Figure 2.22: A fully equiaxed Ti6Al4V microstructure (Ivanova et al., 2002). 39
Figure 2.23: Ti6Al4V bimodal microstructures (a) Optical micrograph (Nalla *et al*., 2002), (b) BSD-SE micrograph (Ter Haar *et al*., 2018)....40
Figure 2.24: Illustration of triple heat treatment strategy (Zhao et al., 2018)....41
Figure 2.25: Illustration of cycling heat treatment (Sabban et al., 2019). 41
Figure 3.1: Powder morphology of the Ti6Al4V powder (a) SEM-SEI image, (b) HS circularity curve. 44
Figure 3.2: Convexity of the Ti6Al4V powder (a) SEM-SEI image, (b) Convexity curve.....44
Figure 3.3: Aeroswift^{TM} 3D printing machine available at CSIR, Pretoria. 45
Figure 3.4: Horizontal heat treatment furnace available at the CSIR. 46
Figure 3.5: Vertical heat treatment furnace available at Pretoria University. 47
Figure 3.6: Micro-hardness testing machine available CSIR NLC. 50
Figure 3.7: Schematic diagram of a tensile sample. 51
Figure 4.1: High speed SLM produced Ti6Al4V rod samples. 53
Figure 4.2: Microstructures of the sample after heat treatment at different temperatures (a) as-received, (b) 700°C, (c) 950°C and (d) 1000°C....54
Figure 4.3: Cooling paths of Ti6Al4V (Galarraga et al., 2017)....57
Figure 4.4: Hardness profiles of the samples after heat treatment at various temperatures. ...58
Figure 4.5: Microstructures of the sample after different cooling methods (a) As-received (b) WQ (c) AC and (d) FC after heat treatment at 1000°C and holding time of 2 hrs. 60
Figure 4.6: Hardness profiles of the samples after cooling with different methods. 62
Figure 4.7: Microstructures of the samples (a) as-received, (b) 15 min, (c) 30 min, (d) 1 hr, (e) 2 hrs, (f) 4 hrs, and (e) 8 hrs. 64
Figure 4.8: Hardness profiles of the samples after heat treatment at various residence times.67
Figure 5.1: Image of the as-received sample that were used for heat treatment....70
Figure 5.2: High resolution 2D micro-ct scan image of the as-received rod sample....71
Figure 5.3: Images of the as-received Ti6Al4V sample (a) 2D micro-ct scan (b) Optical microstructure. 72

Figure 5.4: Microstructures of the as-received and heat treated samples using optimized parameters, (a) As-received (b) 1000°C for 2 hrs followed by FC and (c) 1000°C for 8 hrs followed by FC. 73
Figure 5.5: Hardness profiles of the as-received samples and the heat treated samples after heat treating using optimized parameters. 74
Figure 5.6: Stress versus extension curves of heat treated Ti6Al4V samples using optimized parameters. 76

List of Tables

Table 2.1: Physical properties of Ti6Al4V (Yan and Yu, 2015). 11
Table 2.2: Mechanical properties of Ti6Al4V (Yan and Yu, 2015). 11
Table 2.3: Phase transformations of Ti6Al4V (Seniawski et al., 2013; Yan and Yu 2015). ... 26
Table 2.4: Phase composition after control cooling from above β-transus temperature (Seniawski et al., 2013). 31
Table 2.5: Relationship between residence time and elongation of Ti6Al4V components (Plaza et al., 1990). 32
Table 4.1: Average hardness of the samples after heat treatment at various temperatures. 58
Table 4.2: Average of hardness of the as-received and heat-treated samples. 62
Table 4.3: Summarised hardness of the as-received and heat-treated samples. 67
Table 4.4: The selected optimized heat treatment parameters. 69
Table 5.1: Summarised porosity analysis of the as-received sample. 72
Table 5.2: Average hardness of the samples after heat treatment using optimized parameters. 75
Table 5.3: Mechanical properties of the Ti6Al4V samples. 76

List of Abbreviations

3D	Three Dimensional
AC	Air cooling
Al	Aluminium
AM	Additive Manufacturing
ASTM	American Society for Testing and Materials
BCC	Body Centred Cubic
CAD	Computer Aided Design
CCT	Continuous Cooling Transformation
CP-Ti	Commercially Pure titanium
CSIR	Council for Scientific and Industrial Research
DED	Directed Energy Deposition
DSI	Department of Science and Innovation
EBM	Electron Beam Melting
EBSD	Electron Backscatter Diffraction
EDS	Energy Dispersive Spectroscopy
HAZ	Heat Affected Zone
HCP	Hexagonally Closed Packed
HIP	Hot Isostatic Pressing
HV	Vickers Hardness
LENS	Laser Engineered Net Shaping
M_f	Martensite finishes temperature
M_s	Martensite start temperature
NLC	National Lase Centre

OM	Optical Microscope
PBF	Powder Bed Fusion
PM	Powder Metallurgy
SEM	Scanning Electron Microscope
SLM	Selective Laser Melting
TMP	Thermomechanical Processing
TTT	Time Temperature Transformation
UTS	Ultimate Tensile Strength
V	Vanadium
WQ	Water Quenching
YS	Yield Strength

Chapter 1 : Introduction

This chapter gives background knowledge on selective laser melting (SLM) of Ti6Al4V alloy. The effect of heat treatment on SLM produced Ti6Al4V into producing an improved bimodal microstructure is highlighted. The research gap, problem statement and research objectives are defined, and the hypothesis is given. Lastly, the dissertation structure is reported.

1.1 Background

1.1.1 Metal additive manufacturing

Metal additive manufacturing (AM) is an emerging technology that provides advantages such as energy savings, material savings and high efficiency, to several industries (Lee *et al*., 2017; Sabban *et al*., 2019). AM is highly recognised because of its ability to deposit material successfully, at designated targeted areas, and by coherently delivering either laser or electron beam on it. Consequently, the powder is melted and solidifies, thereby enabling manufacturing of high precision components (Lee *et al*., 2017). AM processes are identified primarily by the type of an energy source they use to consolidate the depositing materials, and the way in which the deposited material is fed during manufacturing (Hrabe *et al*., 2013; Leuder *et al*., 2013).

The function of the laser or electron is to melt pure metals or alloys of definitive particle size range (0.6-400µm) during manufacturing, leading to the development of either laser or electron beam melting AM process. Material can either be overlaid or blown before melting, leading to either pre-placed or powder blown platform classification (Hrabe *et al*., 2013). Laser technologies have attracted interest in various manufacturing industries and research fields; hence one of the AM technologies, in this case, selective laser melting was used to achieve the objective of this research work.

1.1.2 Selective laser melting

In selective laser melting (SLM), a laser is used to melt various metal powders. The SLM technique uses computer aided design (CAD) models to produce parts layer upon layer (Sallica-Leva *et al*., 2016; Chicos *et al*., 2018; Zhang *et al*., 2018). SLM products, such as aircraft

turbines, pressure vessels and surgical implants, are used in the aerospace, automotive, biomedical and other technology industries, respectively (Jovanovic *et al*., 2006; Yaidroitsev *et al*., 2014; Tong *et al*., 2017). SLM has become a preferred technique because of its advantages which include manufacturing of complex, finished shapes and material, furthermore, the process is time saving (Yadroitsev *et al*., 2014; Wang *et al*., 2016). Furthermore, SLM is capable of accommodating many alloy powders including, stainless steel, cobalt, and chromium (Rafi *et al*., 2013; Gong *et al*., 2014; Dong *et al*., 2017). In this work SLM machine was used to process Ti6Al4V alloy.

1.1.3 Titanium and titanium alloys

Over the last 20 years, commercially pure titanium (CP-Ti) and its alloys have attracted more interest in the modern fabrications, overriding conventional materials such as steel and aluminium (Wysocki *et al*., 2017). These materials are widely used for the manufacturing of metallic components due to their attractive properties of strength, toughness, biocompatibility, exceptional corrosion resistance at high temperatures (Wu *et al*., 2016; Wysocki *et al*., 2017; Shipley *et al*., 2018). CP-Ti can be mixed with other several elements to develop its characteristics.

For example, titanium can be alloyed with aluminium and vanadium to achieve titanium aluminium grade 5 alloy called Ti6Al4V which is a widely used and researched material. The success of Ti6Al4V is linked to the advantages it offers such as high strength, reduced weight and toughness (Teo *et al*., 2008; Wu *et al*., 2016; Tong *et al*., 2017). The two phases of Ti6Al4V ($\alpha + \beta$) permit for its structure to be refined during heat treatment. This leads to possible phase transformations when the alloy undergoes heat treatment.

1.1.4 Selective laser melting produced Ti6Al4V

Literature shows a considerable difference between SLM Ti6Al4V microstructure and wrought microstructure of the same composition (Kasperovich *et al*., 2015; Ter Haar and Becker, 2018). Several studies on the SLM produced Ti6Al4V microstructure have revealed large prior β grains that were made of sharp martensitic α'-phase. Studies by Kasperovich *et al*. (2015) and Zhao *et al*. (2018) compared the microstructure of SLM Ti6Al4V in its as-produced condition to that of wrought Ti6Al4V. The observed microstructures are presented in Figure 1.1.

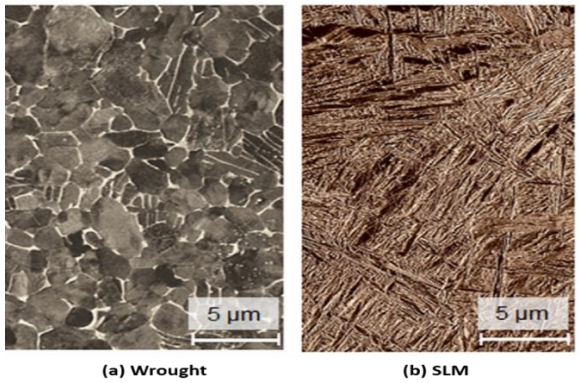


Figure 1.1: Microstructures of Ti6Al4V (a) Wrought, (b) SLM (Kasperovich *et al*., 2015).

Figure 1.1(a) depicts that microstructure of wrought Ti6Al4V components consist of equiaxed α and β grains while the SLM produced Ti6Al4V compose of a sharp acicular martensitic α'-phase. The acicular martensitic α'-phase is associated with low ductility (elongation less than 10%) and residual stresses resulting in the compromised mechanical properties. Studies by Joshi (2006) and Khorosani *et al*. (2017) discussed that SLM produced Ti6Al4V components do not meet the same material properties compared to their wrought counterparts. To overcome this challenge, the SLM produced Ti6Al4V parts are heat treated after production. Heat treatment is able to transform the martensitic α'-phase into stable phases and achieve the microstructure that is comparable to that of wrought parts.

1.1.5 Heat treatment of SLM Ti6Al4V components

Heat treatment is typically applied to SLM produced Ti6Al4V components to improve the microstructure, relieve residual stresses, eliminating the metastable martensitic α'-phase with the purpose of obtaining a stable microstructure (Yan and Yu, 2015). This results in microstructural improvement that leads to part enhancement. The existence of the two phases (α + β) of Ti6Al4V allows for the transformation between phases during heat treatment leading to a variety of microstructures with different and desired mechanical properties (Weiss *et al*., 1986; Semiatin *et al*., 1997; Lutjering *et al*., 1998). Furthermore, heat treatment improves the ductility of Ti6Al4V products manufactured by SLM (Vrancken *et al*., 2012; Wu *et al*., 2016). Several studies (Ter Haar and Becker, 2018; Zhao *et al*., 2018; Sabban *et al.,* 2019) have shown that a bimodal microstructure achieves excellent strength and superior ductility, and it can be achieved by duplex or triple heat treatment strategies. The aim of the current study is to improve

the microstructure of Ti6Al4V components produced by SLM process by developing a bimodal microstructure using a single heat treatment strategy as opposed to the approach proposed by Ter Haar and Becker (2018) and Zhao *et al*. (2018) who respectively used a duplex heat and triple treatment strategies to obtain a bimodal microstructure. This research project concentrated on varying heat treatment temperature, cooling methods and heating residence time, on high speed SLM produced Ti6Al4V coupons to produce a bimodal microstructure.

1.2 Gaps and significance of the research

Over the years, AM has become a preferred manufacturing technology over traditional manufacturing methods due to its cost savings, reliability, material saving and parts accuracy (Liu *et al*., 2016; Zhao *et al*., 2018). Due to these advantages, there has been an increase in demand of high precision geometrical parts (with repeatability) that were difficult or impossible to manufacture using conventional methods. The abilities of AM technologies are rapidly evolving, hence there are several types of AM techniques that are used worldwide.

Aeroswift^{TM} SLM machine, available at the Council for Scientific and Industrial Research (CSIR), is capable of producing components using high speed and power laser of 5 kW. The ability of using high speed and power enables increased productivity, while also adding scientific knowledge and understanding of the SLM process. Although AM of Ti6Al4V and investigation of its heat treatment is not a new area of study, little is known about heat treatment of Ti6Al4V AM components manufactured with SLM at high speed and power. Therefore, this study investigated heat treatment effects on the improvement of the microstructure of the Ti6Al4V coupons that were manufactured from a SLM machine with high speed and power. To the best of the author's knowledge, no work has been reported in open literature at the time of writing on heat treatment of Ti6Al4V produced by SLM at 5 kW power laser.

1.3 Problem statement

Although AM offers a variety of advantages over conventional methods, there are some challenges associated with Ti6Al4V parts manufactured by this technology. The microstructure of the as-built Ti6Al4V component is inhomogeneous, different from its wrought counterparts, and has high residual stresses that are due to repeated thermal cycles, fast heating and cooling

during fabrication (Vilaro *et al*., 2011; Ter Haar and Becker, 2018) which affect their performance. These thermal cycles produce an undesired martensitic α'-phase which alters the microstructure and results in undesired changes in mechanical properties, with parts having low ductility, low toughness and low cycle fatigue property (Ter Haar and Becker, 2018; Zhao *et al*., 2018; Sabban *et al*., 2019). This low ductility hinders AM produced parts the potential in engineering application such as aerospace industry (Zhao *et al*., 2018). For industry applications, ductility and low circle fatigue need to be improved.

For example, the microstructure of SLM produced Ti6Al4V component obtained by Vrancken *et al*. (2012) is shown in Figure 1.2.

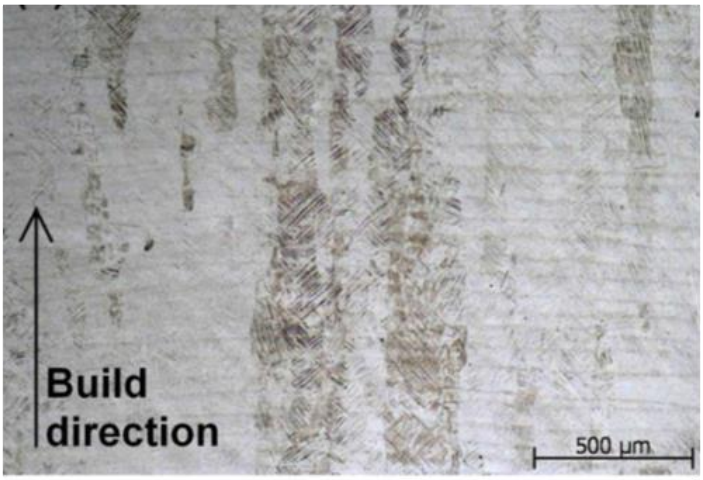


Figure 1.2: Microstructure of SLM produced Ti6Al4V (Vrancken *et al*., 2012).

This type of microstructure is characterized by a sharp acicular martensite α'-phase which is associated with low ductility (Chen *et al*., 2017; Xu *et al*., 2017; Shipley *et al*., 2017; He *et al*., 2019). Heat treating the parts improve the microstructure of the SLM built Ti6Al4V parts leading therefore to a residual stress-free part with improved mechanical properties in ductility and fatigue (Yan and Yu, 2015). Proper heat treatment parameters are required in order to improve the microstructure because some heat treatments may improve the ductility, however at the cost of strength (Zhao *et al*., 2018). Studies by Ter Haar and Becker (2018) used duplex heat treatment strategy and Zhao *et al*. (2018) used triple heat treatment strategy to obtain a bimodal microstructure, which is considered superior balance in strength and ductility. In this study, a single heat treatment strategy was implemented by varying temperature, cooling method and residence time during heat treatment in an attempt to producing a bimodal

microstructure. It is more beneficial to use single heat treatment strategy over duplex and triple strategies because it saves both time and energy.

1.4 Research objectives

Heat treatment is known to affect microstructural transformation that governs its effectiveness in mechanical properties of SLM Ti6Al4V components. A bimodal microstructure achieves good balance of strength and superior ductility. The aim of the study was to produce a bimodal microstructure in Ti6Al4V samples produced by SLM method. The microstructure was achieved by varying temperature, cooling method and residence time. The research objectives were:

- Determine the effect of heat treatment parameters (temperature, cooling methods and residence time) on the microstructure and mechanical properties of Ti6Al4V parts produced with SLM process.

- Determine the optimum heat treatment parameters which ensure formation of bimodal microstructure and improves mechanical properties including tensile properties in SLM fabricated Ti6Al4V.

1.5 Hypothesis

It has been shown that a bimodal microstructure achieves superior tensile ductility Ti6Al4V components produced by SLM process. Water quenching from above the critical temperature achieves a bimodal microstructure of α-phase in a matrix of martensite α'-phase. The second annealing strategy is required to decompose the unwanted martensite α'-phase (Ter Haar and Becker, 2018). Based on this understanding, it is hypothesized that a bimodal microstructure can be achieved without using the second annealing strategy (single heat treatment strategy) on high speed SLM produced Ti6Al4V components by varying temperature, cooling method and residence time.

1.6 Delineations and limitations

This research focused on characterising the as-received and heat-treated high speed and power SLM Ti6Al4V coupons. The coupons were produced on a continuously pre-heated base plate at a temperature of 200°C. Heat treatment was done in an argon protected atmosphere.

1.7 Structure of dissertation

The structure of this dissertation is as follows:

This chapter discussed the importance of heat treatment on the improvement of SLM produced Ti6Al4V samples microstructure and mechanical properties. It captured that an improved microstructure can be obtained if heat treatment parameters are appropriately adjusted. Such an improved microstructure is known as bimodal microstructure which has better tensile properties.

Chapter 2 focuses on literature review and some of the important aspects that are related to this study and review important findings that were made by other authors. The processing of Ti6Al4V alloys using traditional methods and AM techniques followed by post heat treatment is discussed. Chapter 3 gives a detailed description of the experimental procedure. Chapter 4 presents heat treatment results for process development while Chapter 5 reports on heat treatment results obtained using selected heat treatment parameters. Chapter 6 summarises the findings and give the recommendations and future work. References and publications are included at the end of the dissertation.

Chapter 2 : Literature Review

This Chapter focus on revision, findings and important concepts that contribute to the knowledge areas of this project. The comparison of microstructure produced by AM and traditional methods is reviewed in detail. Improving the microstructure of Ti6Al4V by employing different heat-treating strategies is the main focus area. The contribution of heating and cooling on microstructural formation is mainly highlighted. Moreover, the possible microstructures that can result from heat treatments of Ti6Al4V are also reported.

2.1 Metallurgy of titanium and titanium alloys

Titanium and its alloys are essential for various structural applications. Their attractive property of producing light weight structures have made them more desirable in biomedical, marine and automobile industries (Poondla *et al*., 2009; Shipley *et al*., 2018). They owe their success to their low density of 4.43 g/cm^3. Titanium can crystallize in various structures which are depicted in Figure 2.1.

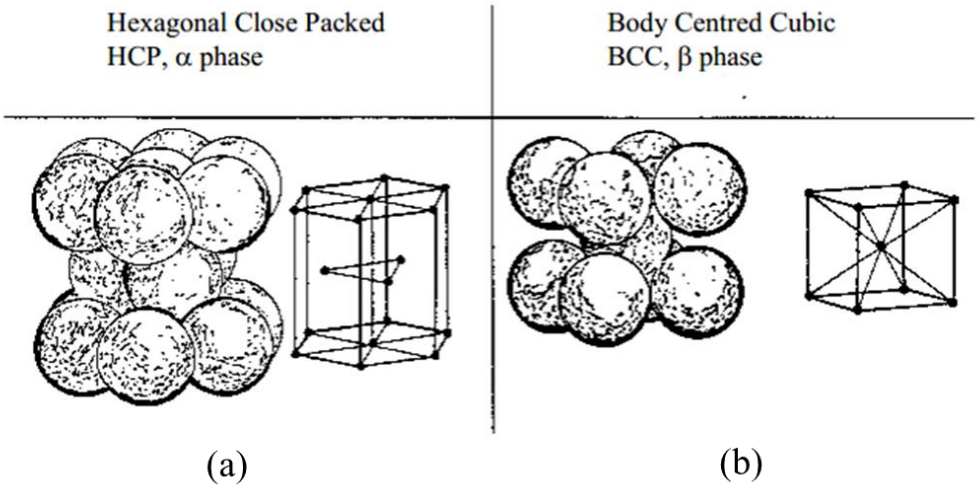


Figure 2.1: Crystal structures of titanium (a) hcp and (b) bcc (Pederson, 2002).

Titanium crystallizes in a familiar hexagonally close packed (hcp) pattern at room temperature as presented in Figure 2.1(a) and they are referred as α-titanium. When the temperature is raised, they crystallize in a stable body centred cubic (bcc) arrangement as presented by Figure 2.1(b), referred to as β-titanium (Lutjering and Williams, 2007). The presence of the two

different structures together with their transformation temperatures is significant to the alloys because they form as a foundation for formation of different structures and mechanical properties.

2.1.1 Titanium alloying

Alloying is the addition of specific elements to titanium in sufficient quantity to improve its material properties. The alloying elements are classified according to the phases that they stabilize. For instance, in case of Ti6Al4V alloy, vanadium (V) is responsible for stabilizing the β-phase and aluminum (Al) stabilizes the α-phase. Elements that added to titanium are grouped as α and β stabilizers or neutral depending their effect on β-transus (Leyens and Peters, 2003; Lutjering and Williams, 2007). Figure 2.2 demonstrate the influence of titanium alloying on β-transus.

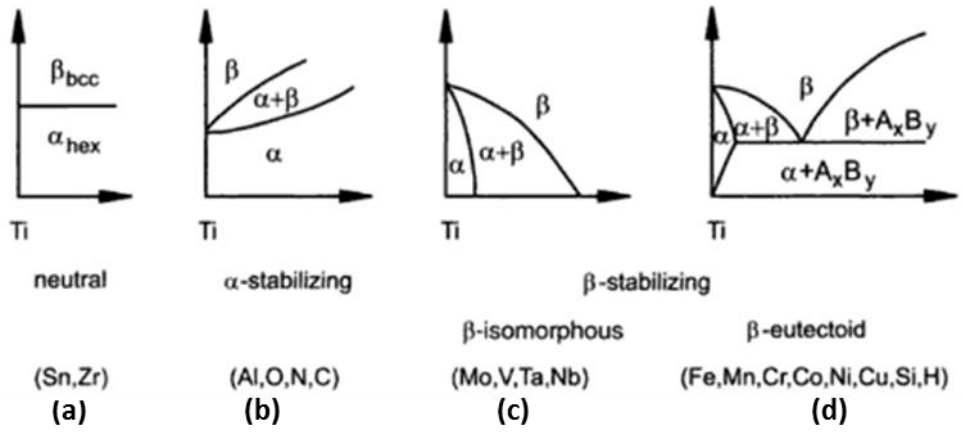


Figure 2.2: Illustration of alloying elements transformation temperatures (Leyens and Peters, 2003).

Elements that do not have an impact β-transus are called neutral elements (Figure 2.2a). On the other hand, elements that increase or decrease the β-transus are called α-stabilizers and β stabilizers, respectively as depicted by Figures 2.2(b), 2.2(c) (Leyens and Peters, 2003). There are two groups of β-stabilizing elements, namely β-isomorphous and β-eutectoid elements (Figures 2.2c, 2.2d). The β-isomorphous elements are favourable because they are mostly soluble in titanium (Leyens and Peters, 2003).

2.1.2 Classification of titanium alloys

2.1.2.1 α-alloys

Titanium alloys are divided into three groups, namely, α, α + β and β alloys. However, near-α and metastable β groups exist as supplementary categories (Leyens and Peters, 2003). These types of alloys are characterized by excellent creep and strength. Moreover, the α-alloys cannot undergo a heat treatment process to manipulate their microstructure because of their single phased hcp structure. In addition, they are known to have very low ductility and anisotropic properties (Weiss and Semiatin, 1999). The stability of α-alloys occurs at temperatures lower than 650°C (Leyens and Peters, 2003). A mixture of this type of alloys with β-stabilizers creates sub-division of near-α group.

2.1.2.2 α + β-alloys

The α + β group stabilizes at 450°C. This type of alloys can undergo heat treatment process to change the material properties (Leyens and Peters, 2003). When properly heat treated, the α + β alloys can have excellent strength and corrosion resistance along with suitable ductility (William *et al*., 2001; Lutjering and William, 2007). With sufficient β favouring alloy element level, transformation to β-phase is produced upon heating and transformed during the cooling. In this category, Ti6Al4V alloy account almost 50% usage over commercial alloys (Semiatin *et al*., 1997; Alcisto *et al*., 2011).

2.1.2.3 β-alloys

The microstructure of this alloys consists mainly of β-phase. They are mostly consumed in the aerospace industry. They are characterized by high strength and ductility (Lutjering and William, 2007; Ghaderi *et al*., 2013). Moreover, this group of alloys are characterized by high concentrations of β-stabilizing elements. These group of alloys are less stable compared to the others and most of them are made of β-phase (Lutjering and William, 2007).

2.1.3 Ti6Al4V alloy

The Ti6Al4V also known as Ti64 is a titanium alloy that is made up of α + β phases. Ti6Al4V is known as the mostly used titanium alloy over other titanium alloys (Semiatin *et al*., 1997; Lutjering, 1999; Alcisto *et al*., 2011). The microstructure of the alloy consists of α and β-phases

at room temperature (Pederson and Babushkin, 2003), with 90% volume fraction of α-phase (Facchini *et al*., 2010). Heat treating this alloy can result in the manipulation of its microstructure which gives improved mechanical properties (Sieniawski, 1997; Lutjering, 1999; Markovskya and Semiatin, 2011). Physical properties of Ti6Al4V are shown in Table 2.1.

Table 2.1: Physical properties of Ti6Al4V (Yan and Yu, 2015).

Physical property	Value
Density of solid (ρ)	4.43 g/cm^3
Density of liquid (ρ)	3.89 g/cm^3
Solidus temperature	1604°C
Liquidus temperature	1660°C

Ti6Al4V is widely used in aero-engine, space shuttles and other high-performance applications (Lutjering and William, 2007). In the aerospace industry, Ti6Al4V alloy is significant for structural materials (William and Starke. 2003). The mechanical properties of Ti6Al4V are given in Table 2.2.

Table 2.2: Mechanical properties of Ti6Al4V (Yan and Yu, 2015).

Mechanical property	Value
Tensile strength, yield (σ)	880 MPa
Tensile strength, Ultimate (UTS)	950 MPa
Elongation ($\mathcal{E}$)	14%
Hardness	349 HV
Young modulus (E)	113.8 GPa
Fatigue strength (at 1*10^7 cycles)	240 MPa
Fatigue strength (unnotched at 1*10^7 cycles)	510 MPa
Fracture toughness	75 MPa

2.1.4 Phase diagram of Ti6Al4V

The microstructure of Ti6Al4V is mainly dependent on how α + β phases are dispersed. A Ti6Al4V phase diagram can be used to understand the behavioral relationship and phase transformations of the alloy. The phase diagram of Ti6Al4V is shown in Figure 2.3.

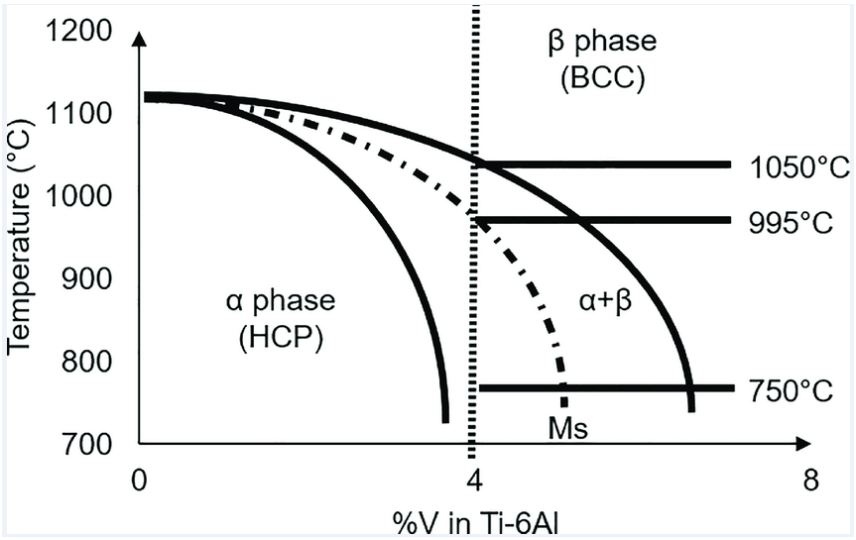


Figure 2.3: Phase diagram for Ti6Al4V (Majumdar *et al*, 2019).

The two phases of Ti6Al4V alloy (α and β) allows its composition to fully transform to β-phase upon heating but return to α-plus or retained/transformed β-phase upon cooling as depicted by Figure 2.3. The β-transus is defined as the temperature whereby other phases transform to full β phase. The β-transus temperature will be discussed in detail in Section 2.5.2. The other important temperatures that are indicated on the phase diagram are the martensite start (M_s) and martensite finishes (M_f) which represents the temperatures where martensite transformation starts and finishes.

2.2 Manufacturing of Ti6Al4V alloy

2.2.1 Traditional methods

Conventional methods are used to manufacture titanium and its alloys. These techniques include casting, forging and powder metallurgy (PM). There are several disadvantages of these techniques that make their processes undesirable in the manufacturing industry. Materials

wastage, long production times and high tooling costs are amongst some of the disadvantages. In addition, manufacturing of complex structures is not possible with the conventional methods (Boyer and Briggs, 2005; Alcisto *et al*., 2011). During the last decade, AM technology has been developed and intensively investigated for manufacturing of various metallic materials for various applications, especially Ti6Al4V alloy (Kasperovich and Hausmann, 2015). The AM technologies offer many advantages over conventional methods because of their improved design freedom (Tiferet *et al*., 2016; He *et al*., 2019).

In terms of microstructures, AM techniques produce microstructures that are different to the ones produced by traditional methods. According to Yan *et al*. (2018), the Ti6Al4V microstructure produced by PM is homogeneous due to the low cooling rates used by most sintered practices. However, porosity is still a major problem on the as-sintered microstructure.

2.2.2 Additive manufacturing techniques

American Standard Testing Method (ASTM) F2921-11 defines AM as a manufacturing method that opposes conventional methods, whereby objects are made by joining material layer upon layer from control aided design (CAD) data. There are various AM techniques that exist but most of them differ according to material feedstock. The AM techniques allow for greater freedom of design, geometrical freedom and material flexibility (Hrabe and Quinn, 2013). AM involves taking information from CAD models to manufacture 3D components. The next sections focused on some of AM techniques used today.

2.2.2.1 Electron beam melting (EBM)

It was mentioned in Section 2.2.2 that there are various AM techniques that exist. The electron beam melting (EBM) is defined as AM technique which uses an electron beam, as an energy source (Galaragga *et al*., 2016). The electron beam melting process is depicted in Figure 2.4.

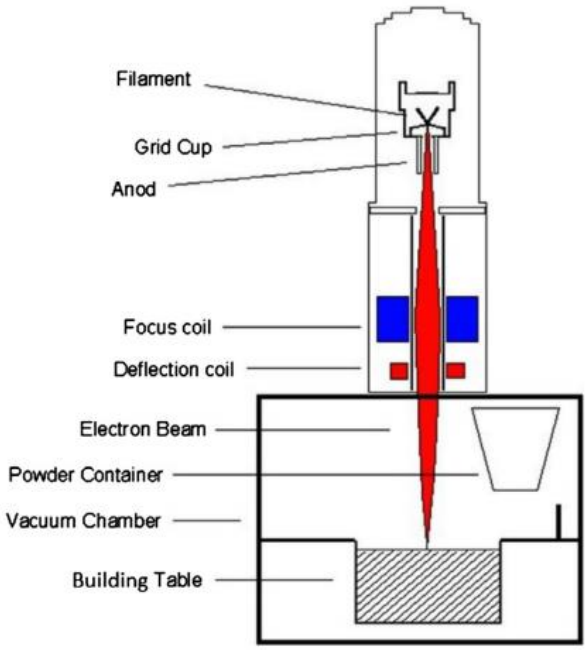


Figure 2.4: EBM process (Biamo *et al*., 2010).

There are four major process parameters that have significant effect on the produced part. These parameters include beam power, beam diameter, scan speed and pre-heat temperature (Gong *et al*., 2014). However, there are other parameters that can be controlled by the software such as line offset, beam current, hatch pattern and rotation angle between consecutive hatches (Mahale, 2014; Rovelo and Fraunhofer, 2016). EBM has attracted attention in the biomedical, aerospace industries, and some application where structural complexity is important (Galarraga *et al*., 2017).

The unique characteristics offered by EBM over other techniques include high energy efficiency, high pre-heating temperature, high scanning and moderate operational cost (Gong *et al*., 2012). The advantages of EBM over conventional manufacturing technologies include less design constrains, geometrical freedom, near-net shape production and weight reduction (Cormier *et al*., 2004; Gaytan *et al*., 2009; Yu *et al*., 2009). In addition, EBM offers the ability to eliminate additional post processing after the component is produced. The ability to melt powder with an electron makes EBM a manufacturing process that accommodates different materials alloys including aluminum alloys, cobalt-based superalloys, titanium alloys and others (Gaytan *et al*., 2009; Yu *et al*., 2009).

There are two important magnetic coils, namely, focus and deflection coils that controls the electron beam to preferred point and diameter, respectively (Figure 2.4). Once the electron beam has scanned the powder, another powder layer is deposited. The process repeats and stops when the component has formed (Gong *et al*., 2012). The entire process is conducted in vacuum to minimise reaction with oxygen on the produced components. When building of the component is completed, it is removed from the chamber when it is at low temperature.

Despite all the interesting advantages displayed by EBM, there are some few process deficiencies that come with this technique. These deficiencies include part defects, quality variation and process instability (Zah and Lutzmann, 2010). The electron beam may result in insufficient energy transmission to the powder, which may cause melt pool instabilities and that result in the balling effect (Cansizoglu *et al*., 2008). Porosity due to gas entrapment is a usual defect in EBM. Gaytan *et al*. (2009) studied porosity formation during EBM, and it was found that it is possible to eliminate the pores and voids on the produced component by using heat treatment that is commonly known as hot isostatic pressing (HIP). Another EBM deficiency is the build-up of residual stresses which are induced by large thermal gradients. In some cases, the bonding ability amongst the layers is less, which may lead to delamination of the produced part (Schwerdtfeger *et al*., 2009).

There are several studies that focused on microstructural and mechanical properties of EBM coupons, comparing them with wrought Ti6Al4V parts. It is important to compare the microstructure because they act as fingerprints of the mechanical properties. Koike *et al*. (2011) compared Ti6Al4V microstructures that were produced by EBM and that of casted Ti6Al4V. The microstructures are shown in Figure 2.5.

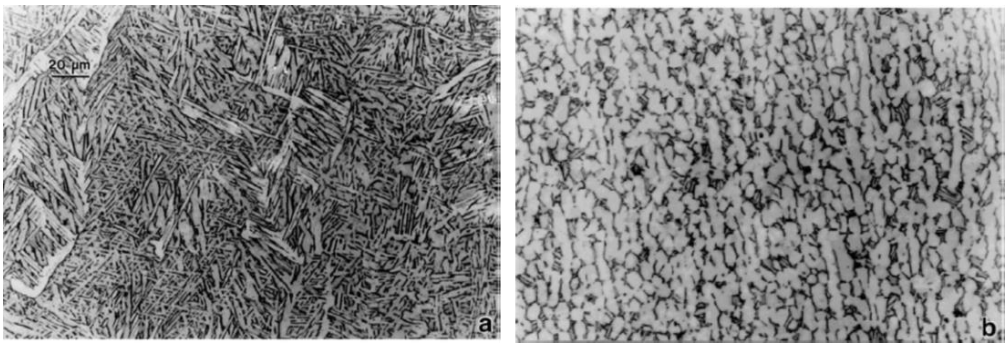


Figure 2.5: Microstructures of Ti6Al4V produced by (a) EBM and (b) Casting (Murr *et al*., 2009).

The EBM produced Ti6Al4V microstructure exhibited a lamella α-phase and martensite α'-phase platelets as shown in Figure 2.5(a) which gave rise to increased hardness (Murr *et al*., 2009). The martensite α'-phase formation was due to rapid cooling and solidification during EBM printing. The microstructure obtained by casting composed of globular α + β grains. As compared to the microstructure obtained by casting presented in Figure 2.5(b), α-phase of the EBM produced Ti6Al4V was found on the β grain boundaries and it was finer (Gulzar *et al*., 2009). In contrast, a basket weave α + β microstructure was observed by Safdar *et al*. (2012) on EBM produced Ti6Al4V parts. However, in this case, α and β phases formed platelets and β rod-like shapes, respectively in the columnar prior β grains on the microstructure.

In addition, Safdar *et al*. (2012) has indicated that Ti6Al4V samples produced from EBM shows fully lamellar microstructure, made up of fine grains due to rapid cooling. Furthermore, these authors observed the heat conduction direction same to the columnar morphology. They attributed the columnar grains to thermal gradients. A study by Antonysamy *et al*. (2013) has reported that elongated shape is responsible for strong fiber texture and is due to the movement melt pool. Three phases which are α, martensite α' and β phase were reported on EBM Ti6Al4V microstructure (Gulzar *et al*., 2009; Facchini *et al*., 2009).

The EBM Ti6Al4V parts possessed by higher ultimate tensile strength (UTS) and low elongation compared to wrought counterparts (Facchini *et al*. 2009). However, Koike *et al*. (2011) reported an opposite observation by reporting higher UTS and ductility for wrought and cast Ti6Al4V counterparts. The different observations were attributed to the difference in built parameters which does not give the same material features (Gong *et al*., 2012).

2.2.2.2 Laser engineered net shaping

In contrast to PBF, the laser engineered net shaping (LENS) uses a directed energy deposition (DED) powder blown method. This technique involves the injection of metal powder into a melt pool that promote melting and solidification of powder, thereby producing 3D parts (Arthur and Pityana, 2018). This AM technique uses a high-power laser as a source of energy. A diagram showing the process of LENS is depicted in Figure 2.6.

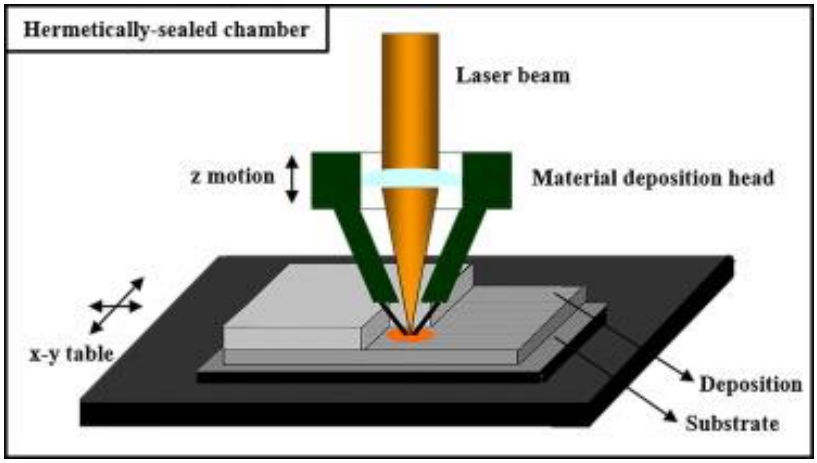


Figure 2.6: Schematic representation of LENS process (Zhai *et al*., 2016).

The processing principle of the LENS includes a deposition substrate that needs to be aligned to a starting position of interest. The process takes place in an inert atmosphere to eliminate oxidation during printing. A small molten pool is created of the powder by the laser. The movement of deposition is created and controlled by CAD files (Mudge and Walt, 2007).

Some of the important characteristics of LENS are low heat inputs and minimal distortion. According to Mudge and Walt (2007), due to the small melt pool used by LENS, the deposited material cools fast, which results in the generation of a fine grain structure that may be comparable to wrought components. Figure 2.7 shows Ti6Al4V microstructures of LENS produced sample and that of wrought samples.

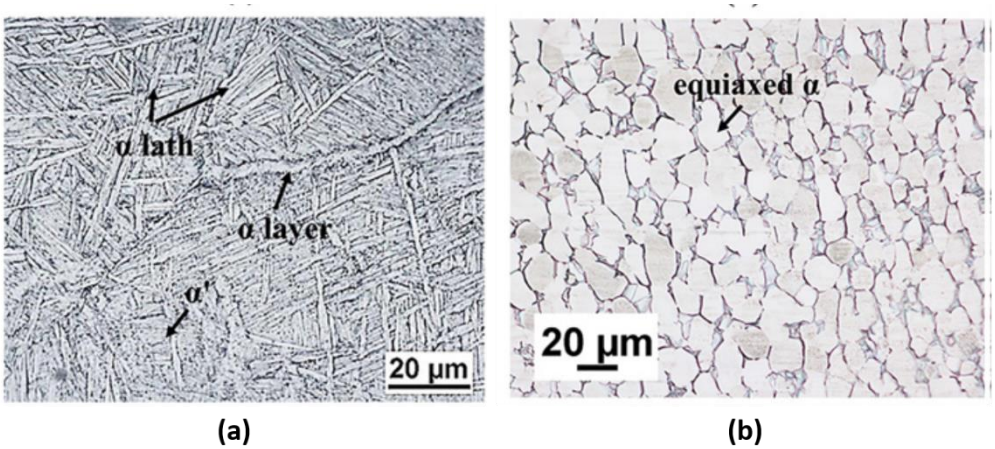


Figure 2.7: Microstructures of Ti6Al4V samples produced by (a) LENS technique (b) Wrought (Zhai *et al*., 2016).

The as-produced microstructure of Ti6Al4V sample produced by LENS process was characterized by sharp needle-like martensitic α'-phase shown in Figure 2.7(a) (Qiu *et al*., 2015). The wrought microstructure presented in Figure 2.7(b) shows equiaxed α-phases. It is evident that LENS produced and wrought Ti6Al4V microstructures are different. LENS offers advantages such as environmental friendliness, creation of smaller heat affected zone (HAZ), production of components in less time, reduced material waste, greater ability for parts repair and digital flexible processing (Qiu *et al*., 2015; Zhai *et al*., 2016).

The LENS is capable of processing different metals and alloys which include titanium, steel and nickel-based super alloys (Zhai *et al*., 2016). Since LENS is an AM technique, it also has its own challenges. Structural defects and part distortion are common issues (Qui *et al*., 2015). On their study on microstructure and texture evolution of Ti6Al4V, Kobryn *et al*. (2003) showed that there are two types of microstructural pores that are found on LENS produced Ti6Al4V components. Spherically shaped gas pores and pores due to insufficient melting which usually forms at the interfaces between layers and show elongated or irregular shape. According to Qui *et al*. (2015), correctly adjusting the rate at which powder is fed, and using moderate laser power achieves a part with minimum porosity.

Thermal stress developments, resultant distortion of substrate of the produced component are other challenges. These challenges may lead to component failure. A study by Moat *et al*. (2011) investigated residual stress measurements on LENS produced Ti6Al4V and showed high level of distributed stress in the produced components.

2.2.2.3 Selective laser melting

Selective laser melting (SLM) is another metal PBF technique, slightly different from EBM that was discussed in Section 2.2.2.1. This manufacturing technique is regarded as a revolutionary emerging technology (Sabban *et al*., 2019). It is an AM technique that is constructed on an infrared fiber laser capable of creating solid near net metallic shaped parts layer-by-layer from powder material according to CAD models (Kruth *et al*., 2007; Thijs *et al*., 2010; Vrancken *et al*., 2012; Simonelli *et al*., 2014). Figure 2.8 illustrate the SLM technique.

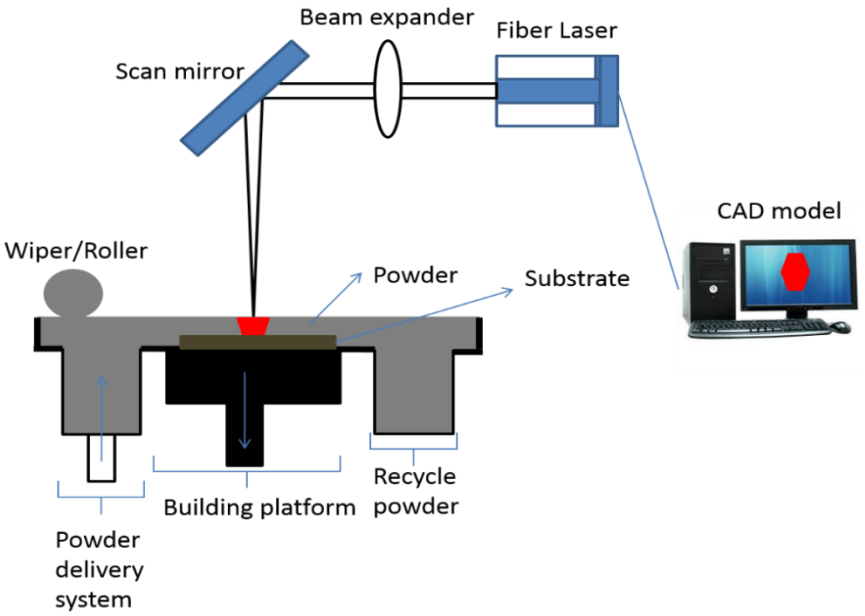


Figure 2.8: Schematic representation of SLM process.

The SLM has gained more interest in the aerospace, electronics, chemical, biomedical and other industries where various products such as aircraft turbines, pressure vessels and surgical implants are used (Alcisto *et al*., 2011; Villaro *et al*., 2011; Shipley *et al*., 2018; Zuback and Debroy, 2018). During production of a component, a CAD model is inserted into the machine, where it is divided into layers (usually between 10-100 µm) by software. A fine powder which is a feed stock is placed on top of the base plate just above the build platform. Then the CAD information leads the laser to scan the metal powder. A small portion of the part is formed when the scanned powder melt and solidifies. The process is repeated severally and complete once a 3D part is formed (Rafi *et al*., 2013; Simonelli *et al*., 2014).

After removal of the part, most of the unconsolidated powder is removed and can be re-used. The main process parameters in SLM are laser power, scanning speed, hatch spacing and layer thickness (Rafi *et al*., 2013). The SLM process usually take place in argon purged environment to reduce oxygen content. The SLM technique is mostly accompanied high heating and cooling rates which result in formation of non-homogeneous structure (Vracken *et al*., 2012; Rafi *et al*., 2013; Kasperovich *et al*., 2016). SLM offers advantages which include production of complex geometries, time saving, ability to produce net-shaped structures, reduced wastage of material, improved flexibility (Villaro *et al*., 2011). Furthermore, SLM is capable of covering complex alloy powders including stainless steel, cobalt, chromium, titanium and many more alloys (Markovskya *et al*., 2011; Rafi *et al*., 2013).

2.2.3 Processing parameters

Defects formation on microstructure depends on processing parameters such as layer thickness, scan strategy, hatch spacing, scan speed and laser power during SLM (Vrancken *et al*., 2012). Improper adjustment of process parameter can form defects. Balling effect (formation of small particles), porosity and lack of fusion are such types of defects. However, balling effect can also be influenced by material properties (Gu *et al*., 2012). If the energy density is not optimal, the working temperature will be insufficient to melt the powder. Energy density (*E*) is a variable that defines the densification of material (Attar *et al*., 2014). The energy density equation defines the average applied energy per volume of material. Equation 1 shows the energy density equation.

$$E = \frac{P}{vht} \qquad (1)$$

Where *P* is the laser power (W), *v* is the laser scanning speed (mm/s), *h* is the hatch spacing (mm) and *t* is the layer thickness (mm). The energy density variables have a tendency to determine a process window for manufacturing completely dense component. Figure 2.9 shows the relationship between relative density and laser energy density as described by Han *et al*. (2017).

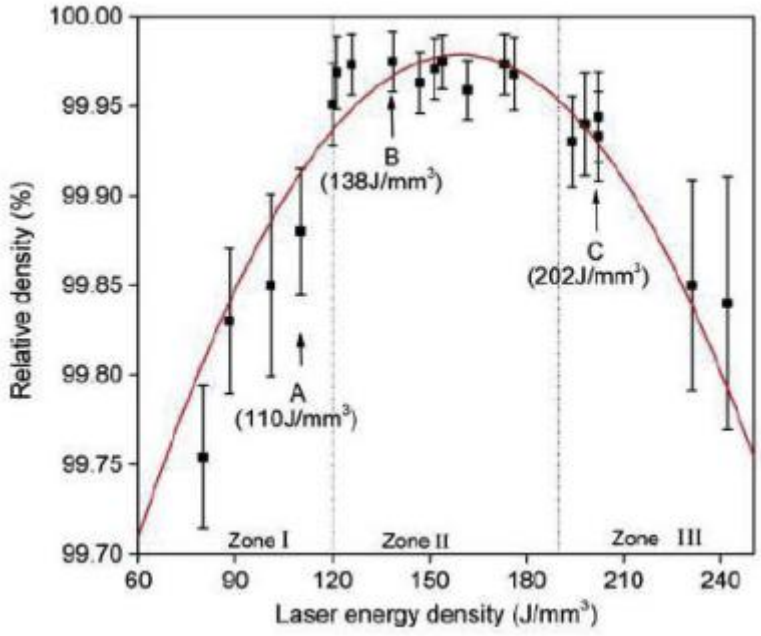


Figure 2.9: Relationship between energy density and relative density (Han *et al*., 2017).

Figure 2.9 shows that relative density increase with increasing laser energy density from 60 J/mm^3 to 120 J/mm^3 as represented by zone I. However, the relative density obtained in this latter region was not maximum. As the energy density increased from 120 J/mm^3 to 180 J/mm^3 (zone II in Figure 2.9), the relative density increased to maximum value above 99.95%. This was an indication processing using the energy densities in this range would result in almost fully dense sample. The relative density decreased when the laser energy density increased from 180 J/mm^3 to 240 J/mm^3 which is demonstrated by zone III in Figure 2.9. This implies that applying energy densities in this region will results in parts with defects, which can lead to part failure. Part failure will result in lowering of the production rate, powder and energy wastage.

Han *et al*. (2017) defined process window of 120-202 J/mm^3 energy densities in order to produce Ti6Al4V components with 99% relative density (Figure 2.9). However, a different process window of 48.61-194 J/mm^3 was reported by Cunningham *et al*. (2016). The reporting of different process windows indicates a difference in parts density that can be obtained by using the same energy densities. This study will make use of samples that are produced with energy density that fall within the range 48.61-194 J/mm^3.

2.2.4 Challenges associated with SLM technique

According to literature, the three main challenges that come with the SLM process are (i) the generation microstructure that is different to microstructure produced by conventional methods (ii) fabrication components with defects such as porosity, delamination, lack of fusion of layers and balling and (iii) the development of residual stresses (Gu *et al*., 2012; Leuders *et al*., 2013; Liu *et al*., 2014; Xu *et al*., 2015; Wysocki *et al*., 2017). Due to high cooling rates, microstructures of SLM produced Ti6Al4V composes of acicular martensite α'-phase which is very brittle (Thijs *et al*., 2010; Vilaro *et al*., 2011; Gu *et al*., 2012; Xu *et al*., 2015; Wysocki *et al*., 2017; Ahmadi *et al*., 2019). As a result, SLM produced Ti6Al4V components have a tendency of having high tensile strength and poor ductility and associated with limited fatigue life (Vilaro *et al*., 2011; Vrancken *et al*., 2012).

The second challenge is fabrication components with porosity, delamination and balling, which then greatly affect the fatigue properties (Gu *et al*., 2012; Leuders *et al*., 2013; Liu *et al*., 2016).

Figure 2.10 demonstrate porosity on SLM produce Ti6Al4V components attained by Kasperovich *et al*. (2016).

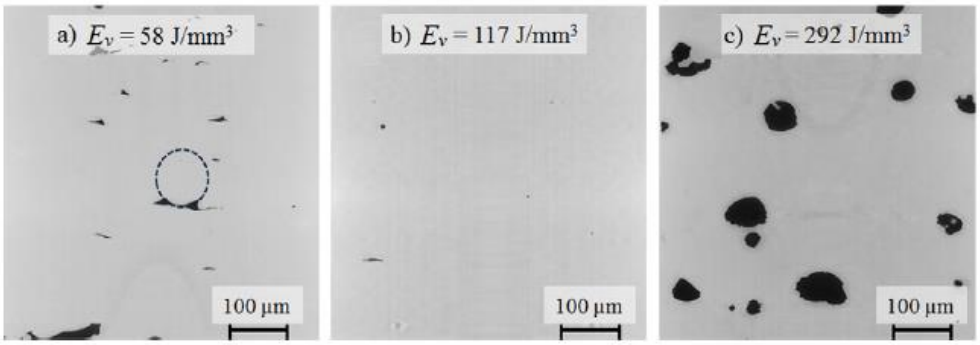


Figure 2.10: Illustration of the effect of energy density on porosity (a) 58 J/mm^3, (b) 117 J/mm^3 and (d) 292 J/mm^3 (Kasperovich *et al*., 2016).

Good control on energy density (or process parameters) determines the amount porosity on the produced components. For example, it can be seen from Figures 2.10(a) and 2.10(c) that lower and higher energy densities, respectively, resulted with high porosity on the produced component whilst moderate energy density as demonstrated by Figure 2.10(b) let to a component with very low porosity. The size of the pores also depends on the energy density (or process parameters) used. Song *et al*. (2012) recommended laser power of 110 W and scan speed of 0.4 m/s in order to obtain Ti6Al4V parts with maximum density. It should be noted that there are other applications such as medical implants whereby porous structures have additional advantage over full-density materials (Warnke *et al*., 2009).

Tong *et al*. (2017) pointed out roughness as another challenge associated with SLM produced part. This results from partially and/or un-melted powder that has a tendency to stick on the surface of the surface part. The development of residual stresses was found to be another challenge associated with SLM. These residual stresses are resulting from high cooling rates and temperature gradients of the SLM technique. However, Rafi *et al*. (2013) and Algius *et al*. (2018) revealed that powder bed pre-heating helps in reducing the build-up of residual stresses when producing the parts.

2.3 Microstructure of SLM Ti6Al4V produced components

It was discussed in Section 2.2, that SLM process parameters and thermal history determine microstructural evolution of Ti6Al4V components (Rafi *et al*., 2013). Their microstructures in the as-produced condition are characterized by large elongated prior β grain that is orientated along the build direction filled with acicular martensitic α'-laths inside (Thijs *et al*., 2010; Vilaro *et al*., 2011; Gu *et al*., 2012; Song *et al*., 2012; Sabban *et al*., 2019). A study by Lekoadi *et al*. (2019) evaluated the microstructure of SLM Ti6Al4V components that were produced at high power and speed. Figure 2.11 shows the microstructure that was obtained.

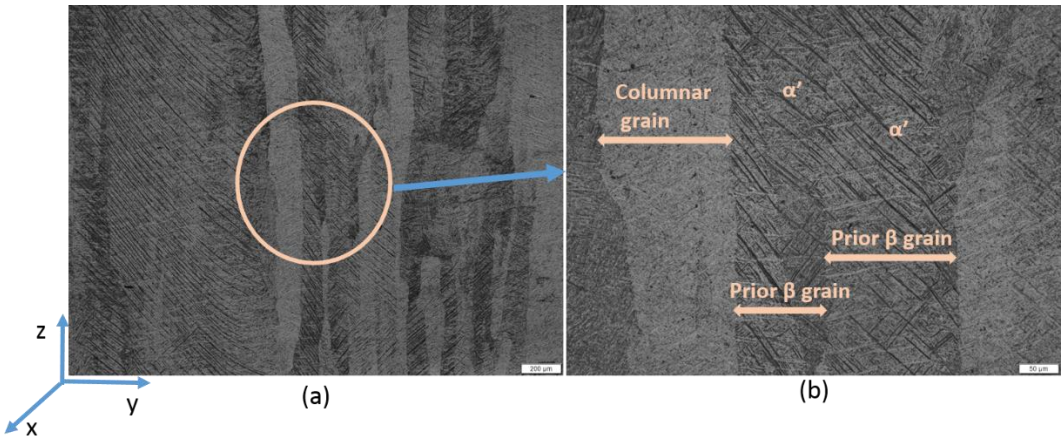


Figure 2.11: SLM produced Ti6Al4V microstructure at different magnifications (Lekoadi *et al*., 2019).

A columnar shaped structure that grew in the direction of build was reported (Figure 2.11b). The columnar morphology was attributed to epitaxial growth of β-phase when newly formed layer partially re-melt previous layers (Eylon and Froes, 1990; Thijs *et al*., 2010; Song *et al*., 2012; Wu *et al*., 2016). The martensitic α'-lath then slowly grow in the columnar grain as the laser moves away across the powder bed (Rafi *et al*., 2013). This martensite α'-phase results in low ductility and anisotropy on the produced components (Vrancken *et al*., 2012; Simonelli *et al*., 2014; Sallica-Leva *et al*., 2018).

This is of major concern because the as-built microstructure is not the same as that of wrought Ti6Al4V components of the same composition. This implies that in the as-built condition, SLM produced sample are not ready for application. There are various measures that can be used to improve the microstructures which include thermomechanical processing or heat treatment. In actual fact, an improved microstructure with improved mechanical properties can be obtained by heat treating SLM processed Ti6Al4V components using appropriate heat treatment parameters.

2.4 Mechanical properties

Due to the acicular martensite α'-phase in the SLM as built condition; the mechanical properties are different from their wrought counterparts (Hrabe and Quinn, 2013; Tong *et al*., 2017). For instance, the as-built microstructure of SLM produced Ti6Al4V exhibit high tensile strengths with low ductility in some cases (Yan and Yu, 2015). Figure 2.12 shows elongation comparison of as-built Ti6Al4V components produced by different AM techniques adopted from a study by Yan and Yu, (2015).

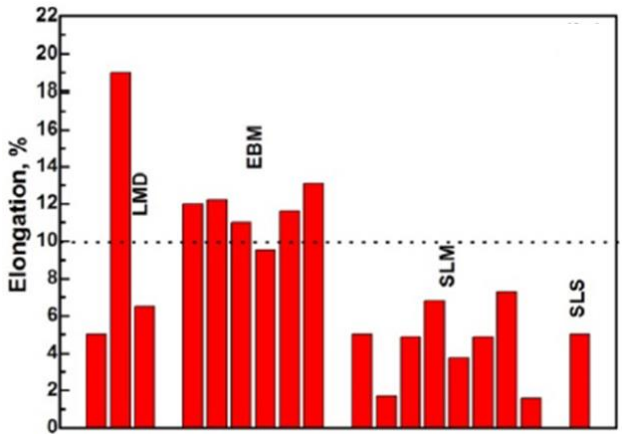


Figure 2.12: Elongation of Ti6Al4V components produced by different AM techniques (Yan and Yu, 2015).

The dotted line in Figure 2.12 represents benchmark elongation value of the corresponding ASTM F2924-14 specification. The ductility of SLM produced Ti6A4V component does not meet the standards since ASTM requires that elongation of the as built sample should not be lower than 10% (Qian *et al*., 2019). The hardness and strength of the as-built are greater than wrought and cast Ti6Al4V counterparts (Attar *et al*., 2014; Han *et al*., 2017). A study by Hrabe and Quinn (2013) observed lower UTS, YS and hardness in EBM fabricated components. The observation was also associated with the martensite α'-phase. These results also add evidence that SLM Ti6Al4V parts require post heat treatment to improve ductility as it was discussed in Section 2.3. Thus, it is important to heat treat the produced components in order to eliminate the martensite α'-phase for improvement of the microstructure.

2.5 Heat treatment

Heat treatment is defined as method of heating and cooling materials to change their material characteristic that makes them more desirable without changing the shape of the material (Leyens and Peters, 2003). Different heat treatments for AM Ti6Al4V components have been carried out by various authors. In other words, heat treatment is important to most of AM Ti6Al4V. Titanium is a highly reactive element at high temperatures; therefore, oxidation is a factor that must be considered during heat treatment of Ti6Al4V. When heat treating Ti6Al4V at temperatures above 427°C, a controlled atmosphere (using either inert gas or vacuum) must be used (Donachi, 2000).

Heat treatments alters the microstructure of SLM Ti6Al4V parts which allows for suitable achievement of their mechanical properties (Gong *et al*., 2014; Dong *et al*., 2017; Li *et al*., 2018). The behavioral relationship of Ti6Al4V alloy system is represented by a phase diagram. The phase diagram plays an important role in determining suitable heat treatment parameters for AM produced Ti6Al4V. Heat treatment of AM Ti6Al4V parts for different applications have been broadly studied with the aim of achieving homogeneous microstructures (microstructures with stable α + β phases), relieving of internal stresses and transforming the metastable martensite α'-phase (Wong and Hernandez, 2012; Zhai *et al*., 2016; Shipley *et al*., 2018). The three most important parameters that play a huge role in microstructural modification are temperature, cooling rate and residence time. However, heat treatment temperature is the most important parameter because cooling method and residence time also depends on the temperature used.

2.5.1 Phase transformations

An improved microstructure and mechanical properties can be achieved by understanding of Ti6Al4V phase transformations. Since Ti6Al4V alloy has two phases (α + β), its composition allows phase transformation to fully transform to β-phase upon heating but return to α + transformed/retained β upon cooling (refer to phase diagram in Figure 2.3). Phase transformation from the β-phase can undergo either diffusional or non-diffusional transformation. A transformation is considered diffusional if the β-phase is transformed into α + β phases and non-diffusional if the β-phase is transformed into martensite α'-phase. However, cooling rate determines the degree of diffusion. More on effect of cooling rate will be discussed in detail in section 2.5.4.

At temperatures within α + β region, Ti6Al4V is composed of α + β phases. Rearrangement of phases can be achieved through transformation of the phases from one phase to another during heat treatment. Table 2.3 presents possible transformations of Ti6Al4V that can take place during heat treatment.

Table 2.3: Phase transformations of Ti6Al4V (Seniawski *et al.*, 2013; Yan and Yu 2015).

Transformation	Temperature (°C)
Temperature of (α + β) → β	980
Temperature of α → β	750
Temperature of martensite phase transformation	780
Temperature of nucleation start (α + β) → β	890
Temperature of precipitation start (α + β) → β	930
Temperature of β → (α + β) start	950
Temperature of β → (α + β) finish	870

There are various phase transformations that SLM produced Ti6Al4V components go through during heat treatment. According to Yan and Yu (2015), martensite α'-phase transformation is reported as 650°C during heating, while α-phase transformation starts at 750°C as can be seen in Table 2.3. Furthermore, β transus temperature was defined as 980°C (Table 2.3). This implies that heating Ti6Al4V parts at temperatures lower than 650°C may not lead to any observable results. However, the low temperatures heat treatment may result in the relieving of residual stresses.

2.5.2 β-transus temperature

The β-transus is defined as transformation temperature of martensite α', α, and β phases transform to full β-phase. The emphasis of β-transus temperature together with the three phases is represented by a phase diagram. In addition, the β-transus separates the α + β region and the β region. Sallica-Leva *et al.* (2016) reported the β-transus as 970 ± 50°C. In contrast, a recent study by Qian *et al*. (2019) reported it as 996 ± 14°C. The β-transus temperature is critical and plays a very important role in heat treatments of Ti6Al4V. The difference in Al and V content

within Ti6Al4V alloy used by these two studies might be the factor that is responsible for the reported variation in β-transus (Shipley et al., 2018).

Other heat treatments are carried out below β-transus, called sub-transus heat treatment while others are performed above, known as super-transus heat treatment (Shipley *et al*., 2018). It was reported by Wood *et al*. (1998) that subjecting Ti6Al4V to thermomechanical processing (TMP) or sub-transus heat treatment may result in improved strength and ductility. It was further discussed that fracture toughness and fatigue crack growth resistance can be enhanced by TMP and super-transus heat treatment.

2.5.3 Effect of heat treatment temperature

As already mentioned, heat treatment of Ti6Al4V is separated into sub-transus and super-transus heat treatments. Roberts *et al*. (2009) reported that heat treating at temperature above the martensite α' start transformation result in elimination of the brittle, metastable martensite α'-phase. The same observation was supported by Wu *et al*. (2016) and Shipley *et al*. (2018) where no major change was observed after heat treatment at temperatures below 600°C. Furthermore, Lutjering *et al*. (1998) and Zhao *et al*. (2018) reported that annealing heat treatment at temperatures below 550°C results in precipitation of very fine $TiAl_3$ which promotes age hardening and embrittlement. Figure 2.13 shows a diagram that emphasise the formation of Ti_3Al and also shows the relationship between α and β phases with respect to temperature that was developed by Zhao *et al*. (2018).

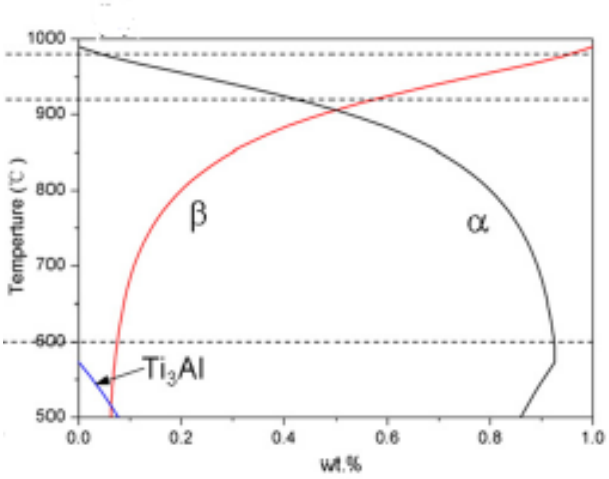


Figure 2.13: Illustration of phase fractions at elevated temperatures calculated by Thermo-Calc software (Zhao *et al*., 2018).

Heat treatment at low temperatures introduces $TiAl_3$ as presented in Figure 2.13. Performing heat treatment in the α + β region or even at higher temperatures higher result in transformation of α-phase and martensite α'-phase to fully β-phase. Heat treatment in the range 750-990°C degenerates the acicular martensitic by forming α-phase platelets with α-phase volume fraction decreasing as the heat treatment temperature increases (Shipley *et al*., 2018).

Super-transus heat treatment transforms the other phases to full β-phase but transforms back to α + β phases upon cooling. Shipley *et al*. (2018) showed that heat treating Ti6Al4V above 1000°C led to the original prior β grain transforming into large equiaxed β grains and that results in ductility improvement but with a slight decrease in tensile strength. In contrast, Sallica-Leva *et al*. (2016) discussed that annealing heat treatment above β-transus (super-transus) should be avoided due to excessive grain growth of the β-phase in this region. The graph in Figure 2.14 shows the behavior of ductility as the temperature is increased reported by other studies (Vilaro *et al*., 2011; Sallica-Leva *et al*., 2016; Vrancken *et al*., 2017).

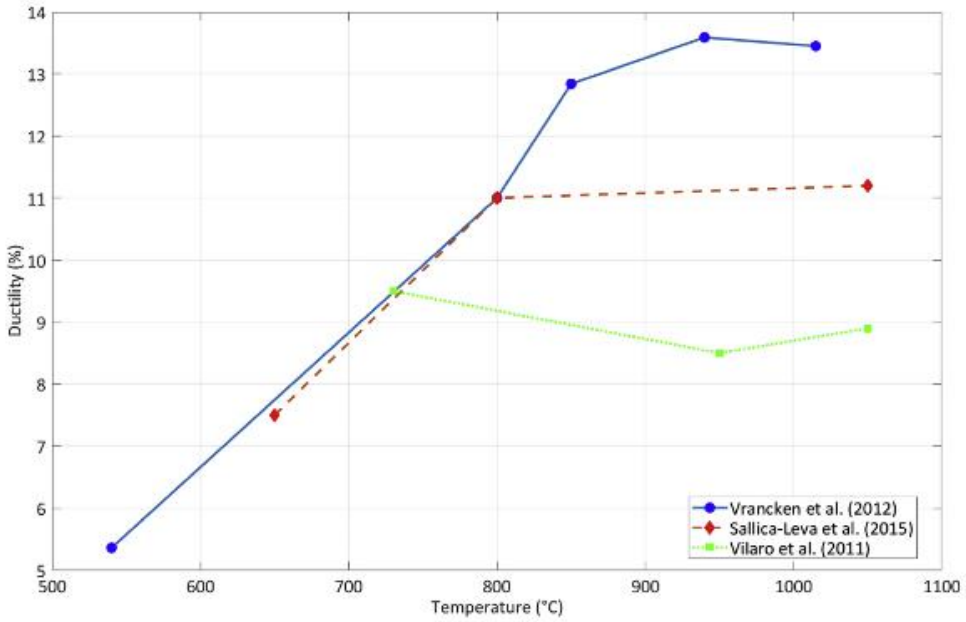


Figure 2.14: Relationship of heat treatment temperature and ductility (Shipley *et al*., 2018).

Sallica-Leva et al. (2015) observed that as temperature increases, ductility also increases until 800°C and then remained constant afterwards as presented by Figure 2.14. However, for the study conducted by Vilaro *et al*. (2011), ductility started decreasing at a temperature around 750°C. The most improvement in ductility of about 13.5% was obtained by Vrancken *et al*.

(2012) at temperature between 800°C and 1000°C. This observation was corresponded with that of Fan *et al*. (2011) who concluded that annealing heat treatment in the α + β region can improve the ductility of Ti6Al4V. Furthermore, Vrancken *et al*. (2012) observed an increase of β-phase as the temperature was increased. Conversely, a different observation was made on YS. The YS decreased as temperature increased (Vilaro *et al*., 2011; Vrancken *et al*., 2012). The findings in Figure 2.14 influences the methodology of the study influencing the selection of heat treatment parameter (temperature, residence time and cooling method) to use in order to obtain the desired improved microstructure in ductility. For example, both Vrancken *et al*. (2012) and Vilaro *et al*. (2011) performed heat treatment at 950°C but obtained different ductility values of ~13.5% and 8.5%, respectively, showing that proper selection of parameters can yield better results.

2.5.4 Effect of cooling rate

Different cooling methods do not give the same phase composition of titanium alloys (Seniawski *et al*., 2013). Semiatin *et al*. (2013) reported that cooling rate influence the arrangement of α and β phases on the microstructure of SLM Ti6Al4V parts. High cooling rates resulting from water quenching (WQ) and air cooling (AC) disturbs the thermodynamic path during heat treatment while low cooling rates resulting from furnace cooling (FC) provide equilibrium thermodynamic path (Ramosoe *et al*. 2010). In terms of diffusional and non-diffusional transformation, slow cooling rates allow complete diffusion to occur whereas fast cooling does not allow complete transformation. A Ti6Al4V continuous-cooling transformation (CCT) diagram can be used to understand the effect of cooling rate on microstructural formation. However, it was discussed by Galaragga *et al*. (2017) that the CCT diagram works better for super-transus heat treatments. This is because α-phase dominate at low temperatures, which result in microstructural evolution being minimal (Shipley *et al*., 2018). A CCT diagram of Ti6Al4V alloy is presented in Figure 2.15.

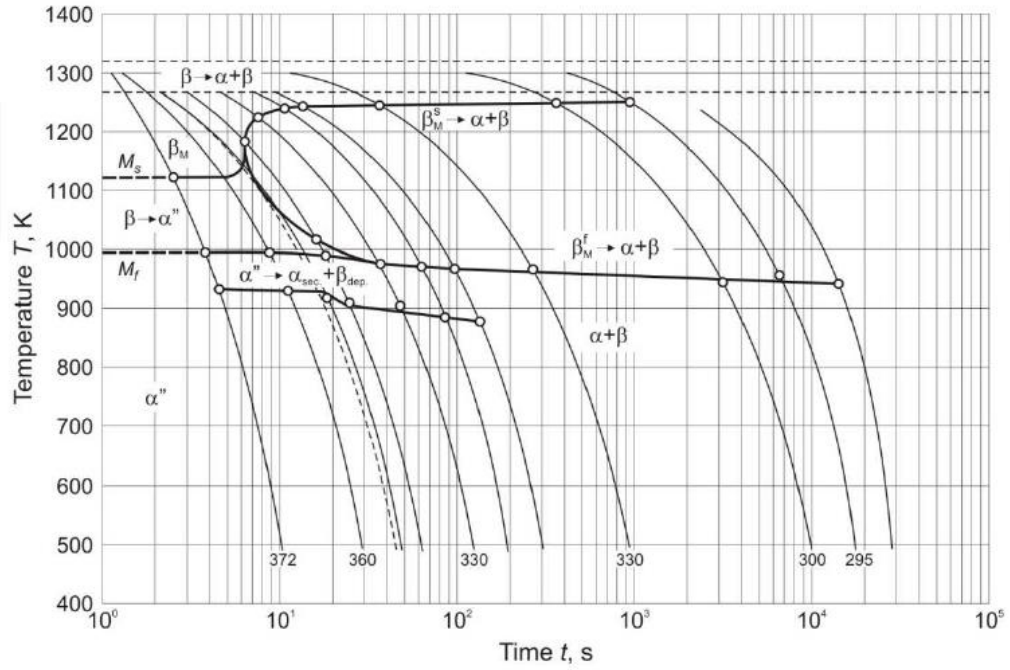


Figure 2.15: CCT diagram of Ti6Al4V (Seniawski *et al*., 2013).

Increasing the temperature leads to formation of more β-phase, therefore at high temperatures below and above β-transus, cooling rate determines the primary α-phase morphology (Lutjering, 1998; Gil *et al*., 2001). According to Lamirand *et al*. (2006) cooling rates below 10°C/min are considered slow cooling, those between 10-50°C/min are classified as medium cooling rates while those above 50°C/min are considered high cooling rates. The CCT diagram clearly shows that high cooling rates offered by WQ and AC produces a metastable martensitic α'-phase (or α'') from high temperatures above β-transus temperature. However, AC is likely to produce a secondary α-phase from the martensite α'-phase as presented in Figure 2.15. High cooling rates supports diffusionless transformation of β-phase into martensite α'-phase (β → α') and that result in increased hardness and brittleness of the whole structure (Gupta *et al*., 2018).

At low cooling rates (usually offered FC), a microstructure that composes α + β phases result without the formation of martensite α'-phase (Figure 2.15). This observation was supported by Shipley *et al*. (2018) by concluding that heat treatment in the α + β or β regions followed by FC produces a lamella α + β microstructure. On the study of the microstructure of TC21 titanium alloy, Shao *et al*. (2013) reported a diffusionless transformation of β-phase to martensite α'-phase resulting from WQ and β-phase into α + β phases after AC and FC. Table

2.4 demonstrate the effect of cooling rate on phase transformations adopted from Seniawski *et al*. (2013).

Table 2.4: Phase composition after control cooling from above β-transus temperature (Seniawski *et al*., 2013).

Cooling rate (°C/s)	Phase composition
48-18	α'' (α')
9	α + α' (α'')
7	α + α' (α'')
3.5	α + α' (α'') + β
1.2-0.04	α + β
0.024-0.004	α + β

Table 2.4 depict that different cooling rates produce different phase compositions. According to Leyens and Peters (2003), fast cooling can be used to obtain a very fine microstructure whereas slow cooling can be used to obtain a coarse lamella microstructure. Shipley *et al*. (2018) concluded that possible cooling methods to optimise mechanical properties are FC and AC in applications where the martensitic α'-phase is not required. Figure 2.16 shows the microstructures of samples that were heat treated at the same temperatures but cooled using FC and WQ.

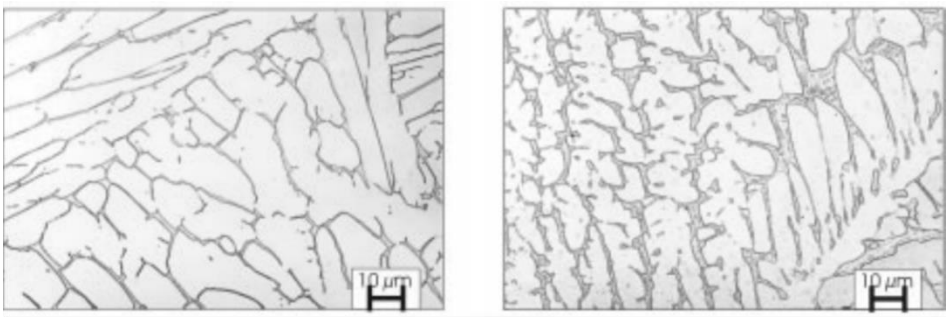


Figure 2.16: Ti6Al4V microstructures after heat treatment at 800°C (a) FC (b) WQ (Layens and Peters., 2003).

The clear observation that was made on these two microstructures is grain growth. The microstructure that resulted from FC sample (Figure 2.16a) showed larger α + β grains than the microstructure that resulted from WQ (Figure 2.16b) which was made-up of martensite α'-phase and α-phase. Similarly, Xu *et al*. (2015) reported formation of lamella and martensitic α'

microstructures at cooling rates in the ranges 15-90°C/s. In addition, Yan and Yu (2015) observed that cooling rate of 20°C/s is suitable for the formation of α-phase while cooling rates higher than 525°C/s produces a sharp acicular martensite α'-phase.

A globular type of microstructure is possible for heat treatments in the α + β region. Damkroger *et al*. (1994) reported that, increasing cooling rate promote nucleation of α-phase. The α-nucleation will result in the formation of α-platelets, with growing α-phase within β grain boundaries. Moreover, cooling rate determine the length and width of α-platelets. When the cooling rate is high, basket weave morphology is created. Finally, WQ from temperature above β-transus may result in partial or full transformation into martensite α'-phase.

2.5.5 Effect of residence time

Residence time also play a role in microstructural formation during heat treatment. Plaza *et al*. (1990) reported that Ti6Al4V samples that were heat treated at high temperatures consisted of α-phases which their size depended on residence time. Moreover, Vrancken *et al*. (2012) and Shipley *et al*. (2018) reported an increasing grain size as residence time was increased. Grain size is known to have an impact of mechanical properties (Plaza *et al*., 1990; Vrancken *et al*., 2012). Table 2.5 shows the relation between residence time and elongation.

Table 2.5: Relationship between residence time and elongation of Ti6Al4V components (Plaza *et al*., 1990).

Temperature (°C)	Residence time (hrs)	Elongation (%)
930	1	14.2
930	2	16.1
930	4	15.8
945	4	15.5
960	4	15.5

It can be seen from Table 2.5 that elongation increased as the residence time was increased to 2 hrs but decreased as the residence time was increased to 4 hrs at a temperature of 930°C. Vrancken *et al*. (2012) reported less impact of residence time after heat treatment was carried

out in the α + β region and this observation was attributed to the level of α-phase in this region. According to these authors, α-phase grows to a certain level which result in a high α-phase content and that consequently leads to hindering of β-phase growth. In contrast, Shipley *et al*. (2018) showed that the effect of residence time is noticeable for super-transus heat treatments.

Longer residence time leads to β grain size increase, which result in formation of bigger α-colonies (Vrancken *et al*., 2012). Grain coarsening depends mainly on the heating process. This implies that residence time for elevated temperatures eventually determines the size of the grain. Therefore, shorter residence times yields small grain sizes while longer residence time exhibit larger grains (Zuback and Debroy, 2018). Figure 2.17 demonstrate the effect of residence time on the Ti6Al4V microstructures.

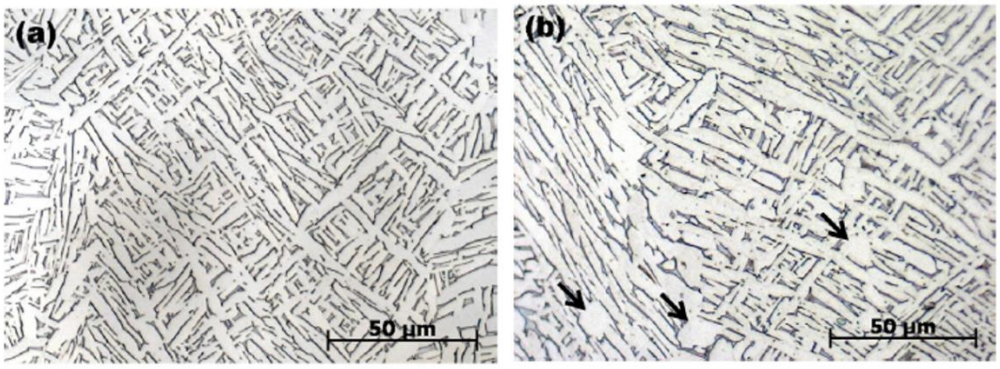


Figure 2.17: Ti6Al4V microstructures after heat treatment at 940°C for (a) 2 hrs, (b) 20 hrs (Vrancken *et al*., 2012).

The two residence times gave obvious different grain sizes. Heat treatment for 2 hr (Figure 2.17a) resulted in smaller size of lamella α + β phases, while heat treatment for 20 hrsresulted in bigger sizes of the lamella α + β phases (Figure 2.17b). Furthermore, the 20 hrs residence time revealed globular α-phases (indicated by arrows) in Figure 2.17(b) (Vrancken *et al*., 2012).

Grain size refinement is known to improve properties such as strength and hardness of Ti6Al4V (Zuback and Debroy, 2018). The Hall-Petch relation is the well-known equation that relates yield strength and grain size.

$$\sigma_y = \sigma_0 + \frac{ky}{\sqrt{d}} \qquad (2)$$

Where σ_y is the yield strength, *d* is the grain size, σ_0 and k_y are material constants that represent the yield strength of a grain free material and the strengthening coefficient, respectively (Zuback and Debroy, 2018). A recent study by Keist and Palmer (2017) compared the relationship between hardness and yield strength of PBF and DED of Ti6Al4V alloy. Figure 2.18 shows their relationship.

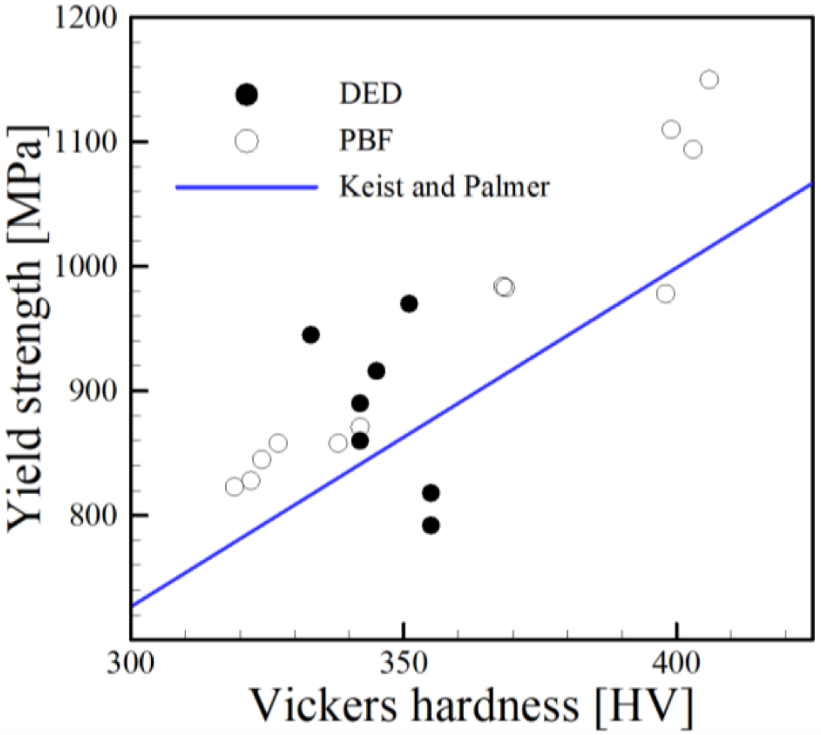


Figure 2.18: Relationship of hardness and yield strength of Ti6Al4V (Keist and Palmer, 2017).

It is clear from Figure 2.18 that these two AM methods yielded different results, with PBF showing higher strength and hardness compared to DED. The variation in these results is attributed to difference in grain sizes associated with these techniques. Although Ti6Al4V parts produced by both PBF and DED methods are characterized by columnar type of grains, PFB is characterized by smaller grains while DED is characterized by larger grains (Zuback and Debroy 2018), which account for the high and lower strength and hardness results observed for PBF and DED, respectively. The relationship observed for PBF graph in Figure 2.18 is that hardness increases with increase in yield strength. This implies that the Hall-Petch relation can be written as a relation of hardness (HV) and grain size (*d*).

$$HV = HV_0 + \frac{ky}{\sqrt{d}} \qquad (3)$$

Where HV_0 and ky are the material constants representing the hardness of a grain free material and hardening coefficient, respectively (Zuback and Debroy, 2018).

2.5.6 Stress relieving

Stress relieving is a type of heat treatment whereby a component is heat treated to a temperature at which the YS is sufficiently low to the point where internal stresses can relieve themselves. Most of AM techniques are associated with residual stress on the built components due to high temperature gradients. Knowles *et al*. (2012) showed that residual stresses in AM produced Ti6Al4V can be higher than 1000 MPa. These residual stresses strongly influence crack initiation and growth. Stress relieving eliminates undesirable residual stresses.

A study by Mercelis *et al*. (2006) has discussed that residual stresses have a negative effect on mechanical behaviour of SLM Ti6Al4V parts. Therefore, the built components need to be stress relieved in order to relieve residual stresses (Yan and Yu, 2015). Gong *et al*. (2012) has shown that Ti6Al4V can be stress relieved at 650°C for 2 hrs. The removal of these stresses helps in maintaining the shape stability of the produced component. In contrast, Donachie *et al*. (2000) recommended temperature and time range of 480-650°C for 1-4 hrs. Quenching must be avoided during stress relieve because the cooling rate need to be uniform.

2.5.7 Hot isostatic pressing

The HIP is a type of heat treatment which simultaneously applies high temperature and externally applied gas pressure (Tong *et al*., 2017; Qian *et al*., 2019). The HIP is widely used today to eliminate internal defects, specifically pores in metallic materials produced by AM techniques, specifically, powder bed fusion. As already discussed, porosity is a characteristic of the SLM process that acts as stress concentration and crack initiation point in the produced components which affect the performance of the component. The purpose of using high pressure is to reduce the amount of porosity (Qian *et al*., 2019). An example of the effect of HIP on pore closure is shown on the Ti6Al4V microstructures in Figure 2.19. The samples were produced with EBM and then HIPed at 800°C with pressure of 200 MPa.

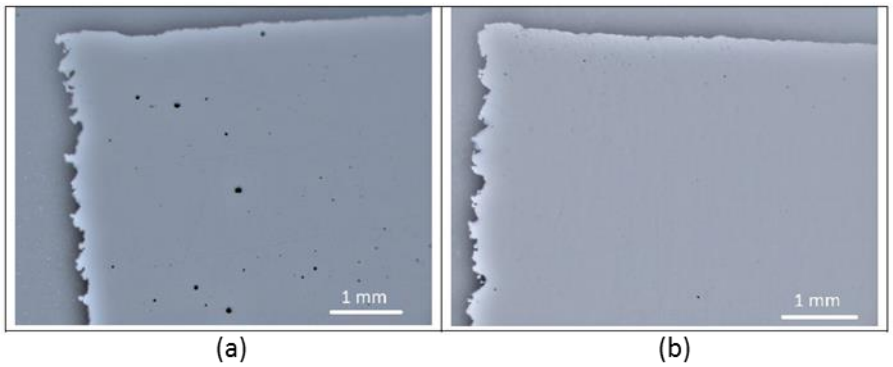


Figure 2.19: Ti6Al4V microstructures (a) As-built (b) HIPed (Eklund *et al*., 2018).

Clearly most of the pores were no longer observed after HIP (Figure 2.19b). ASTM standard F2924-14 for Ti6Al4V powder bed AM states a HIP temperature range of 895-955°C, minimum pressure of 100 MPa and minimum residence time of 2 hrs. Literature shows that HIP is typically performed at temperatures above 900°C for Ti6Al4V. HIP does not only have impact on porosity but can also influence the type of the microstructure produced. Qiu *et al*. (2013) reported that HIP at 900°C with 102 MPa for a period of 4 hrs close porosity on Ti6Al4V components and further transform the martensitic α' structure. Moreover, these authors also observed an improved ductility. A study by Mower *et al*. (2016) reported increased α-lath thickness on HIPed Ti6Al4V components at 900°C at 102 MPa pressure for 2 hrs.

In other instances, Facchini *et al*. (2009) observed coarse microstructure HIPed components and also observed a decrease in strength accompanied by increased ductility. According to these authors, HIP improves the ductility of SLM produced components but leads to reduction in strength. Eklund *et al*. (2018) discussed that HIP of EBM and SLM produced Ti6Al4V eliminate these defects and results in ductility and fatigue properties of the components.

With suitable processing and heat treatment parameters, various types of microstructure ranging from lamella to bimodal can be achieved. Most importantly, the properties of Ti6Al4V alloy depends on the arrangement of α and β phases which determine microstructure. The types of Ti6Al4V microstructures that can be achieved through heat treatment are discussed in detail in Section 2.6.

2.6 Possible microstructure after heat treatment

2.6.1 Fully martensitic α' microstructure

Although a fully martensitic α' microstructure is obtained after the SLM process, a fully martensitic α' can be formed after heat treatment. The determination factors are parameters, especially cooling method. Figure 2.20 shows fully martensitic α' microstructures that were obtained by Wu *et al*. (2016) after sub-transus and super-transus heat treatment.

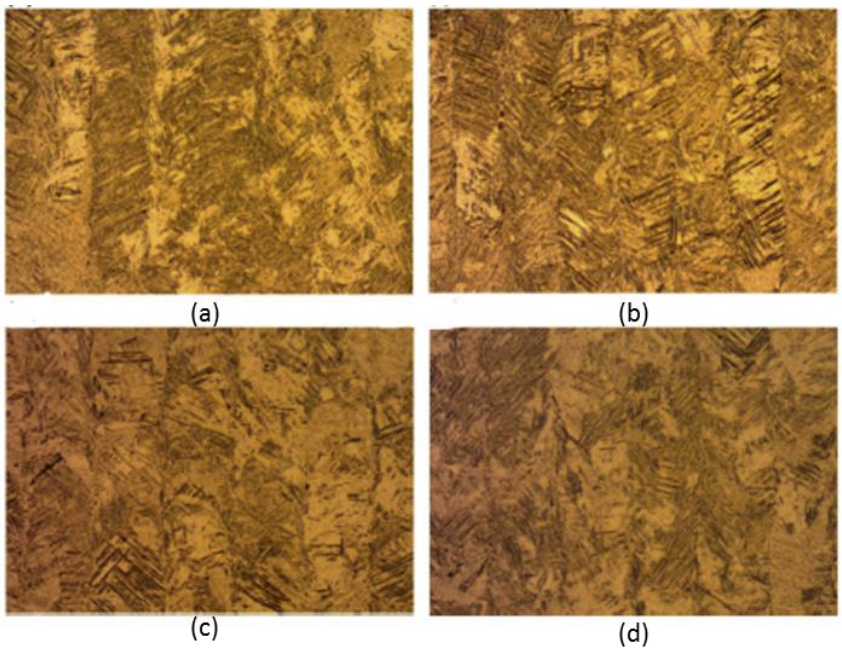


Figure 2.20: Ti6Al4V microstructures after heat treatment for 2 hrs followed by WQ (a) 800°C (b) 840°C (c) 875°C and 900°C (Wu *et al*., 2016).

Figure 2.20 evidently shows fully martensitic α' microstructures that resulted from WQ after heat treating at various temperatures. The main parameter that leads to the production of a fully martensitic α' microstructure is cooling by WQ and sometimes AC (Wu *et al*., 2016). It is expected that the acicular martensite α'-phase will transform into stable β-phase as temperature increases, but WQ introduced the martensitic α'-phase because it is regarded as fast cooling. It was shown by Wu *et al*. (2016) and Ter Haar and Becker (2018) that WQ from sub-transus heat treatment introduces weave type of acicular martensite α' microstructure. It should however be noted that the martensitic α' microstructure is not desired in the aerospace industry and other industries because it is associated with low ductility and high residual stresses.

2.6.2 Fully Lamella microstructure

Heat treatment of Ti6Al4V parts can produce is a fully lamella microstructure. A lamella microstructure is categorized as a microstructure that consists of alternating plates of α and β phases. Figure 2.21 shows a schematic diagram and optical image of examples of fully lamella microstructures.

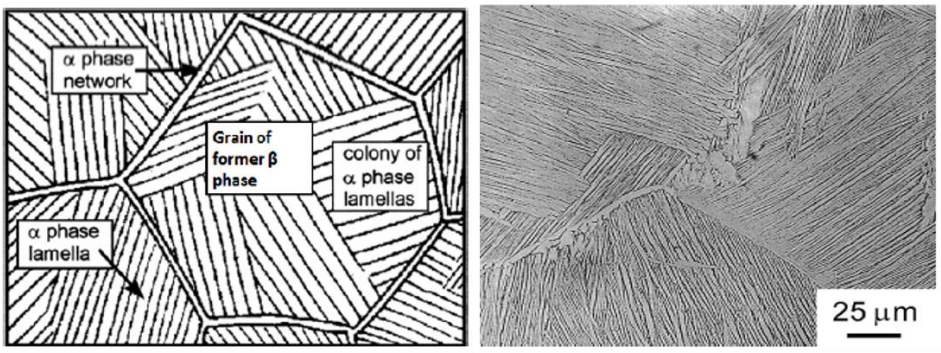


Figure 2.21: Ti6Al4V lamella microstructures (a) schematic diagram (Chraponiski and Szkliniarz, 2001), (b) Optical image (Nalla *et al*., 2002).

Figure 2.21(a) depict a network of α-phase separates the lamella grains. The separation of α-grains is clearly visible in a lamella structure. Heat treating Ti6Al4V above β-transus temperatures can form a lamella microstructure, that is characterized by ductility improvement without affecting the YS of Ti6Al4V components (Lutjering, 1998). This improvement in ductility is attributed to the arrangement of β-phase within the lamella structure that promote slip transfer between the α + β phases (Simonelli *et al*., 2014). According to these authors, the slip transfer that happens between α and β phases result in increased dislocation movement, which results in increased ductility.

The morphology of lamella microstructure depends mostly on the cooling rate. In fact, the α-phase plate width decreases to about 0.5 μm from 100 μm in slowly cooled materials (Lutjering and William, 2007). The lamella microstructure in Figure 2.21(b) resulted from sufficient low cooling from super-transus heat treatment, that formed a mixture of α + β phases (Lutjering and William, 2007).

2.6.3 Equiaxed microstructure

An equiaxed microstructure (also known as globular) is defined as one that is made up of globular α-phase spread along β-phase matrix (Lutjering 1998; Seniawski *et al*., 2013). A fully equiaxed microstructure is shown in Figure 2.22.

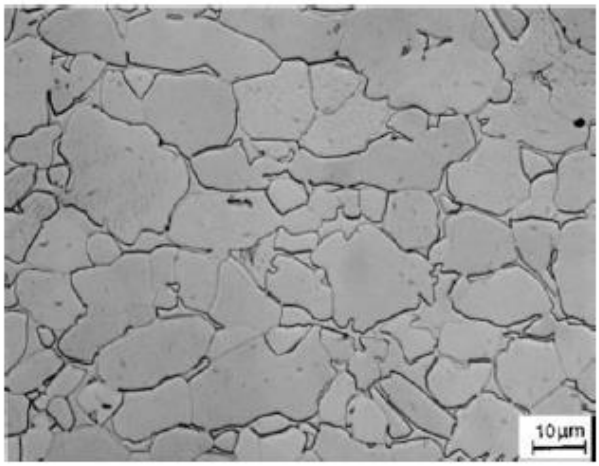


Figure 2.22: A fully equiaxed Ti6Al4V microstructure (Ivanova *et al*., 2002).

Zhao *et al*. (2018) revealed that an equiaxed α + β microstructure obtains superior ductility. In addition, Seniawski *et al*. (2013) showed that an equiaxed microstructure is characterized by an improved balance between strength and ductility. Furthermore, a sequence of TMP can globularize and deform the α-lamellae and form equiaxed microstructure (Gao *et al*., 2017; Roy *et al*. 2017). In contrast, Seniawski *et al*. (2013) showed that heat treating Ti6Al4V higher in the α + β region can produce an equiaxed microstructure.

2.6.4 Bimodal microstructure

Poodla *et al*. (2009) reported that a bimodal microstructure (also known as duplex microstructure) is known to offer an advantage in terms of YS, UTS, fatigue resistance and ductility. In other words, bimodal microstructure offers an advantageous balance of mechanical properties. A study by Sabban *et al*. (2017) has shown that bimodal microstructure improves the ductility and toughness of AM produced Ti6Al4V alloy by 80% and 66%, respectively. Examples of optical and SEM images of bimodal microstructures are depicted in Figure 2.23.

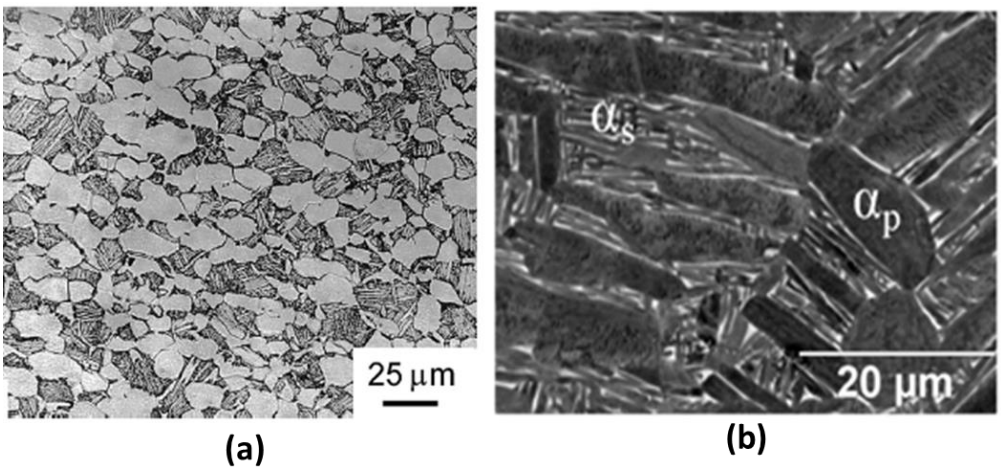


Figure 2.23: Ti6Al4V bimodal microstructures (a) Optical micrograph (Nalla *et al*., 2002), (b) BSD-SE micrograph (Ter Haar *et al*., 2018).

A bimodal microstructure consists of equiaxed primary α-phase (α_p) in a matrix of lamella α (α_s + β phases (Nalla *et al*., 2002, Ter Haar and Becker. 2018). The α_p does not transform during heat treatment as opposed to α-phase that forms due to transformation from the β-phase.

There are various studies that already managed to produce bimodal microstructure using heat treatment. Most of these studies used duplex heat treatment strategies, though there are others that used more than double strategies. For example, Nalla *et al*. (2002) and a recent study by Ter Haar and Becker (2018) both used duplex heat treatment strategies to achieve bimodal microstructures. In the case of Nalla *et al*. (2002), heat treatment at 925°C for 1 hr followed by air cooling was used. The AC samples were subsequently heat treatet at 700°C for 2 hrs as the second treatment strategy. In the case of Ter Haar and Becker (2018), heat treatment at 910°C for 8 hrs and cooling by WQ was carried out. Stress relieving at 700°C for 4 hrs was carried out as the second strategy. The use of the first high temperature annealing strategy is to produce globularized α-phase (Zhao *et al*., 2018; Ter Haar and Becker 2018) while the second low strategy transformed the β-phase into lamella α + β phases, resulting in the production of a bimodal microstructure.

It was recently reported by Zhao *et al*. (2018) that a triple strategy can also be used to produce a bimodal microstructure. The summary of the triple heat treatment strategy used by Zhao *et al*. (2018) is presented in Figure 2.24.

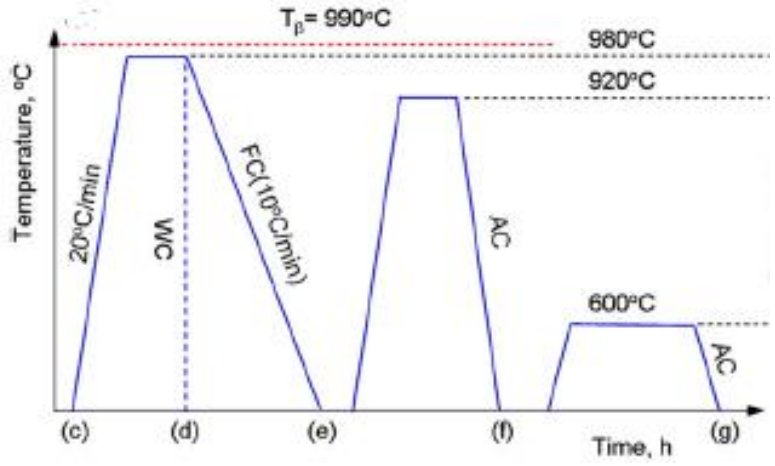


Figure 2.24: Illustration of triple heat treatment strategy (Zhao *et al*., 2018).

These authors came to a conclusion that annealing at 980°C for 1 hr, followed by solution treatment at 920°C for 1 hr, and lastly aging at 600°C for 4 hrs, cooling by AC achieves a bimodal microstructure as presented by Figure 2.24.

As already mentioned, this study aimed at producing a bimodal microstructure by using a single heat treatment strategy. Single heat treatment strategy is preferred over other strategies due to its benefit of time and energy savings. According to the author's knowledge, there is no study that managed to produce a bimodal microstructure using only a single strategy. However, a recent study by Sabban *et al*. (2019) managed to produce a bimodal microstructure by using several cyclic heat treatments. The strategy that was used by Sabban *et al*. (2019) is presented in Figure 2.25.

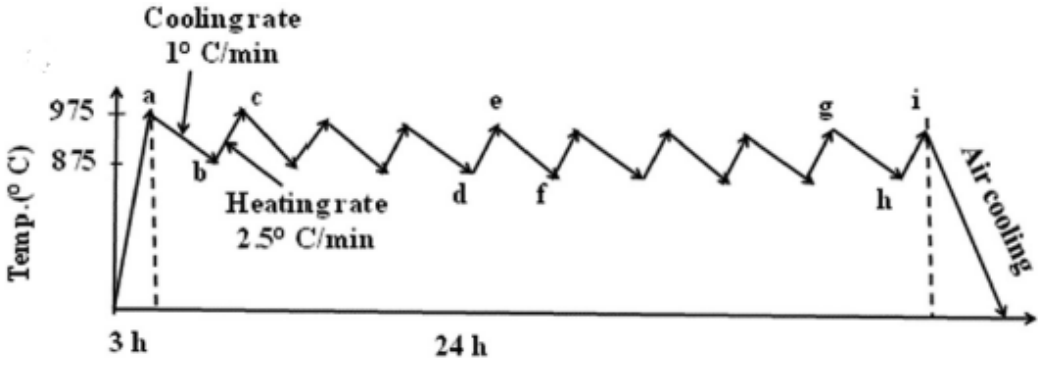


Figure 2.25: Illustration of cycling heat treatment (Sabban *et al*., 2019).

The heating and cooling cycles were performed using sub-transus heat treatments between 975°C and 875°C, taking advantage of the important phase change between these temperature range. This temperature ranges enable diffusion and thereby rapid transformation. The circles were repeated 18 times for 24 hrs to allow formation of globular α-phase while cooling at 1°C/min throughout, leading a bimodal microstructure. This bimodal microstructure significantly improved the ductility to 25% in comparison to maximum reported 12% of SLM produced Ti6Al4V with a slight decrease in strength (Sabban *et al*., 2019).

2.7 Summary of Chapter 2

This chapter has evaluated effect of processing history on microstructural and mechanical properties of Ti6Al4V produced via AM. The evaluation gave a clear understanding of the starting microstructure before heat treatment is applied. It was discussed that AM produced Ti6Al4V microstructures do not meet the required ASTM standards and therefore requires post heat treatment. The manipulation of heat treatment temperature, cooling method and residence time to obtain various types of microstructures on SLM produced Ti6Al4V was also successfully discussed. This chapter also showed that bimodal microstructure can form in different ways depending on the heat treatment parameters.

Chapter 3 : Experimental Procedure

This chapter gives a full description on the materials and methodological steps that were developed to accomplish the objectives of this study. A detailed report of the equipment and facilities that were used together with their respective locations are also reported. The characterization of the Ti6Al4V powder used in this study is also reported.

3.1. Materials

Spherical Grade 5, pre-alloyed Ti6Al4V powder with particle size distribution in the range of 20-60 µm was used as the deposition material during the production of the test samples. The powder was produced and supplied by TLS Technik GmbH & Co from Germany and was used in its as received form. The samples were produced on a Ti6Al4V base plate substrate of dimensions 320 mm × 340 mm × 30 mm.

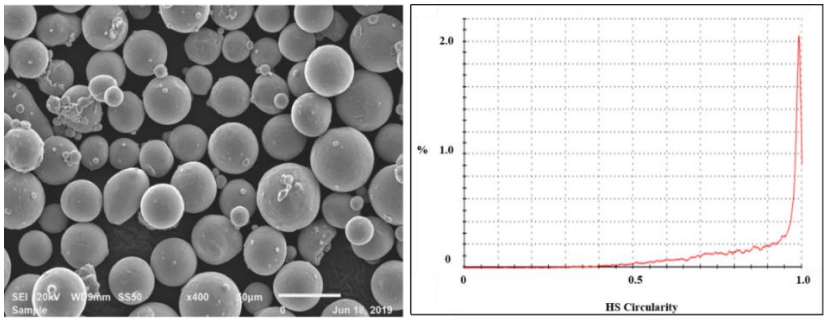
3.2. Powder Characterization

Particle analysis of the Ti6Al4V powder was conducted at the University of North West (Potchefstroom Campus). A Malvern PANalytical G3 advanced particle characterization machine (RAMANXRN System) was used for the measurement of particles shape and size from 0.5 µm to several millimetres. A Joel JSM-6010PLUS/LA Scanning Electron Microscope (SEM) was used to study particle morphology.

3.2.1. Powder analysis

Powder characterisation of Ti6Al4V was conducted before manufacturing of the samples for identifying and quantifying particles size and also to verify the specifications given by the supplier. Moreover, powder characterization was also conducted to investigate if there was porosity on the powder particles which may affect the quality of the produced coupons.

The SEM and high sensitive (HS) circularity (the measurement of the closeness to a perfect circle) were used to analyze the morphology of the powder. Figure 3.1 shows SEM image and shape distribution curve measured on more than 7225 particles of Ti6Al4V powder.

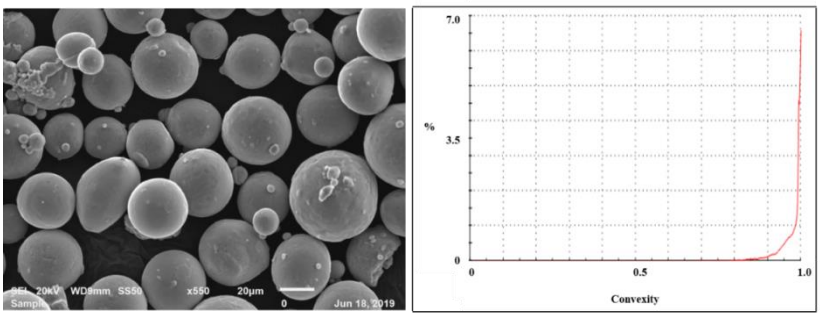


(a) (b)

Figure 3.1: Powder morphology of the Ti6Al4V powder (a) SEM-SEI image, (b) HS circularity curve.

The Ti6Al4V powder was made of spherically shaped particles as presented by Figure 3.1(a). Similar observation of spherical particles of Ti6Al4V powder were reported in literature (Yadroitsev *et al*., 2014; Wu *et al*., 2016; Zhao *et al*., 2016; He *et al*., 2019). The shape distribution curve in Figure 3.1(b) confirms the observation by indicating a high percentage peak at 1.0 HS circularity. A perfect circle must have a HS circularity of 1. The minimum and maximum HS circularity of Ti6Al4V powder particles were found to be 0.1 and 1.0, respectively, suggesting that some of the powder particles were not perfectly spherical but most were perfectly spherical. The powder had particle size of 30-100 µm. Particle size within this range was reported in other studies (Wu *et al*., 2016; He *et al*., 2019). The supplier gave particle size distribution in the range 20-60 µm.

Figure 3.2 shows powder morphology image and convexity curve of the powder measured over 10104 particles. Particle convexity is defined as the measurement of the surface roughness of the powder particles.



(a) (b)

Figure 3.2: Convexity of the Ti6Al4V powder (a) SEM-SEI image, (b) Convexity curve.

The powder particles were smooth as presented in Figure 3.2(a). Similarly, smooth Ti6Al4V powder particles were reported by He *et al*. (2019). However, some of the particles were not perfectly smooth. The mean convexity of the powder particles was found to be 0.973. The results complemented the observation made in Figure 3.2(a) which showed that most of the particles were smooth. A smooth spherical particle is expected to have a convexity of 1. The minimum and maximum convexity values were measured to be 0.7 and 1.0, respectively. It must be noted that spherical and smooth surfaced powder is desirable for the SLM process because it contributes to powder flowability, packing density and thermal conductivity, which affects the properties of the produced part (Shipley *et al*., 2018).

3.3. Sample production

The Ti6Al4V rod samples with diameter and length of 1.5 cm and 8 cm, respectively, were produced from the SLM Aeroswift^{TM} 3D printing machine using optimized process parameters. Due to the confidentiality of this work, the optimized process parameters used were not disclosed. The process parameters were previously optimized to obtain fully dense components. It should be noted that the machine uses a PBF method. The image of the Aeroswift^{TM} machine is depicted in Figure 3.3.



Figure 3.3: Aeroswift^{TM} 3D printing machine available at CSIR, Pretoria.

Aeroswift^{TM} 3D printing machine has a build volume of 2000 mm × 600 mm × 600 mm. The system uses a high-power single fiber Ytteribium laser mode 5 kW, with wavelength of 1076 nm. Before the samples were printed, the oxygen content inside the chamber was reduced to 300 ppm by purging an inert argon gas to prevent oxidation. Moreover, the base plate was heat treated to 200°C in order to reduce building up of thermal stresses.

Before the commencement of the printing process, moisture was removed from Ti6Al4V powder by drying the powder at a temperature of 120°C for 4 hrs in an oven. Printed samples were removed from the base plate using a titanium cutting plate and subjected to heat treatment.

3.4. Heat treatment design

Two different furnaces were used for heat treatment. The first furnace was a horizontal column tube furnace, and the second furnace was a vertical tube furnace. Both furnaces were operated under argon atmosphere. The reason for using two different furnaces was that the horizontal tube furnace allowed only one method of cooling which was furnace cooling (FC), while the vertical tube furnace allowed for air cooling (AC) and water quenching (WQ). The image of the horizontal tube furnace is shown in Figure 3.4.

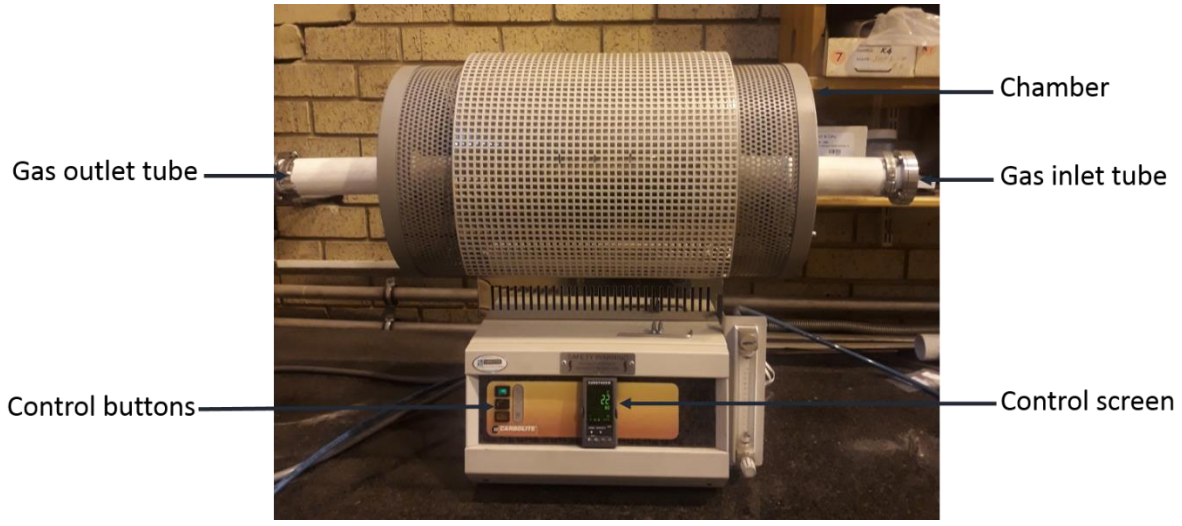


Figure 3.4: Horizontal heat treatment furnace available at the CSIR.

A STF 16/180 Carbolite furnace with length of 50 mm and internal tube diameter of 1 m was used as horizontal furnace. The furnace was manufactured by Parson Lane in England and was capable of heat-treating samples up to maximum temperature of 1600°C. To avoid samples

from oxidizing during heat treatment the furnace was flooded with argon gas continuously. The experiments were carried out once the oxygen content inside the furnace was lower than 100 ppm. Before heat treatment, the argon gas was continuously purged at a gas flow rate of 2 liters per minute to maintain the 100 ppm oxygen content.

The furnace was set to a constant heating rate of 10°C/min for all heat treatments. The furnace was equipped with a K-type thermocouple which measured and monitored the inside temperature. Samples were placed inside graphite crucible before they were placed inside the furnace.

Figure 3.5 shows the image of the other furnace that was used, which was a vertical tube furnace.

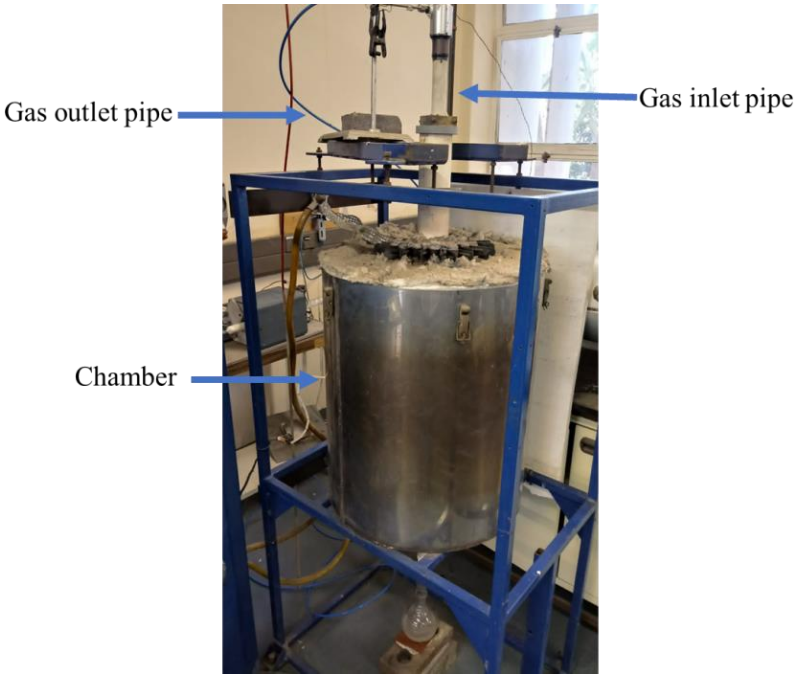


Figure 3.5: Vertical heat treatment furnace available at Pretoria University.

A Lenton LFT 15 model furnace with length of approximately 55 mm and internal tube diameter of 1 m was used for the vertical furnace. The furnace was manufactured by Lenton Company and capable of heat-treating samples up to 1500°C. Similarly, the oxygen content inside the furnace was dropped to 200 ppm by purging with argon. The argon was then continuously purged at a flow rate of 0.8 liters per minute. The furnace was constantly operated at heating rate of 4°C/min for all the heat treatments in the range 700-1000°C. The samples

were held with a thin wire for support. This vertical furnace also uses a K-type thermocouple which measure and monitor the temperature inside the chamber during heat treatment.

3.5. Heat treatment

During heat treatment, three heat treatment parameters which are temperature, cooling methods and residence time were varied. These heat treatment parameters were varied in order to obtain optimized parameters.

3.5.1. Optimizing heat treatment temperature

Temperature was the first parameter that was evaluated. Several small samples, of 10 mm × 7 mm dimensions, were cut out from the rod sample and were taken for heat treatment under different temperatures. The samples were placed inside a ceramic crucible, before they were placed inside the tube furnace. The samples were heat treated to temperatures of 700°C, 950°C and 1000°C, respectively. A residence time of 2 hrs was used. The samples were then furnace cooled. Furnace cooling was obtained by switching off the furnace after heat treatment and allowing the samples to cool inside the furnace. The samples were removed from the furnace when the furnace was at room temperature.

3.5.2. Optimizing cooling method

The second study focused on achieving optimized cooling method. The aim was to obtain a cooling method that achieves a mixture of primary and secondary α-phase, so as to achieve a bimodal microstructure. Heat treatment was carried out at 1000°C, for residence time of 2 hrs, and then cooled using three different cooling methods, namely, WQ, AC and FC. The WQ was attained by immersing the samples inside tap water that was at a temperature of 25°C; AC was obtained by cooling the sample in air at room temperature, while FC was obtained by switching off the furnace and allowing the samples to cool inside the furnace.

3.5.3. Optimizing residence time

The study mainly focused on the optimization of residence/holding time. Samples were heat treated to 1000°C, using various residence times of 15 min, 30 min, 1 hr, 2 hrs, 4 hrs, and 8 hrs, respectively and then cooled using FC method.

3.6. Characterization of samples

3.6.1. Metallographic sample preparation

The as-received rod sample was cut into smaller samples for preparation and characterization. A Struers Labotom-5 cutting machine was used to cut the sample using a Struers high quality titanium cutoff wheel (20S25). The cutting machine was an abrasive machine that used a rotating disc and water as coolant. The coolant protected the samples against thermal and mechanical damage.

Mounting of the as-received and heat-treated samples was conducted on AMP 50 automatic mounting press machine in order to obtain required size and shape for analyses. An Aka Resin Phenolic SEM black conductive resin was used to mount all samples. Mounted samples were mechanically grinded with Struers Tegrapol-25 grinding and polishing machine. Silicon carbide (SiC) grinding papers from grit size 80, 320, 1200 to 4000 were used for grinding the samples. Polishing of the samples was conducted with Daipro MD-Mol 3 µm diamond suspension for 3 min and colloidal silica 0.04 µm OP-S suspension for a period of 3 min as the final polishing stage.

Cleaning of polished samples was prepared with a soap suspension, rinsed and dried in ethanol for metallographic observations. Samples were etched in Kroll's reagents, a solution containing, 100 mL H_2O, 1-3 mL HF and 2-6 mL HNO_3, to reveal the microstructure of the samples. The etching time used for all sample was between 10-15 s.

3.6.2. Microstructural analyses

The metallographically prepared and etched samples were characterized for microstructural characteristics, defects, phases, grain and grain sizes, and chemical composition using an Olympus BX51M Optical microscope (OM) and Joel JSM-6010PLUS/LA Scanning Electron

Microscope (SEM) available at CSIR NLC. To obtain overview of the whole samples, microstructural images were taken at various position using magnifications of 5X, 10X, 20X and 50X.

3.6.3. Hardness measurements

Hardness measurements were measured using Matsuzawa Seiko Vickers model MHT-1 micro-hardness automatic indentation machine that is available at CSIR NLC. The hardness testing machine that was used is shown in Figure 3.6.

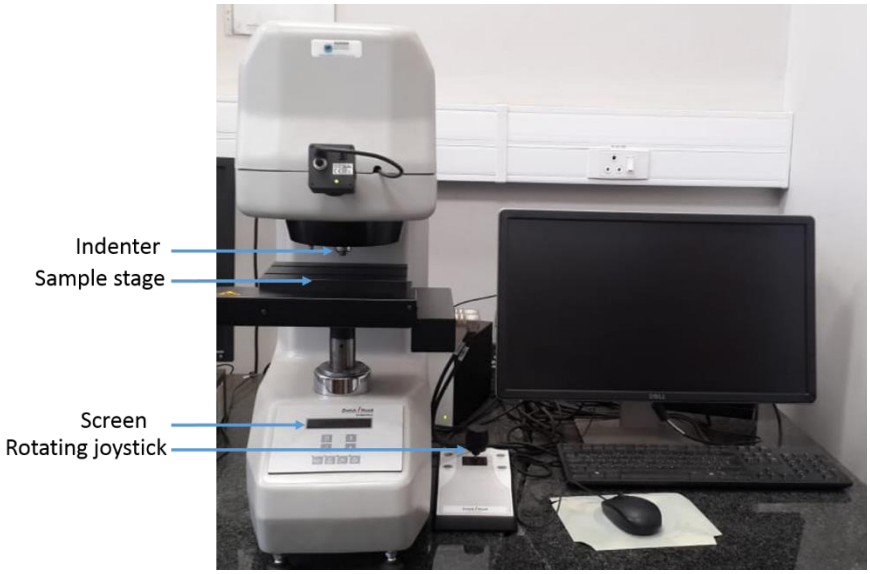


Figure 3.6: Micro-hardness testing machine available CSIR NLC.

All hardness measurements were performed using a diamond-shaped type of indenter. The measurements were done by applying a load of 0.3 kgf and dwell time of 10 s. The depth spacing was set as 300 µm, at 10X magnification. Indentation measurements were taken in the middle of the samples, parallel to the z-axis. Three hardness patterns were measured on each sample and the average of the measurement was calculated as hardness of the material.

3.6.4. X-ray micro-computer tomography scan (micro-CT-scan)

Porosity measurements and analysis were conducted using General Electric Phoenix VITome[X L240] X-ray micro-computer tomography scan (micro-CT scan). The micro-CT scan was performed at Stellenbosch University before heat treatment was carried out.

Characterization using this technique was only applied to the sample that was heat treated using optimized process parameters. During measurements, the scanning current and voltage were set to 80 µA and 160 kV, respectively. A maximum of 1600 images were generated in a single rotation. Copper filters of 0.5 mm and scan resolution of 30 µm were used for minimizing beam hardening.

3.6.5. Tensile testing

All the tensile specimens were machined at M & H Engineering in Pretoria according to ASTM E8-E8M standard. The machining process was prepared by machining of rod samples to standard dimensions into a dog bone shape (Figure 3.7). All dimensions were in mm.

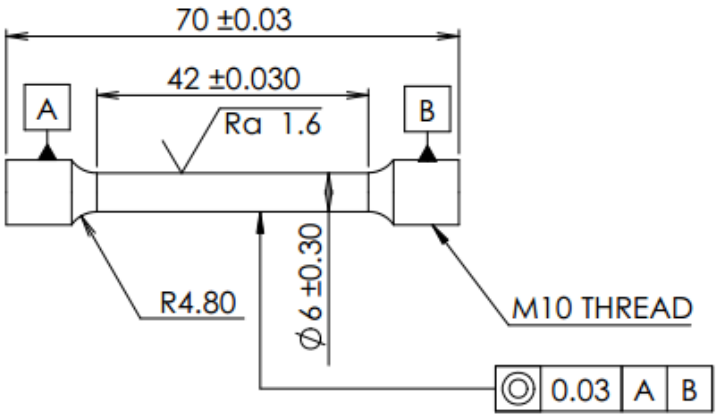


Figure 3.7: Schematic diagram of a tensile sample.

The Ti6Al4V samples were machined and prepared before they were taken for heat treatment. Tensile tests were performed at the CSIR Material Testing Laboratory on an Instron^{TM} 1342 tensile testing machine at constant crosshead 0f 0.5 mm/min. During testing, strain measurement was done by attaching the extensometer to the gauge section on the test specimen. The extensometer was removed at a strain of 5% to prevent damage during specimen fracture. The tensile extension was also recorded by using Linear Variable Differential Transform (LVDT) gauge. Three samples of each heat treatment temperature were tested for tensile properties.

3.7. Summary of Chapter 3

It was important to identify materials and also develop methodological steps that will be used to achieve the objectives of this study. This chapter has demonstrated the development of the experimental procedure and identified the equipment and facilities together with their respective locations. The heat treatment procedure was developed and discussed in this chapter. Moreover, selection heat treatment parameter together with their strategies for improving the microstructure of the SLM Ti6Al4V coupons was the main focus. Moreover, the capability of OM and SEM to reveal the phases, grain size and morphology makes it easier to link the microstructures with their hardness and tensile properties plays an important role for this study.

Chapter 4 : Heat treatment for process development

This chapter present the analyses of results and discussions obtained from heat treatment for process development. Heat treatment optimisation was very important for this study, therefore analyses of the results before selecting parameters for carrying out heat treatment experiment to achieve a bimodal microstructure is reported. The evaluation of microstructures and hardness properties after heat treatment was the main focus. Figure 4.1 shows three rod samples that were produced and used for heat treatment optimisation.

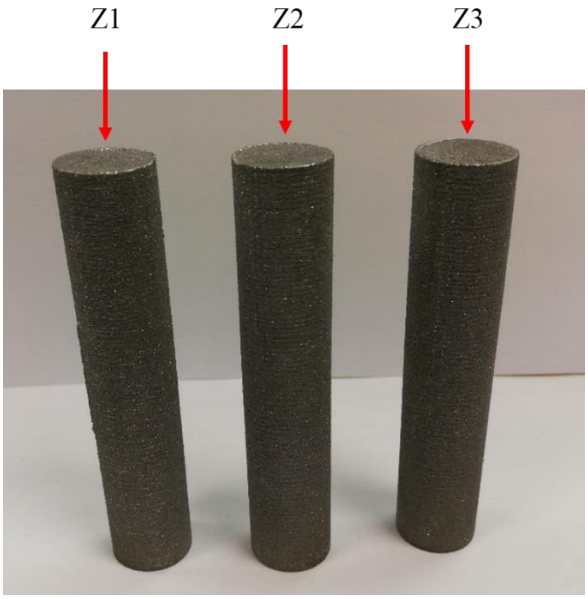


Figure 4.1: High speed SLM produced Ti6Al4V rod samples.

The samples that were produced with same process parameters were labelled Z1, Z2 and Z3 for identification purposes as indicated in Figure 4.1. These rod samples had the same diameter and length of 1.5 cm and 8 cm, respectively. The three samples were cut into small pieces for heat treatment experiments. Other samples were heat treated in an argon rich atmosphere using the horizontal tube furnace while others were heat treated in the vertical furnace to study the effect of different cooling methods. Three heat treatment parameters that were extensively studied are temperature, cooling method and residence time. The microstructure and hardness results are reported in the next section.

4.1. Process development for heat treatment optimisation

Temperature optimisation on the Ti6Al4V samples was studied by heat treating samples at different temperatures (700°C, 950°C and 1000°C) and residence time of 2 hrs followed by FC. The microstructural and hardness properties of the samples are reported next.

4.1.1. Microstructures of the samples after heat treatment

Figure 4.2 shows the microstructures of the as-received and the heat-treated samples. The images were taken at the same position for all the samples using same magnification for comparison purpose.

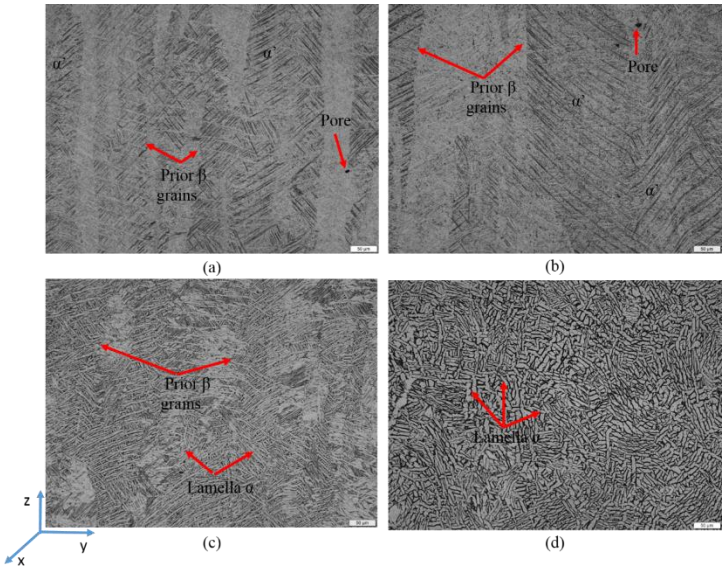


Figure 4.2: Microstructures of the sample after heat treatment at different temperatures (a) as-received, (b) 700°C, (c) 950°C and (d) 1000°C.

The microstructural defects that were observed on the as-received microstructure were spherical pores as presented in Figure 4.2(a). These types of pores are common to SLM produced Ti6Al4V samples (Murr *et al*., 2009; Zhao *et al*., 2016; Shipley *et al*., 2018; Zhang *et al*., 2018). The spherical pores are due to gas entrapment in the melt pool during SLM processing (Zhao *et al*., 2016; Shipley *et al*., 2018). Proper adjustment of processing parameters can lead to minimal porosity. According to a study by Shipley *et al*. (2018), porosity on SLM produced Ti6Al4V is caused by non-optimal process parameters during production of the samples.

The as-received microstructure also showed large columnar prior β grains that were orientated parallel to the z-axis which was the build direction as shown in Figure 4.2(a). The columnar prior β grains are known to be the fingerprint of SLM produced Ti6Al4V samples (Zhang *et al*., 2018; Chicos *et al*., 2019). The large columnar prior β grains resulted from partial re-melting of previous layers during the SLM process (Vilaro *et al*., 2011; Algius *et al*., 2018). In other words, during scanning of the powder by the laser beam, automatic remelting of top columnar grain behaves as a nucleating site for the epitaxial growth. The melt pool remains liquid for a certain time, before the sample solidifies, which results in epitaxial growth of the prior β grain, depending on the solidification rate (Vilaro *et al*., 2011, Zhang *et al*., 2018).

Inside these large columnar prior β grains, a fine single acicular needle-like martensitic α'-phase was observed as seen from Figure 4.2(a). According to Tiferet *et al*. (2016), during SLM processing, the acicular martensite α'-phase grows spontaneously to a specific width along a given direction ordered by specific Burgers relation guided by the other phases. Burgers relation is described as one in which both α (hcp) and β (bcc) phases share the same closest plane (Zheng *et al*., 2018). This type of microstructure was similar to the one reported by various authors (Qiu *et al*., 2013; Simonelli *et al*., 2014; Chen *et al*., 2017; Xu *et al*., 2017; Shipley *et al*., 2017; He *et al*., 2019) on Ti6Al4V manufactured by SLM. The martensitic α'-phase was due to high cooling rates and steep thermal gradients that are present during SLM production. It must be noted that the formation of the martensite α'-phase resulted from non-diffusionless transformation of the β-phase during sample production (Xu *et al*., 2017; Zhang *et al*., 2018).

Samples that were heat treated at 700°C did not show any observable microstructural change in comparison to the as-received microstructure. Similar findings were reported by other authors, who investigated the heat treatment of SLM Ti6Al4V components at temperatures below 730°C (Vilaro *et al*., 2011; Shipley *et al*., 2018; Wu *et al*., 2018). Furthermore, heat treatment for stress relieving of Ti6Al4V is carried out in the temperature ranges 600-700°C (Donachie *et al*., 2000; Gong *et al*., 2012), which support the results.

A study by Vilaro *et al*. (2011) reported similar observations after heat treating SLM produced Ti6Al4V coupons at 730°C for 2 hrs. The columnar prior β grains were clearly observed after heat treatment at 700°C as shown in Figure 4.2(b). Due to the overlapping of the layers during production of the components, the size of the columnar prior β grains on the 700°C samples

were slightly larger than the one of the as-received sample, but this observation was not associated with the heat treatment temperature, but processing history. Vilaro *et al*. (2011) reported that 730°C does not change the size of the β grain. Because of the above-mentioned observation, the length of the acicular martensite α'-phases on the 700°C microstructure was longer than the one of the as-received microstructure.

Heat treatment at 950°C transformed the microstructure from fully martensitic α' structure into fully lamella α + β structure (α' → α + β) as seen in Figure 4.2(c). This observation was expected because the temperature was slightly below β-transus (Vrancken *et al*., 2012). According to Gil *et al*. (2001), complete decomposition of martensite α'-phase is observable at temperatures above 800°C. The columnar prior β grains were still visible after heat treating at 950°C. The observed columnar prior β grains were associated with the 950°C temperature because is considered a temperature that is higher in the sub-transus region (Wu *et al*. 2016; Zhang *et al*., 2018; Vilaro *et al*., 2011; Shipley *et al*., 2018). A similar type of microstructure was reported by Zhang *et al*. (2018) on Ti6Al4V components manufactured by SLM, and heat treated at 950°C for residence time of 2 hrs.

Heat treatment at 1000°C also transformed the fully martensitic α' microstructure into fully lamella α + β microstructure, but with evidence of slight grain growth as can be seen in Figure 4.2(d). This implied that heat treating at 1000°C was able to fully transform the martensitic α'-phase structure into lamella α + β phases, while allowing grains to grow. As it was already mentioned in Chapter 2, heat treatment at 1000°C is categorised as super-transus, which means that the material transformed into fully β-phase during heating and formed α + β phases upon cooling, followed by grain growth. The FC method also played a role in the formation of the microstructure since it is a slow cooling process. The same reason also accounted for the disappearance of the large columnar prior β grains.

A diagram showing cooling paths of Ti6Al4V from temperatures above β-transus was reported by Galaragga *et al*. (2017), shown in Figure 4.3. The figure shows that the transformation of martensite α'-phase into α + β phases was as expected because of the high temperature (1000°C) and slow cooling rate provided by FC method.

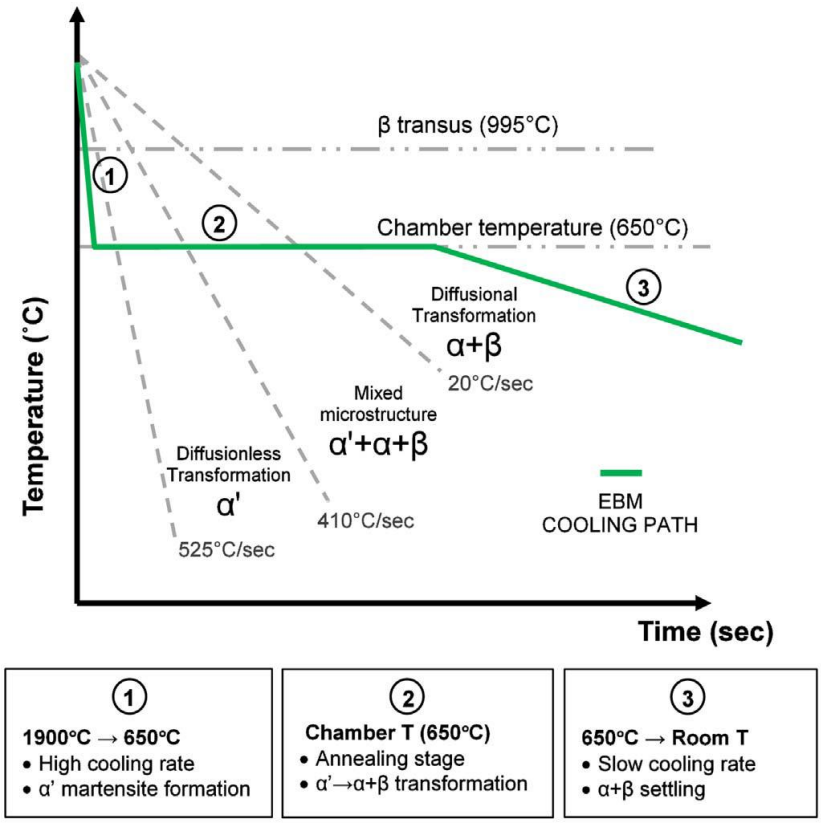


Figure 4.3: Cooling paths of Ti6Al4V (Galarraga *et al.*, 2017).

Slow cooling at 20°C/min from high temperature above β-transus lead to diffusional transformation of β-phase to stable α + β phases (Figure 4.3). Furthermore, intermediate cooling at 410°C/sec from super-transus treatments gave a mixture of martensite α', α and β phases.

4.1.2. Hardness

Figure 4.4 and Table 4.1 presents the graph and hardness results of the as-received and the heat-treated samples. An average of three hardness measurements were calculated and the results were plotted against the depth.

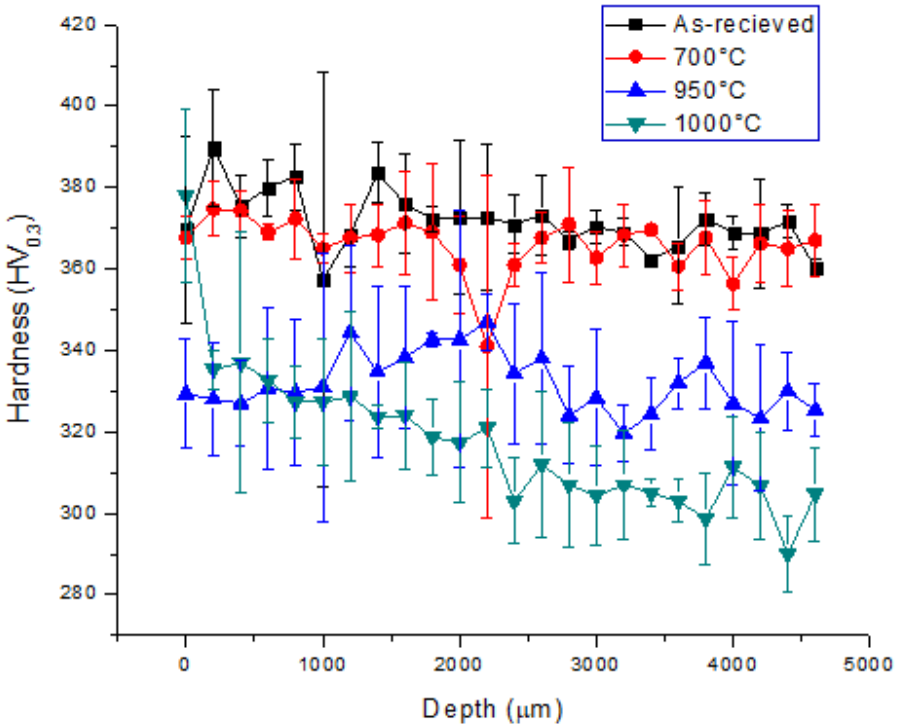


Figure 4.4: Hardness profiles of the samples after heat treatment at various temperatures.

Table 4.1: Average hardness of the samples after heat treatment at various temperatures.

Sample	**Hardness ($HV_{0.3}$)**
As-received	372 ± 10
700°C	362 ± 12
950°C	328 ± 15
1000°C	317 ± 12

All the samples displayed wavy hardness profiles as presented in Figure 4.4. The waviness of the profiles was due to the indentation made on the different phases during the measurements (Gupta *et al.*, 2018; Zhang *et al.*, 2018). It is noteworthy that the microstructure of all the samples was homogeneous throughout the entire samples. The as-received sample gave the highest hardness, with the sample recording hardness of 372 HV. These results were supported by other studies (Gupta *et al.*, 2018; Zhang *et al.*, 2018), who observed that the α-phase is softer compared to martensitic α'-phase. It is worth mentioning that martensite α'-phase and α-phase are made up of the same crystal structure.

A small decrease in hardness profiles was observed after heat treatment at 700°C as presented in Table 4.1. This small decrease was observed even though the microstructures of the as-received and 700°C samples were similar. The explanation behind the reduction in hardness was that at 700°C residual stresses were relieved by the heat treatment (Vilaro *et al*., 2011). According to Vilaro *et al*. (2011) and Gong *et al*. (2012), heat treatment at 700°C promotes sufficiently low yield strength at which only the internal stresses are relieved without changing the microstructure. A similar observation was reported by Vilaro *et al*. (2011) who recorded hardness of 354 ± 8 HV and 344 ± 8 HV for the as-produced and the heat-treated sample (at 730°C), respectively.

Heat treatment at 950°C and 1000°C resulted in noticeable hardness reduction, with the 1000°C heat treated sample showing the lowest hardness as presented in Table 4.1. This decrease in hardness was also observed on their hardness profiles as presented in Figure 4.4. The low hardness profiles of the two samples were associated with the transformation of the martensitic α'-phase into α + β phases. The results also confirmed the observations by Gupta *et al*. (2018) and Zhang *et al*. (2018) who reported soft stable α-phase than the harder metastable martensite α'-phase. A further low hardness profile was obtained on the 1000°C heat treated sample, as shown in Figure 4.4 and Table 4.1. Zhang *et al*. (2018) also reported decreased hardness values of 330 HV from 365 HV after heat treating at the same temperature.

4.1.3. Selection of heat treatment temperature

It was observed from results presented in Sections 4.1.1 and 4.1.2 that phase transformation of the martensite α'-phase into α + β phases (α' → α + β) was depended on temperature. Moreover, the phase transformation from martensite α'-phase into α + β phases resulted in the reduction in hardness. The hardness decreased with an increasing temperature. Most importantly, heat treatment at 950°C and 1000°C was able to fully transform the unwanted acicular martensitic α'-phase into stable α + β phases. Considering the outcomes of transformation of martensite α'-phase to more stable α + β phases, transformation of the columnar prior β grains and reduction of hardness to the lowest hardness value of 317 ± 12 HV that resulted from heat treatment at 1000°C, this temperature was selected as the optimised temperature.

Various cooling methods were considered when heat treating the samples under optimised temperature of 1000°C. The subsequent section presents results on the effects of cooling methods.

4.2. Optimisation of cooling method

The study on cooling methods was done by heat treating the samples to 1000°C and residence time of 2 hrs, followed by AC, WQ and FC. The microstructural characteristics and hardness properties of the samples are reported next.

4.2.1. Microstructures

The obtained microstructures before and after heat treatment, followed by cooling under various schemes are shown in Figure 4.5. Microstructural measurements were taken at the same position for all the samples, using the same magnification for comparison of grain sizes and the resulting morphologies.

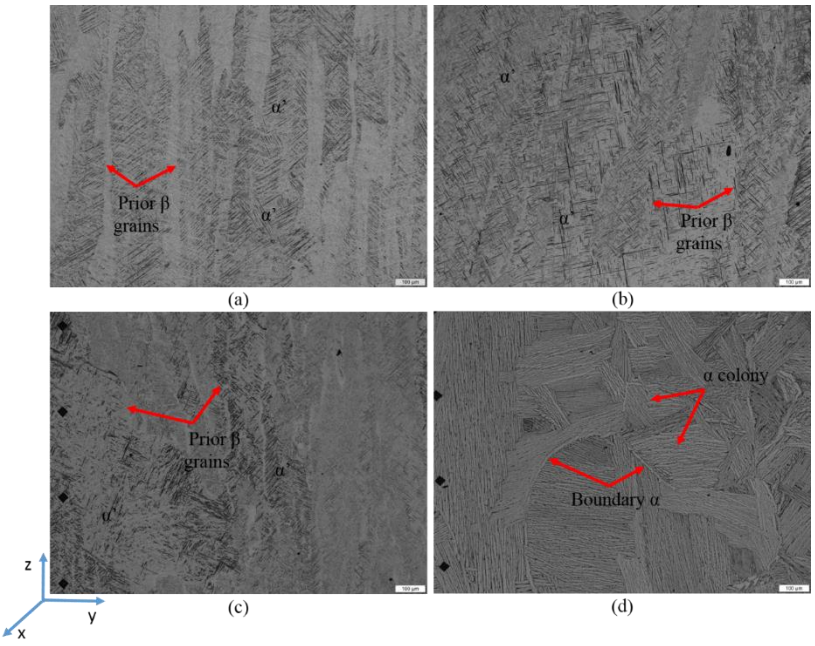


Figure 4.5: Microstructures of the sample after different cooling methods (a) As-received (b) WQ (c) AC and (d) FC after heat treatment at 1000°C and holding time of 2 hrs.

The as-received microstructure was discussed in Section 4.1.1 and will not be discussed in this section. The fingerprints of the SLM process which are the columnar prior β grains, acicular

martensitic α'-phase and porosity were observed on the as-received sample as shown in Figure 4.5(a). The large columnar prior β grains were also observed on the samples that were cooled using WQ and AC. These results were as expected because WQ and AC methods do not allow grains to grow and change shape. A similar microstructure was reported by Shipley *et al*. (2018) after heat treatment in the sub-transus followed by WQ and AC.

It was discussed in Chapter 2 that a fully martensitic α' microstructure can be produced after heat treatment, depending on the cooling rate or method used (Wu *et al*., 2016). It should be noted that the martensite α'-phase that was observed after WQ and AC was coarser than the microstructure of the as-received sample. These observations corresponded well with the outcomes of Ahmed and Rack (1998), Vilaro *et al*. (2011) and Vrancken *et al*. (2012), who identified the martensite α'-phase that formed after WQ as new martensite α'-phase. The new α'-phase was found to be thicker than the α'-phase identified in the as-received microstructure. Furthermore, Jovanovich *et al*. (2006) and Wu *et al*. (2016) also reported a fully martensitic α' structure after WQ of Ti6Al4V from 1010°C and 1100°C, respectively. Vilaro *et al*. (2011) attributed the increase in thickness of martensite α'-phase to different cooling rates possessed by the SLM and WQ (Ahmed and Rack, 1998; Vilaro *et al*., 2011).

The FC method clearly showed different microstructural characteristics compared to the as-received, WQ and AC samples. FC method resulted in a fully lamella α + β morphology containing large α-colonies within the prior β grain. Firstly, the microstructure transformed from fully martensitic α'-phase into lamella α + β phases. This type of microstructure was similar to the one reported by Shipley *et al*. (2018), who also observed lamella α + β microstructure after FC from heating Ti6Al4V samples below and above β-transus temperature. Figure 4.5(d) shows that FC (slow cooling) eliminated the formation of the unwanted martensite α'-phase (Vilaro *et al*., 2011).

Secondly, the columnar prior β grains transformed into equiaxed shape, with the microstructure taking basket weave type morphology after FC as presented in Figure 4.5(d). The FC method led to grain growth. Evidence of grain growth was clearly observed mostly on the boundaries of the β grain, as can be seen in Figure 4.5(d). A similar type of microstructure was reported by Vrancken *et al*. (2012) and Zhang *et al*. (2018) and attributed the grain growth to temperature and cooling rate used.

4.2.2. Hardness

The hardness results before and after heat treatment are represented in Figure 4.6 and in Table 4.2, respectively.

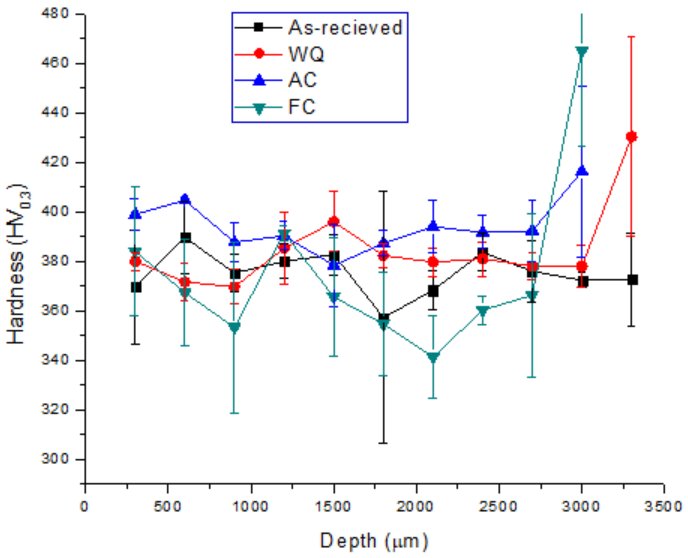


Figure 4.6: Hardness profiles of the samples after cooling with different methods.

Table 4.2: Average of hardness of the as-received and heat-treated samples.

Sample	**Hardness ($HV_{0.3}$)**
As-received	372 ± 10
WQ	385 ± 11
AC	394 ± 11
FC	375 ± 22

The hardness profiles all of the samples showed wavy patterns, indicating the existence of the different phases on the microstructures of the investigated samples (Gupta *et al*., 2018; Zhang *et al*., 2018) as presented in Figure 4.6. It is noteworthy that the microstructures of these samples were homogeneous. The microstructures of the as-receive, WQ and AC samples were fully martensitic α' structure while the FC sample showed fully lamella α + β phases. As already mentioned in section 4.1.2, the martensite α'-phase was found to be harder than the α and β phases (Gupta *et al*., 2018; Zhang *et al*., 2018). Increased hardness was observed for the WQ

and AC samples as presented by Table 4.2. These samples (WQ and AC) had average hardness values of 385 HV and 394 HV, respectively, from 372 HV of the as-received sample. The AC sample had the highest hardness value followed by WQ sample (Figure 4.6 and Table 4.2). Similar findings of increased hardness after AC were reported by Zhang *et al*. (2018), who reported an increased hardness to 350 HV from 330 HV after heat treatment.

High hardness values of the AC and WQ samples were attributed to the presence of the finer acicular martensitic α'-phase on the microstructure of these samples (Vilaro *et al*., 2011; Zhang *et al*., 2018). It is worth mentioning that even though the as-received sample also composed of acicular martensitic α'-phase, the hardness profiles of the samples was lower than WQ and AC because finer martensite α'-phase proved to exhibit higher hardness than coarse martensite α'-phase (Vilaro *et al*., 2011).

The as-received and FC sample showed the lowest hardness profile than the AC and WQ samples as presented by Figure 4.6. Furthermore, Table 4.2 also showed comparable hardness values for the as-received and FC samples. It was expected that the hardness of the FC sample would decrease, but that was not the case. Although FC transformed the fully martensitic α'-structure to α + β phases, the hardness remained the same, which was an unexpected result. In other words, the hardness of the FC sample did not reflect the full transformation. It was discussed in Section 4.1.2, that the martensitic α'-phase was observed to have higher hardness than α and β phases (Gupta *et al*. 2018; Zhang *et al*., 2018). Shipley *et al*. (2018) concluded that the size of α-colony led to increased hardness. The unexpected hardness result of the FC was associated with the presence of large α-colonies.

In brief, it was observed from the results that WQ and AC led to a microstructure with finer acicular martensitic α'-phase which resulted in an increase in hardness. The FC was the only cooling method that formed stable α + β phases, with hardness remaining the same. Given the transformation of the fully martensitic α' microstructure to stable α + β phases together with the resulting hardness results, FC was selected as the optimised cooling method. The optimum residence time had to be attained and this is discussed in the next section.

4.3. Optimisation of residence time

The effects of residence time were effectively studied by heat treating the samples to 1000°C at different residence times of 15 min, 30 min, 1 hr, 2 hrs, 4 hrs and 8 hrs, respectively followed by FC. The microstructures and hardness properties of the samples are reported next.

4.3.1. Microstructures

Figure 4.7 shows the microstructures of the as-received and heat-treated samples at various residence times. The microstructural measurements were taken at the same position for all the samples at the same magnification for comparison purposes.

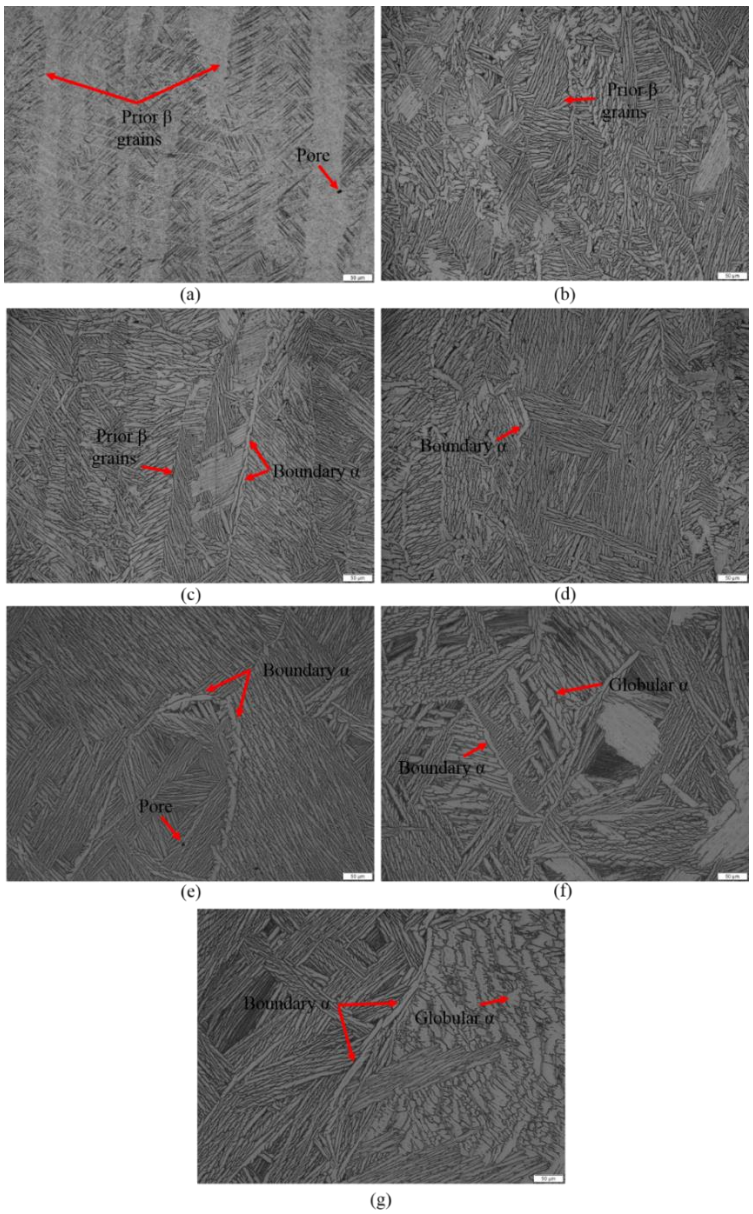


Figure 4.7: Microstructures of the samples (a) as-received, (b) 15 min, (c) 30 min, (d) 1 hr, (e) 2 hrs, (f) 4 hrs, and (e) 8 hrs.

The as-received microstructure was not discussed in detail in this section as it has already been discussed in Section 4.1.1. Heat treatment for 15 min at 1000°C and FC transformed the as-received microstructure from martensitic α' microstructure into a fully lamella α + β microstructure. It would seem that 15 min was a short residence time since the lamella α + β phases were clearly still present in the columnar prior β grains, after heat treatment as presented in Figure 4.7(b). Moreover, due to the FC cooling method, the microstructure was fully lamella α + β, with evidence of grain growth observed. Colonies of the α-phase were observed after heat treatment for 15 min with the microstructure taking basket weave morphology.

As the residence time was increased to 30 min, the columnar prior β grains size increased, as presented in Figure 4.7(c). This was an indication of grain growth. Clearly, the size of the lamella α and β grains was slightly increased after heat treatment for 30 min with α-phase growth originating on the columnar β grain boundaries as shown in Figure 4.7(c). The growth of α-colonies was evident, which also proved that grain growth had occurred.

Grain growth was further noticeable as the residence time was raised to 1 hr. A proof of grain growth was the visibility for the large columnar prior β grains, with the microstructure taking a basket weave morphology as presented in Figure 4.7(d). The lamella α + β grains showed elongation characteristics and more of α growing thicker on the boundaries. In addition, growth of α-colonies was also witnessed after heat treatment for 1 hr. The results were comparable to the one of Chicos *et al*. (2018), who showed the presence of α-colonies after heat treatment for 50 min. Heat treatment for 1 hr resulted into a homogeneous microstructure, indicating that 1 hr was sufficient to homogenize the sample during the heat treatment at 1000°C. The results aligned well with the study of Jovanovic *et al*. (2006), who used 1 hr as a standard residence time during heat treatment of investment cast-Ti6Al4V parts, using same temperature.

Thickening of the lamella α and β phases were observed after resident time was increased to 2 hrs as can be seen in Figure 4.7(e) with the columnar grains no longer visible. Heat treatment for 2 hrs resulted in a homogenised microstructure of stable lamella α + β phases as presented in Figure 4.7(e). The results were in agreement with the findings by Vrancken *et al*. (2011) who reported that increased size of α and β phases when residence time was increased. Most studies in literature use 2 hrs as a standard residence time for microstructural homogenization (Chicos *et al*., 2018; Zhang *et al*., 2018; Ter Haar and Becker 2018) because of its ability to

produce a homogeneous microstructure. Heat treatment for 2hrs produced a microstructure with α-colonies in basket weave morphology.

Excessive grain growth was obvious when residence time was increased to 4 hrs as shown in Figure 4.7(f). Furthermore, 4 hrs produced thicker lamella α + β grains than 2 hrs sample. Heat treatment for 4 hrs initiated globularisation of the α-phase as shown in Figure 4.7(f) because globular of the α + β phases were observed on the microstructure. Globularisation of the α-phase formed along the bigger grain boundaries in a mechanism known as edge spheroidisation (Stefansson and Semiatin, 2003; Sabban *et al*. 2019). According to Stefansson and Semiatin (2003), globularization process follow two stages and requires boundary splitting of the α-phase and requires an internal boundary through the thickness of one of the lamella phases. The globularisation of the α-phase in this case occurred in two stages.

During first stage, microstructural transformation during the initial stage of heat treatment led to segmentation of the lamella phases through boundary splitting, while the second stage was due to the prolonged residence time (Stefansson and Semiatin, 2003). A study by Shipley *et al*. (2018) revealed globular α + β phases after heat treating using a residence time of 20 hrs at 940°C. The globularization of the lamella α + β phases started at the prior β grain boundary. A study by Stefansson and Semiatin (2003) showed that globularisation process can take place as a result of longer residence times. This was due to α-phases at the boundaries which are shorter than the other lamella grain and therefore tend to globularize quicker.

Large α-colonies were also observed after heat treatment of 4 hrs as presented in Figure 4.7(f). A similar type of microstructure was reported by Vrancken *et al*. (2012), who showed larger α-colonies for elongated residence times. Further grain growth was observed after heat treatment of 8 hrs, with lamella α + β phases starting to take an irregular shape as labelled in Figure 4.7(g). Heat treatment after 8 hrs resulted in more globularisation of α and β phases. It was obvious that as the residence time increased, the grains grew larger, α-colonies size also grew larger and the prior β grains were no longer visible (Vrancken *et al*., 2012; Shipley *et al*., 2018).

4.3.2. Hardness

The hardness results of samples are shown on the plots presented in Figure 4.8 and Table 4.3. An average of three patterns was calculated and the results were plotted against the depth.

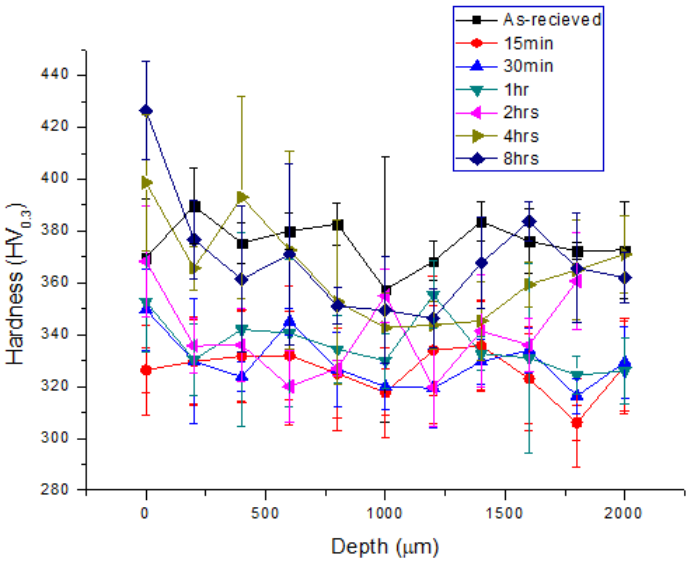


Figure 4.8: Hardness profiles of the samples after heat treatment at various residence times.

Table 4.3: Summarised hardness of the as-received and heat-treated samples.

Sample	**Hardness ($HV_{0.3}$)**
As-received	372 ± 10
15 min	330 ± 19
30 min	337 ± 14
1 hr	342 ± 17
2 hrs	340 ± 14
4 hrs	376 ± 26
8 hrs	369 ± 17

The hardness profiles of all the samples displayed wavy patterns due to the presence of different phases (Figure 4.8). As anticipated, the as-received sample showed the highest hardness value due to martensitic α' structure as presented in Table 4.3. Furthermore, it is obvious that heat treatment at 15 min, 30 min, 1 hr and 2 hrs led to a decrease in hardness, with the sample heat treated at 15 min reporting the lowest hardness. The overall reduction in hardness displayed by

these four samples was attributed to the transformation of the microstructures into stable α + β phases, with very limited grain growth. Moreover, because of similarity of these sample microstructures, their hardness values were comparable.

An increased hardness was recorded after heat treating at 1000°C and holding at the temperature for 4 hrs and 8 hrs, respectively. These two samples also had comparable hardness values. This observation was not expected since the microstructure transformed into stable α + β phases, while grain growth was observed on these samples. This observation was not in agreement with the Hall-Petch relationship (Babu, 2008). The increase in hardness after the 4 hrs and 8 hrs heat treated was associated with the excessive grain growth that resulted from these longer residence times (Vilaro *et al*., 2011; Shipley *et al*., 2018). According to Vilaro *et al*. (2011), longer residence times must be avoided when heat treating Ti6Al4V alloy above β-transus, because they introduce excessive grain growth and larger α-colonies.

In summary, it was observed from the results on the effects of residence time that all the residence times were able to transform the microstructure into stable lamella α + β phases. Moreover, globularisation of the α-phase was originated after heat treating at 1000°C, for 8 hrs, followed by FC. It was also observed that as the residence time increased from 15 min to 2 hrs, hardness decreased, and then slightly increased when the residence time was increased to 4 and 8 hrs. Based on these results, residence times of 2 hrs and 8 hrs were selected as optimized residence times. The residence time of 2 hrs was selected because it was under these conditions whereby homogenised α + β microstructure was produced. The longer holding time of 8 hrs was selected because the microstructure that was achieved under the operating condition was a mixture of globular and lamella α + β morphology, with decreased hardness.

4.4. Discussion of Chapter 4

The aim of heat treatment for process development was to heat treat the Ti6Al4V coupons and select optimized parameters that can produce the desired bimodal microstructure. It was found that sub-transus (950°C) and super-transus (1000°C) heat treatments fully transformed the martensite α'-phase into stable lamella α + β phases, and resulted in a major decrease in hardness, hence these temperatures were selected as optimized temperatures.

The WQ and AC methods led to the introduction of fully martensitic α' microstructure. Since this study aimed at using a single heat treatment strategy to achieve a bimodal microstructure, the microstructures produced by these cooling methods would obviously require a second heat treatment strategy to transform the undesired martensitic α'-phase. Furthermore, these cooling methods led to an increase in hardness; hence they were not selected as optimized cooling methods. The FC method was selected as the optimized cooling method because it introduced the stable lamella α + β phases.

All the residence times used were able to transform the microstructure into fully lamella α + β phases. However, 2hrs and 8hrs were selected as optimized residence times. The 2 hrs was selected because it produced a homogenized α + β microstructure and 8 hrs was selected because of its ability to produce a mixture of globular and lamella α + β morphology.

4.5. Summary of Chapter 4

The evaluation of the three heat treatment parameters, namely, temperature, cooling method and residence time were extensively studied, and optimized parameters were successfully chosen depending on their ability to produce the desired microstructure. The microstructures and hardness properties that were reported in this chapter led to the identification of parameters that could give the desired bimodal microstructure. Table 4.4 shows the selected heat treatment parameters. As discussed in the experimental procedure in Chapter 3, these selected parameters were used as optimised parameters to heat treat as-received tensile samples.

Table 4.4: The selected optimized heat treatment parameters.

Temperature	Cooling method	Residence time
1000°C	FC	2 hrs
1000°C	FC	8 hrs

Chapter 5 : Heat treatment using optimised conditions

This chapter present the results and discussion of samples that were heat treated using optimised parameters. The microstructure, hardness and tensile properties of the samples heat treated using optimised process parameters are reported. The image of the rod sample is shown in Figure 5.1.



Figure 5.1: Image of the as-received sample that were used for heat treatment.

The rod sample had a diameter of 1.5 cm and height of 7.5 cm. The sample was cut into small pieces before they were heat treated. Heat treatment was conducted under argon atmosphere using the vertical heat treatment furnace at the University of Pretoria. Porosity analysis, microstructure and hardness properties are reported, followed by tensile test results.

5.1. Porosity analysis

Porosity of SLM produced Ti6Al4V components is a major shortcoming of the technology (Shipley *et al*., 2018). The cause of porosity on the produced parts is complex and therefore porosity analysis on the samples has to be understood before heat treatment of the samples since tensile test was going to be carried out on the samples. In addition, porosity is critical for SLM produced Ti6Al4V components because it has detrimental effects on mechanical properties (Leuder *et al*., 2013; Kasperovich *et al*., 2015; Shipley *et al*., 2018). A study by Shipley *et al*. (2018) has reported that porosity act as crack initiators and affects properties such

as fracture and fatigue performance. Figure 5.2 shows a high resolution 2D micro-CT scan image of the as-received rod sample.

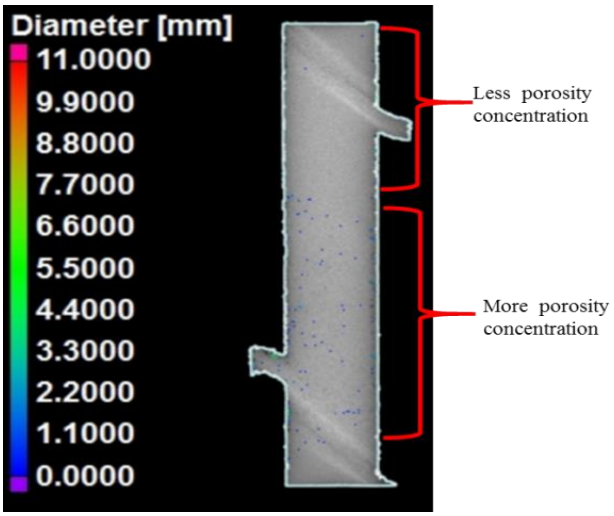


Figure 5.2: High resolution 2D micro-ct scan image of the as-received rod sample.

Porosity on the as-received sample was measured over a volume of 15649 mm^3. The sample showed level of non-uniform porosity throughout the entire sample (Figure 5.2). All the pores were internal pores which resulted from both gas entrapment and lack of fusion.

The major cause of porosity on the components is high roughness on some regions during each layer, which can result in inconsistent powder deposition. As a result, this will lead to the laser insufficiently melting the powder, which will cause lack of fusion between layers, resulting in crack-like pores (Kruth *et al*., 2010). The cause of the second type of pores was surface roughness that caused gas entrapment between the printed layers and newly deposited powder (Shipley *et al*., 2018).

Porosity concentration on the whole sample was also found not to be the same throughout the sample. There is a region that was found to be having less porosity concentration compared to other regions as shown in Figure 5.2. This observation was not expected and was thought to be due to inconsistent powder deposition during the production of the samples. The size of the pores was found not to be the same as can be seen in Figure 5.2. Furthermore, pores of bigger diameter (green colour region on the samples in Figure 5.2) were witnessed on other parts of the sample. Again, this observation might be due to lack of fusion on those regions. The as-received sample measured a maximum pore size with a diameter of approximately 0.9 mm.

The overall percentage porosity of the sample was measured to be 1.21 vol.%. A summary of the porosity results is represented in Table 5.1.

Table 5.1: Summarised porosity analysis of the as-received sample.

Description	Value
Material volume (mm^3)	15648.57
Defects volume (mm^3)	192.54
Defects ratio (vol.%)	1.22

It is obvious from Table 5.1 that the as-received sample gave a porosity percentage of 1.22 vol.%. As it was already mentioned in Chapter 2, ASTM F3001 concerning powder bed manufacturing requires that the manufactured component must not contain defects, cracks, discontinuities, foreign materials or inclusions. However, achieving porosity free component is still a challenge even when the density is greater than 99% (Thijs *et al*., 2010; Cunningham *et al*., 2016; Kasperovich *et al*., 2016). The overall porosity on the as-received sample was measured to be 192 mm^3 over a volume of 15649 mm^3.

The sample was studied for microstructural features after porosity measurements. The microstructure of the as-received sample on a small top region is indicated by an arrow indicated in Figure 5.3.

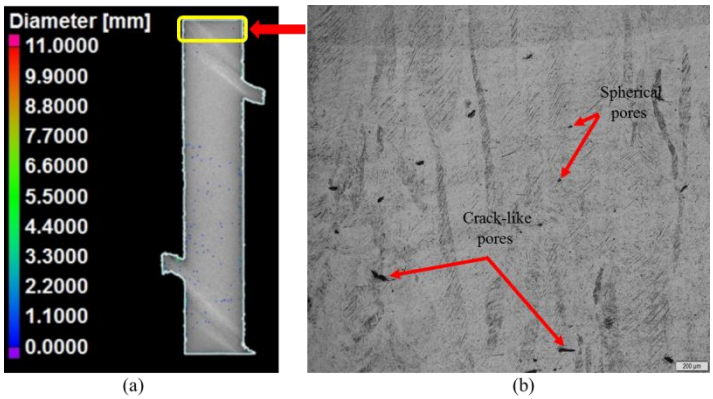


Figure 5.3: Images of the as-received Ti6Al4V sample (a) 2D micro-ct scan (b) Optical microstructure.

Crack-like pores and spherical pores were noticeable on the as-received microstructure as shown in Figure 5.3. These types of pores were also reported in literature (Liu *et al*., 2014;

Kasperovich *et al*., 2016; Shipley *et al*., 2018) on SLM produced Ti6Al4V parts. Spherical pores resulted from gas entrapment in the melt pool and the crack-like pores were result of insufficient melting during production of the components (Liu *et al*., 2014; Gu *et al*., 2016; Kasperovich *et al*., 2016). These pores were associated with the process parameters that were used to produce the sample. It was mentioned in Section 2.2.4 that process parameters that are not optimized can results in porosity and sometimes cracks. The observations of pores on the microstructure complement the one made by the micro-ct-scan results. The columnar prior β grains which are known as the fingerprint of SLM produced Ti6Al4V components were observed on the as-received sample. As expected, the microstructure was fully martensitic, with the martensite α'-phase found inside the columnar prior β grains.

5.2. Optimized heat treatment process

5.2.1. Microstructures

The microstructures of the samples after heat treatment using optimized parameters are depicted in Figure 5.4. The microstructures were taken at the same position for all the samples, with the same magnification for comparison purposes.

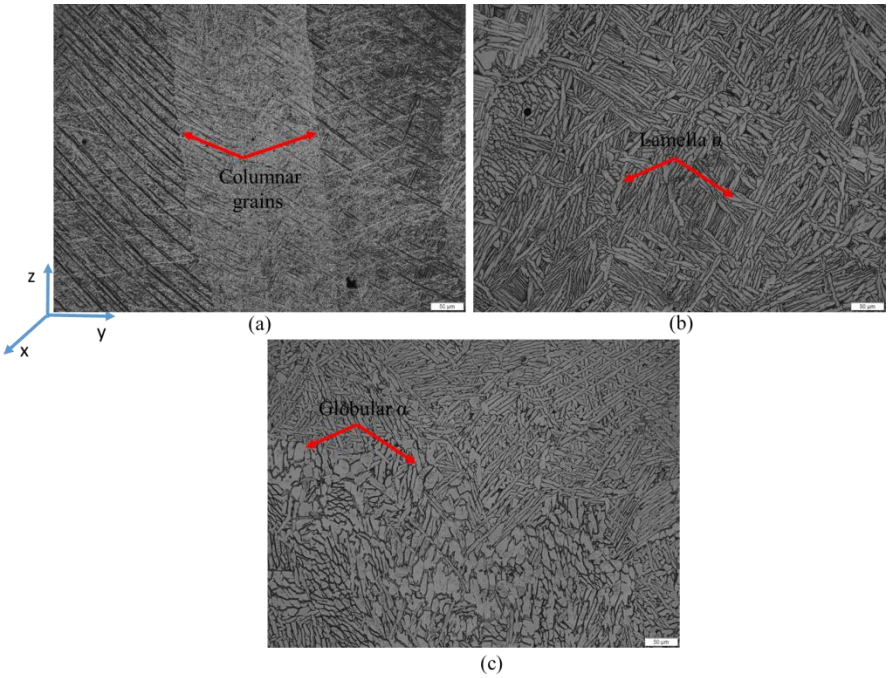


Figure 5.4: Microstructures of the as-received and heat treated samples using optimized parameters, (a) As-received (b) 1000°C for 2 hrs followed by FC and (c) 1000°C for 8 hrs followed by FC.

Heat treating at 1000°C for 2 hrs followed by FC gave fully lamella α + β structure as presented in Figure 5.4(b). The β grains were not observed after heat treatment as presented in Figure 5.4(b), implying that the columnar grains transformed into equiaxed grains. Furthermore, the α-colonies were clearly visible with the microstructure taking a basket weave type of morphology. Heat treating the sample at 1000°C for 2 hrs followed by FC resulted in limited grain growth. On the contrary, a study by Vilaro *et al*. (2011) observed grain growth after super-transus treatment.

Heat treatment at 1000°C for 8 hrs followed by FC produced a combination of globular and lamella α + β phases as presented by Figure 5.4(c), which indicated that the globularization process, took place. Globularization is when the lamella α + β phases change to be globular in shape.

5.2.2. Hardness

The hardness results of the samples after heat treatment using optimized parameters are represented by the graph in Figure 5.5 and Table 5.2, respectively. An average of three hardness patterns was calculated and the results were plotted against the depth.

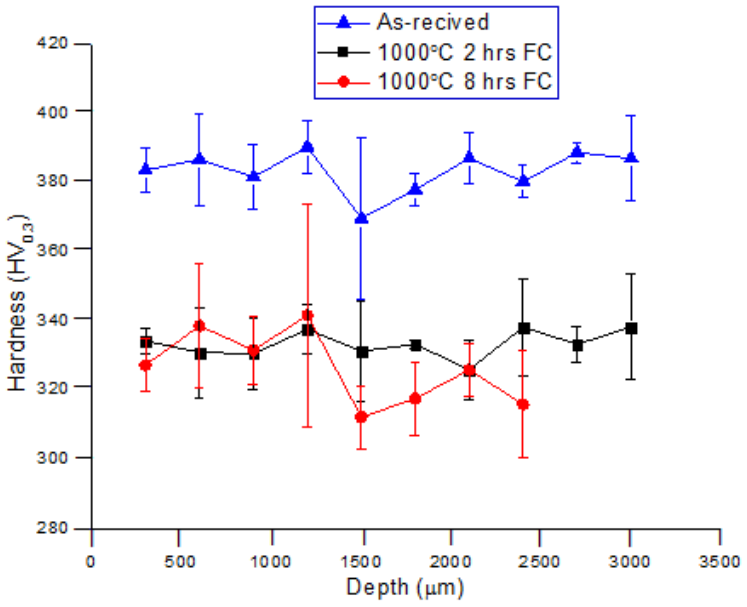


Figure 5.5: Hardness profiles of the as-received samples and the heat treated samples after heat treating using optimized parameters.

Table 5.2: Average hardness of the samples after heat treatment using optimized parameters.

Sample	Hardness ($HV_{0.3}$)
As-received	383 ± 13
1000°C 2 hrs FC	333 ± 9
1000°C 8 hrs FC	327 ± 14

Figure 5.5 and Table 5.2 indicate that hardness decreased after heat treatment using the optimized parameters as expected. The low hardness on the heat-treated samples was attributed to the stable α + β phases that were observed on the microstructures of the latter samples. The as-received sample gave the highest profile (Figure 5.5) with an average hardness of 383 $HV_{0.3}$ (Table 5.2) in relation to its microstructure. Another important observation was the hardness profiles of the heat-treated samples showing comparable results. The similarity in hardness profiles of these samples suggests that all the selected parameters achieved comparable hardness profiles. However, heat treating at 1000°C for 8 hrs and cooling by FC gave the lowest hardness as can be seen in Table 5.2.

5.2.3. Tensile properties

Tensile testing was performed after heat treatment using optimized parameters. Tensile testing was conducted at the CSIR Material Testing Laboratory as per ASTM E8 M standard. Figure 5.6 shows the stress versus extension curves of the samples. The figure shows ductility improvement as a result of heat treatment using the optimized parameters.

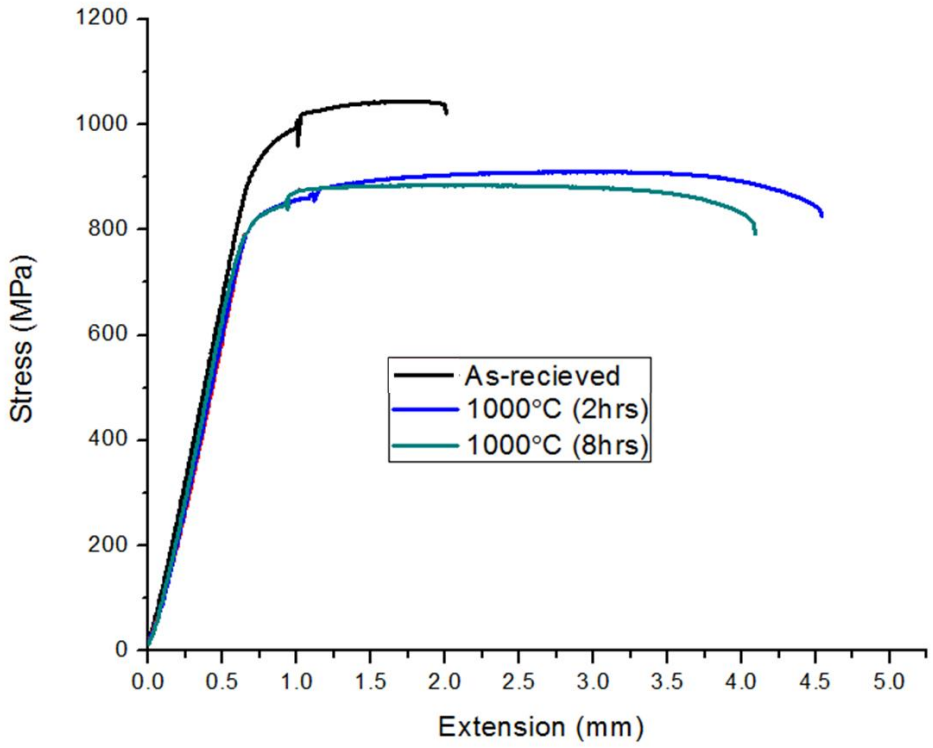


Figure 5.6: Stress versus extension curves of heat treated Ti6Al4V samples using optimized parameters.

Figure 5.6 shows that the ductility (% elongation) of the as-received sample was low compared to the heat-treated samples. The low ductility was associated to the martensitic α'-phase that was seen on the as-received microstructure in Figure 5.4(a) (Vrancken *et al*., 2012; Fachinni *et al*., 2010; Ter Haar and Becker, 2018; Zhang *et al*., 2018). Figure 5.6 further present that heat treatment resulted in improvement on ductility. The improved ductility was associated with the transformation of the martensitic α'-structure to a more stable α + β phases (Tong *et al*., 2017). All the selected heat treatment parameters improved the ductility of the samples.

The ductility improvement observed after heat treatment was associated with the homogeneous microstructures that were observed for all the heat-treated samples. It is noteworthy that all the optimized parameters resulted in ductility improvement that was comparable. The resulting tensile properties are summarised in Table 5.3.

Table 5.3: Mechanical properties of the Ti6Al4V samples.

Sample	Specimen	YS (MPa)	UTS (MPa)	Elongation (%)

	S1	943.05	1044.03	3.92
As-received	S2	960.09	1049.14	6.30
	S3	943.30	1042.50	4.56
	Average	**948.81**	**1045.22**	**4.92**
	S1	828.44	910.39	10.67
1000 2hrs FC	S2	827.61	906.51	13.90
	S3	847.47	916.95	13.17
	Average	**834.51**	**911.28**	**12.58**
	S1	807.85	885.20	13.30
1000 8hrs FC	S2	811.34	889.63	12.73
	S3	806.75	882.84	12.23
	Average	**808.65**	**885.89**	**12.76**

It was mentioned in Chapter 2 that ASTM F2924-14 requires that the elongation of AM produced Ti6Al4V must at least be more than 10%. It is presented in Table 5.3 that the as-received sample had the lowest ductility that does not meet the required standard. Similar results of low ductility for SLM produced Ti6Al4V were reported in literature (Facchini *et al*., 2010; Vilaro *et al*., 2011; Ter Haar and Becker, 2018). Moreover, the results support Zhang *et al*. (2018) who discussed that the needle shaped martensite α'-phase that is found on SLM Ti6Al4V is brittle in nature. The martensitic α'-phase is known to be highly anisotropic because it results from high cooling rates with large temperature gradients; hence it is associated with low ductility.

It is well known that the tensile strengths of Ti6Al4V are determined by their microstructures, which mean that can be altered by heat treatment (Tong *et al*., 2017). ASTM F2924-14 requires a minimum yield strength (YS) and ultimate tensile strength (UTS) of 795 MPa and 860 MPa, respectively. The tensile properties of SLM produced Ti6Al4V are known to be superior to those of wrought or cast components (Shipley *et al*., 2018). Even though ductility was improved after heat treatment, the YS and UTS were reduced, albeit the desired two-phase

microstructures. It is noteworthy that even though the YS and UTS decreased, they were still within the required standard. Similar result of decreased YS and UTS were made in literature after heat treatment of Ti6Al4V (Vilaro *et al*., 2011; Zhang *et al*., 2018).

5.3. Discussion of Chapter 5

This study proposed a method of producing a bimodal microstructure using an innovative single heat treatment strategy on SLM Ti6Al4V coupons. As reported in Chapter 2, this type of microstructure is characterized by improved ductility of SLM produced Ti6Al4V (Nalla *et al*., 2002; Poondler *et al*., 2009; Ter Haar and Becker, 2018; Zhao *et al*., 2018; Sabban *et al*., 2019). Therefore, the selected optimized heat treatment parameters had a tendency of producing the bimodal microstructure (globular α-phase in a matrix of lamella α + β phases), with fully martensitic α' structure as the starting microstructure. Two main heat treatment conditions were selected. The conditions were 1000°C for 2 hrs followed by FC and 1000°C for 8 hrs followed by FC.

1000°C for 2 hrs and cooling with FC was able to produce the desired lamella α + β matrix but failed to produce the globular α-phase. In other words, this heat treatment produced a fully lamella α + β microstructure (Figure 5.4b), instead of a bimodal microstructure. Super-transus heat treatments are recommended for grain growth purposes (Vrancken *et al*., 2012; Vilaro *et al*., 2011), therefore, heat treatment at 1000°C for 2 hrs followed by FC was expected to produce the globular α-phase in the lamella α + β matrix, however it this was not achieved. Although this heat treatment resulted in grain growth, a fully lamella α + β microstructure was achieved (Figure 5.4c).

The mechanical properties depend largely on constituent phases and their morphology (Xu *et al*., 2015; Tong *et al*., 2017). Since hardness of SLM Ti6Al4V is inversely proportional to ductility (Babu, 2008), Heat treatment at 1000°C for 2 hrs, cooling by FC was characterized by a decrease in hardness from 383 ± 13 HV to 333 ± 9 HV, with the ductility improved from 4.92% to 12.58%. It is well known that heat treatment improves the ductility of SLM produced Ti6Al4V components at the cost of strength (Vilaro *et al*. 2011; Zhang *et al*. 2018). Even though 1000°C for 2 hrs, cooling by FC improved the ductility, the YS decreased to 835 MPa and UTS decreased to 949 MPa.

Heat treatment at 1000°C for 8 hrs followed by FC was able to produce a microstructure that was composed of combination of equiaxed and lamella α + β phases (Figure 5.4c). This heat treatment condition was able to globularize the α-phase, owing to the long residence time of 8 hrs. Globularization of the α-phase formed on the boundaries of the bigger grain in a mechanism known as edge spheroidization (Stefansson and Semiatin, 2003; Sabban *et al*. 2019). Boundary splitting of the α-phase requires an internal boundary through the thickness of one of the lamella phases. The globularization of the α-phase in this case occurred in two phases. In the first phase, the microstructural transformation during the initial stage of heat treatment led to segmentation of the lamella phases through boundary splitting, while the second stage was due to the prolonged residence time (Stefansson and Semiatin, 2003).

The microstructure composed of sections of lamella α + β phases and globular α + β phases, therefore it was not considered bimodal because the globular α-phase did not form in matrix of lamella α + β phases. However, the microstructure was close to the bimodal microstructure. The microstructure was characterized by hardness decrease to 327 ± 14 HV from 383 ± 13 HV. The ductility increased to 12.76% from 4.92%. YS and UTS decreased to 807 MPa and 886 MPa, respectively.

5.4. Summary of Chapter 5

Porosity analysis showed two types of pores on the SLM produced Ti6Al4V coupons due to lack of fusion and gas entrapment. This chapter further showed that the selected heat treatment parameters improved the microstructure of the Ti6Al4V coupons by producing lamella fully α + β and mixture of globular and lamella α + β phases. Furthermore, tensile results also showed that the selected parameters improved the ductility of the coupons by at least 13%. The results showed that a single heat treatment strategy did not produce a bimodal microstructure as anticipated. However, an improved microstructure was obtained.

Chapter 6 : Conclusions

This chapter present conclusion based on the evaluation of the microstructural features, hardness and tensile properties of SLM produced Ti6Al4V coupons. Improving the microstructure of high speed SLM produced Ti6A4V by obtaining a bimodal microstructure using post heat treatment was significant because it resulted in improved ductility.

The Ti6Al4V rod samples were manufactured on SLM Aeroswift^{TM} machine. The Ti6Al4V powder was successfully characterized before production of the components. Different heat treatments were performed on the produced Ti6Al4V coupons with the aim of improving their microstructure. Porosity analysis was conducted on the produced samples before microstructural, hardness and tensile properties were studied and discussed. The summary of the findings is given in the next section.

6.1. Summary of findings

The Ti6Al4V powder that was used in the production of Ti6Al4V rod samples had smooth spherically shaped particles. Moreover, the powder was characterized by particle size distribution in the ranges of 30-100 µm. The high speed SLM produced Ti6Al4V samples were found to have spherical and crack-like pores, which were due to gas entrapment and lack of fusion, respectively, in the melt pool during production.

The microstructure of the produced Ti6Al4V coupons was composed of sharp acicular martensitic α'-phase, which was characterized by high hardness. Moreover, the SLM produced microstructure was characterized by low ductility of 4.95% that was below the required standard of 10% (requirement for ASTM F2924-14 standard). Hence it was important to perform heat treatment on the produced coupons, with the ability to produce an improved bimodal microstructure.

Heat treatment at lower temperature of 700°C did not bring about any microstructural changes. This was because 700°C was a low temperature to initiate any phase transformation. Even though there was no microstructural change that was observed, this temperature caused a small

decrease in hardness of 362 ± 12 HV from 372 ± 10 HV was observed after heat treatment at 700°C. The decrease in hardness was associated with the relief of residual stresses.

Heat treatment at 950°C transformed the microstructure to fully lamella α + β, with columnar prior β grains still visible. Minimal grain growth was observed after heating at this temperature. Furthermore, 950°C resulted in a decrease in hardness to 328 ± 15 HV from 372 ± 10 HV.

Super-transus treatment at 1000°C produced a fully lamella α + β microstructure with basket weave morphology. This heat treatment also led disappearance of the columnar β grains and subsequent grain growth observed. The phase transformation also led to a decrease in hardness to 317 ± 12 HV from 372 ± 10 HV.

The WQ and AC methods led to the formation of finer martensitic α'-phase than the coarser martensitic α'-phase that was observed on the as-received sample. This was because the cooling rate introduced by WQ and AC was higher than the one introduced by the SLM process. The transformation to the new finer martensitic α'-phase resulted in an increase in hardness to 394 ± 11 HV and 385 ± 11 HV for the AC and WQ samples, respectively, from 372 ± 10. The FC proved to be the only cooling method that showed no formation of the unwanted martensitic α'-phase. The FC method produced a fully lamella α + β microstructure, leading to a hardness of 375 ± 22 HV.

Heat treatment for 15 min, 30 min, 1 hr, and 2 hrs all led to similar transformed α + β microstructures. The similarities of the microstructures of these samples were reflected by the comparable hardness values. Heat treatment at 4 hrs and 8 hrs led to the formation of a mixture globular and lamella α + β microstructure, with excessive grain growth observed. Hardness also proved to increase after heat treatment at 4 hrs and 8 hrs, with the samples recording hardness of 376 ± 26 HV and 369 ± 17 HV from 340 ± 14 HV of the 2 hrs samples.

The optimized heat treatment parameters were unable to yield a bimodal microstructure but resulted in improved microstructures of the Ti6Al4V coupons. The selected temperature, residence time, cooling method of 1000°C, 2 hrs, FC, respectively produced fully lamella α + β microstructures which improved the ductility by 12.58%. In addition, 1000°C, 8 hrs, FC produced a mixture of lamella and globular α + β phases, which was not bimodal, but close to being bimodal. The microstructure was characterised by ductility improvement of 12.76%.

6.2. Main conclusions

The study and objectives of conducting heat treatment of high speed SLM produced Ti6Al4V coupons led to the following conclusions;

- The microstructure of the high speed SLM Ti6Al4V is characterized by fully martensitic α'-structure, columnar prior β grains and porosity.

- Low heat treatment strategy at 700°C does not lead to any observable microstructural phase transformation. This heat treatment leads only to a slight decrease in hardness.

- The WQ and AC method must be avoided since they introduce back a finer acicular martensitic α'-phase, resulting in increased hardness and low elongation. The FC is recommended for the full transformation of the martensite α'-phase.

- Heat treatment at 1000°C 2 hrs and FC produced lamella α + β structure accompanied by smaller grain growth. This microstructure was characterized by increased ductility to 12.58%.

- Heat treatment at 1000°C 8 hrs followed by FC produced a microstructure that composed of mixture of globular and lamella α + β phases, but the microstructure was not consider bimodal because of the arrangement of the phases. This microstructure was characterized by ductility improvement to 12.76%.

- Heat treatment at 1000°C 8 hrs and FC resulted in highest ductility improvement of SLM produced Ti6Al4V coupons.

- Single heat treatment using the selected optimized parameters failed to produce the desired bimodal microstructure. The hypothesis that a bimodal microstructure can produced using single heat treatment strategy is disproved.

6.3. Recommendations

This given recommendations are based on the obtained results for future research on heat treatment of high speed SLM Ti6Al4V alloy.

- Use XRD and EBSD to quantify the phases present after heat treatment using the optimized parameters.

- Study the effect of controlling cooling rate when heat treating Ti6Al4Vto produce a balance between martensite α', α and β phases.

- Perform porosity measurements after heat treatment using optimized parameters, with an attempt to determine porosity effect on mechanical properties.

References

Ahmadi, SM., Kumar, R., Borisov, EV., Petrov, R., Leeflang, S., Li, Y., Tumer, N., Huizenga, R., Ayas, C., Zadpoor, AA., Popovich, VA. (2019), From microstructural design to surface engineering: A tailored approach for improving fatigue life for additively manufactured meta-biomaterials, *Acta Materialia*, vol. 83,pp.153-166.

Alcisto, J., Enriquez, A., Garcia, H., Hinkson, S., Steelman, T., Silverman, E., Valdovino, P., Gigerenzer, H., Foyos, J., Ogren, J., Dorey, J., Karg, K., MacDonald, T., Es-said, OS. (2011), Tensile properties and microstructure of laser formed Ti6Al4V, *Journal of Material Engineering and Performance*, vol. 20, no, 2,pp.203-212.

Algius, D., Kourousis, KI., Wallbrink, C. (2018), A review of the As-Built SLM Ti6Al4V Mechanical Properties towards Achieving Fatigue Resistance Designs, *Metals*, vol. 8, no, 75.pp.1-24.

Antonysamy, AA., Meyer, J., Pragnell, PB. (2013), Effect of build geometry on the β-grain structure in additive manufacture by selective electron beam melting, *Material Characterization*, vol. 84,pp.153-168.

Arthur, NKK., and Pitjana, S. (2018), Microstructure and material properties of LENS fabricated Ti6Al4V components, *Journal of the South African Institution of Mechanical Engineering*, vol. 34,pp.33-36.

ASTM F2921-11, (2011), *Standard Terminology for Additive Manufacturing Coordinate System and Test Methodologies*, ASTM International, West Conshohocken, PA.

ASTM F2924-14, (2012), *Standard Specification for Additive Manufacturing Titanium-6 Aluminum-4 Vanadium with Powder Bed Fusion*, ASTM International, West Conshohocken, PA.

Attar, H., Haghighi, S., Kent, D., Wu, X., Dargusch, MS. (2017), Comparative study of commercially pure titanium produced by laser engineered net shaping, selective laser melting and cast processes, *Material Science and Engineering A*, vol. 705,pp.385-393.

Babu, B. (2008), Physically based model for plasticity and creep of Ti6Al4V, *Journal of Mechanics of Materials*, vol. 3,pp.311-314.

Biamo, S., Penna, A., Ackelid, U., Sabbadini, S., Tassa, O., Fino, P., Pavese, M., Gennero, P., Badini, C. (2010), Electron beam melting of Ti-48Al-2Cr-2Nb alloy: Microstructure and mechanical properties investigation, *Intermetallics*, vol. 19,pp.776-781.

Boyer, RR., and Briggs, RD. (2005), The use of β titanium alloys in the aerospace industry, *Journal of Materials Engineering and Performance*, vol. 14,pp.681-685.

Chicos, LA., Zaharia, SM., Lancea, C., Pop, MA., Canadas, I., Rodriguez, J., Galindo, J. (2018), Concentrated solar energy used for heat treatment of Ti6Al4V alloy manufactured by selective laser melting, *Solar Energy*, vol.173,pp.76-88.

Chraponski, J., and Szkliniarz, W. (2001), Quantitative metallography of two-phase titanium alloys, *Material Characterization*, vol. 46,pp.149-154.

Cormier, D., Harryson, O., West, H. (2004), Characterization of H13 steel produced via electron beam melting, *Rapid Prototyping Journal*, vol. 10,pp.35-40.

Cunningham, R., Narra, SP., Montgomery, C., Beuth, J., Rollet, AD. (2016), Synchrotron based X-ray microtomography characterization of the effect of processing variables on porosity formation in laser powder-bed additive manufacturing of Ti6Al4V, *Journal of Minerals, Metals and Materials*,pp.2-7.

Damkroger, BK., Dixon, RD., Cotton, JD. (1994), Microstructure and mechanical properties of Ti6Al4V welds with filler additions of tantalum and FS58, *Office of Science*, vol. 273,pp.10-15.

Donachie, MJ. (2000), Titanium: A technical guide, 2nd edition, ASM international.

Dong, E., Yu, W., Cai, Q. (2017), Alpha-case kinetics and high temperature plasticity of Ti6Al4V alloy oxidized in different regions, *Procedia Engineering*, vol. 207,pp.2149-2154.

Eklund, A., Ahlfos, M., Bahbou, F., Wedenstrand, J. (2018), Optimizing HIP and printing parameters for EBM Ti6Al4V, *Key Engineering Materials*, vol. 770,pp.174-178.

Eylon, D., and Froes, FH. (1990), Titanium Powder Metallurgy Products, 10th edition, ASM Handbook, vol. 2,pp.647-660.

Facchini, L., Magalini, E., Robotti, P., Molinari, A. (2009), Microstructure and mechanical properties of Ti6Al4V produced by electron beam melting of pre-alloyed powders, *Rapid Prototyping Journal*, vol. 15,pp.171-178.

Facchini, L., Magalini, E., Robotti, P., Molinari, A., Hoges, S., Wissenbach, K. (2010), Ductility of a Ti6Al4V alloy produced by selective laser melting of pre-alloyed powders, *Rapid Prototyping Journal*, vol. 16, no, 6,pp.450-459.

Fan, Z., Liu, G. (2011), Soldification behaviour of AZ91D alloy under intensive forced convection in the RDC process, *Acta Materialia*, vol. 53,pp.4345-4357.

Galarraga, H., Lados, DA., Dehoff, RR., Kirka, MM., Nandwana, P. (2016), Effect of the microstructure of Ti6Al4V ELI alloy fabricated by electron beam melting (EBM), *Additive Manufacturing*, vol. 10,pp.47-57.

Galarraga, H., Warren, RJ., Lados, DA., Dehoff, RR., Kirka, MM. (2017), Effect of heat treatment on the microstructure and properties of Ti6Al4V ELI alloy fabricated by electron beam melting (EBM), *Material Science and Engineering A*, vol. 685,pp.417-428.

Gao, X., Zeng, W., Zhang, S., Wang, Q. (2017), A study of epitaxial growth behaviors of equiaxed alpha at different cooling rates in near alpha titanium alloy, *Acta Materialia*, vol. 122,pp.296-309.

Gaytan, SM., Murr, LE., Medina, F., Martinez, E., Lopez, MI., Wicker, RB. (2009), Advanced metal powder based manufacturing of complex components by electron beam melting, *Materials Technology*, vol. 24,pp.181-190.

Gil, FJ., Ginebra, MP., Manero, JM., Planell, JA. (2001), Formation of α-Widmanstatten structure: effect of grain size and cooling rate on the Widmanstatten morphology and on the mechanical properties in Ti6Al4V, *Journal of Alloys and Compounds*, vol.329,pp.142-152.

Gong, H., Rafi, K., Gu., H., Starr, T., Stucker, B. (2014), Analysis of defect generation in Ti6Al4V parts made using powder bed fusion additive manufacturing process, *Additive Manufacturing*, Vol. 4, pp.87-98.

Gong, X., Anderson, K., Chou, K. (2012), Review on powder-based electron beam additive manufacturing technology, *Manufacturing Review*, vol. 1, no, 2,pp.507-515.

Gu, D., Hagedom, YC., Meiners, W., Meng, G., Batista, RJS., Wissenbach, K., Poprawe, R. (2012), Densification, microstructure evolution and wear performance of selective laser melting processed pure titanium, *Acta Materialia*, vol. 60,pp.3849-3860.

Gulzar, J., Akhter, JI., Ahmad, M., Ali, G., Manhood, M., Ajmal, M. (2009), Microstructure evolution during surface alloying of ductile iron and austempered ductile iron by electron beam melting, *Applied Science Surface*, vol. 255,pp.8527-8532.

Gupta, A., Khatirkar, RK., Kumar, A., Parihar, MS. (2018), Investigations on the effect of heating temperature and cooling rate on evolution of microstructure in α+β titanium alloy, *Material Research Society*, vol. 54,pp.1-12.

Han, J., Yang, J., Yu, H., Yin, J., Gao, M., Wang, Z., Zeng, X. (2017), Microstructure and mechanical properties of selective laser melted Ti6Al4V dependence on laser energy density, *Rapid Prototyping Journal*, vol. 23,pp.217-226.

He, J., Li, D., Jiang, W., Ke, L., Qin, G., Ye, Y., Qin, Q., Qui, D. (2019), The Martensitic Transformation and Mechanical Properties of Ti6Al4V Prepared via Selective Laser Melting, *Materials*, vol. 12, no, 321,pp.1-14.

Hrabe, N., and Quinn. T. (2013), Effect of processing on microstructure and mechanical properties of titanium alloy (Ti6Al4V) fabricated using electron beam melting (EBM) part 1: Distance from build plate and part size, *Materials Science and Engineering A*, vol. 573,pp.264-270.

Ivanova, SG., Biederman, RR., Sisson Jr, RD. (2002), Investigation of fatigue crack initiation in Ti-6Al-4V during tensile-tensile fatigue, *Journal of Materials Engineering and Performance*, Vol. 11, No, 2,pp.226-231.

Joshi, VA. (2006), An Atlas of Structures and Fracture Features, Titanium Alloys, ISBN-9781420006063, 1st edition, CRC Press: Boca Raton, FL, USA.

Joshi, VA. (2006), An Atlas of Structures and Fracture Features, Titanium Alloys, CRC Press: Boca Raton, FL, USA.

Jovanovic, MT., Tadic, S., Zec, S., Miskovic, Z., Bobic, I. (2006), The effect of annealing temperatures and cooling rates on the microstructure and mechanical properties of invest cast Ti6Al4V alloy, *Material and Design*, vol. 27,pp.192-199.

Kasperovich, G., and Hausmann, J. (2015), Improvement of fatigue and ductility of Ti6Al4V processed by selective laser melting, *Journal of Materials Processing Technology*, vol. 220,pp.202-214.

Kasperovich, G., Haubrich, J., Gussone, J., Requena, G. (2016), Correlation between porosity and processing parameters in Ti6Al4V produced by selective laser melting, *Materials and Design*, vol. 105,pp.160-170.

Keist, JS., and Palmer, TA. (2017), Development of strength-hardness relationship in additively manufactured titanium alloys, *Material Science and Engineering*, vol. 693,pp.214-224.

Khorasani, A., Gibson, I., Golberg, M., Littlefait, G. (2017), On the role of different annealing heat treatments on mechanical properties and microstructure of selective laser melted and conventional wrought Ti6Al4V, *Rapid Prototyping Journal*, vol. 23,pp.295-304.

Knowles, CR., Becker, TH., Tait, RB. (2012), Residual stress measurements and structural integrity implications for selective laser melted Ti6Al4V, *South African Journal of Industrial Engineering*, vol. 23, no, 2,pp.119-129.

Kobryn, PA., and Semiatin, SL. (2001), The laser additive manufacturing of Ti6Al4V, *Journal of Minerals, Metal and Materials*, vol. 53,pp.40-43.

Koike, M., Martinez, K., Guo, L., Chahine, G., Kovacevic, R., Okabe, T. (2011), Evaluation of titanium alloy fabricated using electron beam melting system for dental applications, *Journal of Material Processing Technology*, vol. 211,pp.1400-1408.

Kruth, JP., Levy, G., Klocke, F., Childs, THC. (2007), Consolidation phenomena in laser and powder-bed based layered manufacturing, *Manufacturing Technology*, vol. 56, no, 2,pp.730-759.

Lamirand, M., Bonnentien, JL., Ferrierre, G., Guerin, S., Chevalier, JP. (2006), Effect of interstitial oxygen on microstructure and mechanical properties of Ti-48Al-2Cr-2Nb with fully lamella and duplex microstructure, *Metallurgical and Materials Transaction A*, vol. 37A,pp.2369-2378.

Lee, H., Lim, CHJ., Low, MJ., Tham, N., Murukeshan, VM., Kim, YJ. (2017), Lasers in additive manufacturing: A review. *International Journal of Precision Engineering and Manufacturing-Green Technology*, vol. 4, no,3,pp.307-322.

Leuders, S., Thone, M., Riemer, A., Niendorf, T., Troster, T., Richard, HA., Maier, HJ. (2013), On the mechanical behavior of titanium alloy Ti6Al4V manufactured by selective laser

melting: Fatigue resistance and crack growth performance, *International Journal of Fatigue*, vol. 48,pp.300-307.

Leyens, C. and Peters, M. (2003), Titanium and titanium alloys, Fundamental Applications, Wiley-VCH Verlag GmbH & Co. KGaA, Weinheim.

Li, H., Zhao, Z., Ning, Y., Guo, H., Yao, Z. (2018), Characterization of Microstructural Evolution for Near-α Titanium Alloy with Different Initial Lamella Microstructures, *Metals*, vol. 8, no, 1045,pp.1-17.

Liu, Q., Wang, Y., Zheng, H., Tang, K., Ding, Li., Li, H., Gong, S. (2016), Microstructure and mechanical properties of LMD-SLM hybrid forming Ti6AL4V alloy, *Material Science and Engineering*, vol. 660,pp.24-33.

Lutjering, G. (1998), Influence of processing on the Microstructure and Mechanical Properties of α + β Titanium Alloys, *Materials Science and Engineering*, vol. A243,pp.32-45.

Mahale, TR. (2014), (2009) Electron Beam Melting for advanced materials and structures, N.C. State University

Majumdar, T., Bazin, T., Ribeiro, E.M., Frith, E., Birbilis, N. (2019), Understanding the effect of PBF process parameter interplay on Ti6Al4V surface properties, *Plos One*, vol. 48,pp.2-24.

Markovskya, PE., and Semiatin, SL. (2011), Tailoring of microstructure and mechanical properties of Ti6Al4V with local rapid heat treatment, *Material Science and Engineering*, vol. A528, no,7-8,pp.3079-3089.

Mercelis, P., and Kruth. (2006), Residual stresses in selective laser sintering and selective laser melting, *Rapid Prototyping Journal*, vol. 12, no, 5,pp.254-265.

Moat, RJ., Pinkerton, AJ., Li, L., Withers, PJ., Preuss, M. (2011), Residual stresses in laser direct metal deposited Waspaloy, *Material Science and Engineering A*, vol. A528,pp.2288-2298.

Mower, TM., and Long, MJ. (2016), Mechanical behaviour additively manufactured powder-bed laser fused materials, *Material Science and Engineering A*, vol. 651,pp.198-213.

Mudge, RP., and Wald, NR. (2007), Laser engineered net shaping advances additive manufacturing and repair, *Welding Journal*, vol. 86,pp.44-48.

Murr, LE., Esquivel, EV., Quinones, SA., Gaytan, SM., Lopez, MI., Martinez, EY., Medina, F., Hernandez, DH., Martinez, E., Martinez JL., Stafford, SW., Brown, DK., Hoppe, T., Meyers, W., Lindle, U., Wicker, RB. (2009), Microstructure and mechanical properties of electron beam-rapid manufactured Ti6Al4V, *Materials Characterization*, vol. 60,pp.96-105.

Nalla, RK., Boyce, BL., Campbell, JP., Peters, JO., Ritchie, RO. (2002), Influence of microstructure on high-circle fatigue of Ti6Al4V: Bimodal vs Lamella structures, *Metallurgical and Materials Transactions,* vol. 33A, no,3,pp.899-918.

Paderson, R., Babushkin, O., Skystedt, F., Warren, R. (2001), The Use of High Temperature X-ray Diffractometry to Study Phase Transition in Ti6Al4V in Titanium Alloy at Elevated Temperature, *Structural Development and Science Behaviour*, Institute of Materials, ISNN 1336-5510, London.

Plaza, L., Irisarri, A., Gil-Negrete, A. (1990), Improvement of Ti6Al4V fracture toughness by sub-transus heat treatment, *Scripta Metallurgica*, vol. 24,pp.1765-1769.

Poondla, N., Srivatsan, TS., Patnaik, A., Petraroli, M. (2009), A study of the microstructure and hardness of two titanium alloy: Commercially pure and Ti6Al4V, *Journal of Alloys and Compounds*, vol. 486,pp.162-167.

Qian, M., Xu, W., Brandt, M., Tang, HP. (2019), Additive manufacturing and post processing of Ti6Al4V for superior mechanical properties, *Materials Research Society*, vol. 41,pp.775-783.

Qiu, C., Adkins, JEN., Attallah, MM. (2013), Microstructure and tensile properties of selectively laser melted and of HIPed Ti6Al4V, *Material Science and Engineering A*, vol. 578,pp.230-239.

Qiu, C., Ravi, GA., Dance, C., Ranson, A., Dilworth, S., Attar, MM. (2015), Fabrication of large Ti6Al4V structures by direct laser deposition, *Journal of Alloys and Compounds*, vol. 269,pp.351-361.

Rafi, HK., Karthik, NV., Gong, H., Starr, TL., Stucker, BE. (2013), Microstructure and mechanical properties of Ti6Al4V parts fabricated by selective laser melting and electron beam melting, *Journal of Material Engineering and Performance*, vol. 22, no, 12,pp.3872-3883.

Ramosoeu, ME., Chikwanda, HK., Bolokang, AS., Booysen, G., Ngonda, TN. (2010), Assitive Manufacturing: Characterization of Ti6Al4V alloy intended for biomedical application, *The*

South African Institute of Mining and Metallurgy Advance Metal Initiative Light Metal Conference,pp.337-344.

Roberts, IA., Wang, CJ., Esterlein, R., Stanford, M., Mynors, DJ. (2009), A three dimensional finite element analysis of the temperature field during laser melting of metal powders in additive layer manufacturing, *International Journal of Machine Tool and Manufacture*, vol.49,pp.916-923.

Rovelo, P., and Fraunhofer IF. (2016), AM Dresden orders new facility for Selective Electron Beam Melting with ARCAM, 3D printing industry.

Roy, S., and Suwas, S. (2017), Orientation dependent spheroidization response and macrozone formation during sub β-transus processing of Ti6Al4V alloy, *Acta Materialia*, vol. 134,pp.283-301.

Sabban, R., Bahl, S., Chatterjee, K., Suwan, S. (2019), Globularization using heat treatment in additively manufactured Ti6Al4V, *Acta Materialia*, vol. 162,pp.239-254.

Safdar, A., Wei, LY., Snis, A., Lai, Z. (2012), Evaluation of microstructural development in electron beam melted Ti6Al4V, *Materials Characterization*, vol. 65,pp.8-15.

Sallica-Leva, E., Caram, R., Jardini, AL., Fogagnolo, JB. (2016), Ductility improvement due to martensitic α' decomposition in porous Ti6Al4V parts produced by selective laser melting for orthopaedic implants, *Journal of the Mechanical Behaviour of Biomedical Materials*, vol. 54,pp.149-158.

Schwerdtfeger, J., Heinl, P., Singer, RF., Korner, C. (2009), Selective electron beam melting: a new way to auxetic cellular structures. *Proceeding of the 20th Annual International Solid Freeform Fabrication Proceedings*, Austin, TX, August 3-5,pp.724-729.

Semiatin, SL., Seetharaman, V., Weiss I. (1997), The Thermomechanical Processing of Alpha/Beta Titanium alloys, *Metals*, vol. 49,pp.33.

Shap, H., Zhao, Y., Ge, P., Zeng, W. (2013), Influence of cooling rate and aging on the lamella microstructure and fractography of TC21 titanium alloy, *Metallography, Microstructure, and Analysis*, vol. 2,pp35-41.

Shipley, H., McDonnell, D., Culleton, R., Coull, R., Lupoi, G., Odonell, D., Trimble, D. (2018), Optimization of process parameters to address fundamental challenges during selective laser

melting of Ti6Al4V: A review, *International Journal of Machine Tool and Manufacture*, vol. 128,pp.1-20.

Sieniawski, J., Ziaja, W., Kubiak, K., Motyka, M. (2013), Microstructure and mechanical properties of high strength two-phase titanium alloys, *Titanium Alloys*, Chapter 4,pp.69-80.

Simonelli, M., Tse, YY., Tuck, C. (2014), On the texture formation of selective laser melted Ti6Al4V, *Metallurgical and Materials Transactions*, vol. 45A,pp.2863-2872.

Song, B., Dong, B., Zhang, B., Liao, H., Coddet, C. (2012), Effect of processing parameters on microstructure and mechanical property of selected laser melting Ti6Al4V, *Material Design*, vol. 35,pp.120-125.

Ter Haar, GM., and Becker, TH. (2018), Selective Laser Melting Produced Ti6Al4V: Post-Process Heat Treatments to achieve Superior Tensile Properties, *Materials*, vol. 11,pp.1-15.

Thijs, L., Verhaeghe, F., Craeghs, T., Van Humbeeck, J., Peirre Kruth, J. (2010), A study of the microstructural evolution during selective laser melting of Ti6Al4V, *Acta Materialia*, vol. 58,pp.3303-3312.

Tiferet, E., Rivin, O., Ganor, M., Ettedgui, H., Ozeri, O., Caspi, EN., Yeheskel, O. (2016), Structural investigation of selective laser melting and electron beam melting of Ti6Al4V using neutron diffraction, *Additive Manufacturing*, vol. 10,pp.3-46.

Tong, J., Bowen, CR., Persson, J., Plummer, A. (2017) Mechanical properties of titanium based Ti6Al4V alloy manufactured by powder bed additive manufacture, *Material Science and Technology*, vol. 33,pp.138-148.

Villaro, T., Colin, C., Bartout, JD. (2011), As-Fabricated and Heat-Treated Microstructures of the Ti6Al4V Alloy Processed by Selective Laser Melting, *Metallurgical and Materials Transactions*, vol. 42A,pp.3190-3199.

Vrancken, B., Thijs, L., Kruth, PJ., Van Humbeeck, J. (2012), Heat treatment of Ti6Al4V produced by Selective Laser Melting: Microstructure and mechanical properties, *Journal of Alloys and Compounds*, vol. 541,pp.177-185.

Wang, L., and Felicelli, S. (2007), Influence of process parameters on the phase transformation and consequent hardness induced by the LENS process, *Material Processing Fundamentals*, pp.63-72.

Wanying, L., Yuanhua, L., Yuhai, C., Taihe, S., Singh, A. (2017), Effect of Different Heat treatments on Microstructure and Mechanical Properties of Ti6Al4V Titanium Alloy, *Rare Metal Materials and Engineering*, vol. 46,pp.0634-0639.

Warnke, PH., Douglass, T., Wollny, P., Sharry, E., Steiner, M., Galonska, S., Becker, ST., Springer, IN., Wiltfang, J., Sivananthan, S. (2009), Rapid Prototyping: Porous titanium alloy scaffolds produced by selective laser melting for bone tissues, *Tissue Engineering*, vol. 15,pp.115-124.

Weiss, I., Froes, FH., Eylon, D., Welsh, GE. (1986), Modification of Alpha Morphology in Ti6Al4V by Thermomechanical Processing, *Metal Transition*, vol. 17A,pp.1947-1953.

William, JC., and Starke jnr EA. (2003), Progress in structural materials for aerospace systems, *Acta Materialia*, vol. 51, no, 19,pp.5775-5799.

Wong, KV., and Hernandez, A. (2012), A Review of Additive Manufacturing, *Mechanical Engineering*, vol. 6,pp.1-11.

Wu, SQ., Lu, YJ., Gan, YL., Huang, TT., Zhao, CQ., Lin, JJ., Guo, S., Lin, JX. (2016), Microstructural evolution and microhardness of selective-laser-melted Ti6Al4V alloy after post heat treatments, *Journal of Alloys and Compounds*, vol. 672,pp.643-652.

Wysocki, B., Maj, P., Krawczynska, A., Rozniatowski, K., Zdunek, J., Kurzydlowski, KJ., Swieszkowiski,W. (2017), Microstructure and mechanical properties investigation of CP titanium processed by selective laser melting (SLM), *Journal of Material Processing Technology*, vol. 241,pp.13-23.

Xu, W., Brandt, M., Sun, S., Elambasseril, J., Liu, Q., Latham, K., Xia, K., Qian, M. (2015), Additive manufacturing of strong and ductile Ti6Al4V by selective laser melting via martensite decomposition, *Acta Materialia*, vol. 85,pp.74-84.

Yadroitsev, I., Krakhmalev, P., Yadroitsava, I. (2014), Selective laser melting of Ti6Al4V alloy for biomedical application: Temperature monitoring and microstructural evolution, *Journal of Alloys and Compounds*, vol. 53,pp.404-409.

Yan, M., and Yu, P. (2015), An overview of densification, microstructure and mechanical properties of additively manufactured Ti6Al4V-comparison among selective laser melting, electron beam melting, laser metal deposition and selective laser sintering, and with conventional powder, *Sintered Material Technology*, vol. 23,pp.374-386.

Yan, W., Lin, S., Kafka, OL., Yu, C., Liu, Z., Lian, Y., Wolff, S., Cao, J., Wagner, GJ., Liu, WK. (2018), Modelling process-structure –property relationships for additive manufacturing, *Frontier of Mechanical Engineering*, vol. 13, no, 4,pp.482-492.

Yu, P., Qian, M., Tomus, D., Brice, CA., Schaffer, GB., Muddle, BC. (2009), Electron beam processing of aluminum alloys, *Material Science Forum*, vol. 618,pp.621-626.

Zah, MF., Lutzmann, S. (2010), Modelling and simulation of electron beam melting, *Production Engineering*, vol. 4,pp.15-23.

Zhai, Y., Galarraga, H., Lados, DA. (2016), Microstructure, static properties and fatigue crack growth mechanisms in Ti6Al4V fabricated by additive manufacturing: LENS and EBM, *Engineering Failure Analysis*, vol. 69,pp.3-14.

Zhai, Y., Lados, DA., Brown, EJ., Vigilante, GN. (2016), Fatigue crack growth behavior and microstructural mechanism in Ti6Al4V manufactured by laser engineered net shaping, *International Journal of Fatigue*, vol. 93,pp.51-63.

Zhang, X., Fang, G., Leeflang, S., Bottger, AJ., Zadpoor, AA., Zhou, J. (2018), Effect of subtransus heat treatment on the microstructure and mechanical properties of additively manufactured Ti6Al4V alloy, *Journal of Alloys and Compounds*, vol. 735,pp.1562-1575.

Zhao, Z., Chen, J., Tan, H., Zhang, G., Lin, X., Huang, W. (2018), Achieving superior ductility for laser solid formed extra low interstitial Ti6Al4V titanium alloy through equiaxial alpha microstructure, S*cripta Materialia*, vol. 146,pp.187-191.

Zheng, Z., Waneed, S., Balint, DS., Dunne, FPE. (2018), Slip transfer across phase boundaries in dual phase titanium alloys and effect on strain rate sensitivity, *International Journal of Plasticity*, vol. 104,pp.23-38.

Zuback, J.S and Debroy T. (2018), The hardness of additively manufactured alloys, *Materials*, vol. 11,pp.2-41.

Appendix A: Metals Journal article 2021

metals

MDPI

Article

Evaluation of Heat Treatment Parameters on Microstructure and Hardness Properties of High-Speed Selective Laser Melted Ti6Al4V

Paul Lekoadi [1,2,*], Monnamme Tlotleng [1,3], Kofi Annan [4], Nthabiseng Maledi [2] and Bathusile Masina [1,*]

[1] Council for Scientific Industrial Research (CSIR), Manufacturing, National Laser Centre, Laser Enabled Manufacturing Group, P.O. Box 395, Pretoria 0001, South Africa; MTlotleng@csir.co.za
[2] School of Chemical and Metallurgical Engineering, University of Witwatersrand, Private Bag 3, Wits, Johannesburg 2050, South Africa; Nthabiseng.maledi@wits.ac.za
[3] Department of Mechanical Engineering Science, University of Johannesburg, Auckland Park Campus, Johannesburg 2012, South Africa
[4] Department of Material Science and Metallurgical Engineering, University of Pretoria, Mineral Science Building, Pretoria 0001, South Africa; Kofi.annan@up.ac.za
* Correspondence: PLekoadi@csir.co.za (P.L.); BMasina@csir.co.za (B.M.); Tel.: +27-012-841-4619 (P.L.); +27-012-841-2121 (B.M.)

Abstract: This study presents the investigation on how heat treatment parameters, which are temperature, cooling method, and residence time, influence the microstructural and hardness properties of Ti6Al4V components produced on Ti6Al4V substrate using high speed selective laser melting technique. Heat treatment was performed on the produced samples before they were characterized for microstructure and hardness. The microstructure of the as-built sample contained large columnar β-grains that were filled with martensite α′ phase and had a high hardness of 383 ± 13 HV. At 1000 °C and residence time of maximum 4 h, better heat treatment parameters were seen for the selective laser melting (SLM) produced Ti6Al4V sample since an improved lamellar α + β microstructure was obtained at this condition. This microstructure is known to have improved tensile properties.

Keywords: selective laser melting; heat treatment; temperature; cooling method; residence time; microstructure; hardness

check for updates

Citation: Lekoadi, P.; Tlotleng, M.; Annan, K.; Maledi, N.; Masina, B. Evaluation of Heat Treatment Parameters on Microstructure and Hardness Properties of High-Speed Selective Laser Melted Ti6Al4V. *Metals* **2021**, *11*, 255. https://doi.org/10.3390/met11020255

Received: 27 December 2020
Accepted: 16 January 2021
Published: 3 February 2021

1. Introduction

Selective laser melting (SLM) is a type of powder bed fusion (PBF) additive manufacturing (AM) technology that creates near net 3D shapes by using a laser as an energy source to melt a metallic powder layer-by-layer according to control aided design (CAD) models [1–3]. The fundamentals of SLM processing are discussed elsewhere [3]. SLM is regarded as a revolutionary manufacturing technique since it is precise when printing

Publisher's Note: MDPI stays neutral with regard to jurisdictional claims in published maps and institutional affiliations.

Copyright: © 2021 by the authors. Licensee MDPI, Basel, Switzerland. This article is an open access article distributed under the terms and conditions of the Creative Commons Attribution (CC BY) license (https://creativecommons.org/licenses/by/4.0/).

regarded as a revolutionary manufacturing technique since it is precise when printing parts with complex geometries and high dimensional accuracy [4,5]. Furthermore, SLM is famously known to process various metallic powders and their alloys [6]. Titanium alloy, Ti6Al4V (also abbreviated as Ti64), has properties that are promising for high-end structures; hence, it is regard best for biomedical and aerospace engineering applications [7]. Ti6Al4V can be manufactured with ease into artifact using conventional processes [2,3]; however, in recent years, the developments of using SLM to produce Ti6Al4V components have been a subject of interest [7].

Ti6Al4V is composed of two primary stable phases commonly known as alpha (α) and beta (β). However, due to high heating and cooling rates that are associated with the SLM process, the microstructure of SLM produced Ti6Al4V parts is characterized by a single acicular sharp martensitic α′ phase [8,9]. The martensite α phase is undesired for many applications, including aerospace, since it is associated with microstructural inhomogeneity, high hardness, low tensile elongation, and high residual stresses [10–12]. This implies that SLM produced Ti6Al4V components requires post-processing techniques, such as heat treatment, before they can be used.

Heat treatment is typically applied to SLM produced Ti6Al4V components since it can, in addition to relieving a print of the inherent internal thermal stresses, dissolve and transform the metastable α′ phase into a desired microstructure with improved mechanical properties [13]. In order to achieve a fully transformed and superior two phase (α + β) Ti6Al4V through post-heat treatment, it is critical to understand the role of heat treatment parameters, such as temperature, cooling method, and residence time, individually and in collective, on the improvement of microstructure and mechanical properties of Ti6Al4V.

Wu et al. [14] using laser power and scanning speed of 95 W and 900 mm/s and layer thickness of 25µm, were able to SLM 3D print Ti6Al4V cubes, which they used to for heat treatment studies. Specimens were heat-treated to different temperatures that varied from 300–1020 °C, followed with water quenching (WQ). The microstructure of the as-printed sample was characterized with a columnar prior β grains that were filled with martensite α′ phase. The columnar grains were associated with epitaxial growth of the β phase while the martensite α′ phase was associated with high cooling rates that are prevalent during SLM processing. A similar SLM microstructure has been reported by several other independent authors [3,12,15]. Post-heat treatment, at 600 °C, Wu et al. [14] did not observe any phase transformation or microstructural change. A change in microstructure was reported in the samples that water quenched after heat treatment in the temperature range between 750–950 °C.

In a different, but related, study, Chicos et al. [15] manufactured cylindrically shaped Ti6Al4V specimens from an SLM machine using laser power of 200 W, layer thickness of 25 µm, hatch spacing of 0.095 m, and scanning speed in the range 1200–1500 mm/s and performed heat treatment on the produced specimens. Samples were heat treated to 705 °C, 850 °C, 940 °C, 1015 °C, and 1050 °C for 2 h in a solar furnace at heating rate of 60 °C and gas flow rate of 200 L/min. Two methods of cooling (furnace cooling (FC) and air cooling (AC)) were used; in this paper, however, results on furnace cooling are reviewed. A phase transformation from fully martensitic α′ structure to a microstructure that contained a mixture of α′, α, and β phase with retained prior β grains was reported for sample that was heat treated to 705 °C. At 850 °C, the sample was characterized of a microstructure that consisted of needle-like α′ and lamella α + β phases in a basket weave structure, while, at 940 °C, the authors reported a microstructure that consisted of mixture of α and β phases, with the columnar β grains no longer visible. This means that a full transformation was observed beginning at 940 °C. Heat treatment at 1015 °C produced a microstructure that contained large α-colonies. The observed α-phase were transformed into equiaxial grains. A full transformation of martensitic structure into a lamellar α structure in the βmatrix was achieved. Finally, 1050 °C produced a microstructure that was composed of a mixture of lamellar α + β, with the α-colonies forming into a basket weave structure and nucleating at the grain boundaries of big β grains.

Finally, Zhang et al. [12] conducted heat treatment on Ti6Al4V samples that were produced with a laser power of 200 W, layer thickness of 30 µm, and scanning speed of 80 mm/s from SLM machine. Samples were heat treated to temperatures of 800 °C and 900 °C, independently, while holding for 2 h (residence time) and followed by cooling in air (AC) and inside the furnace (FC). This study reported a microstructure that contained a high-volume fraction of α and β phase for both heating temperatures. In addition, a grain growth for the α phase was reported at 800 °C. Although these reviewed studies show that heat treatment can be used to obtain various type of microstructures which are obviously characterized by different mechanical properties [3,12,14–16], a broader understanding into the effects of all these heat treatment parameters, concurrently, is yet not fully understood. This study focused on investigating the effect of heat treatment parameters (temperature, cooling method, and residence time) on the microstructure and hardness properties of Ti6Al4V parts produced from a high-speed SLM.

2. Experimental Procedure

2.1. Materials

Spherical grade 5, pre-alloyed Ti6Al4V powder with particle size distribution in the range 20–60 µm was used as a deposition material during printing of the samples. The powder was produced and supplied by TLS Technik GMbH & Co (Bitterfeld, Germany) and was used as received. SEM image of the Ti6Al4V powder is shown in Figure 1.

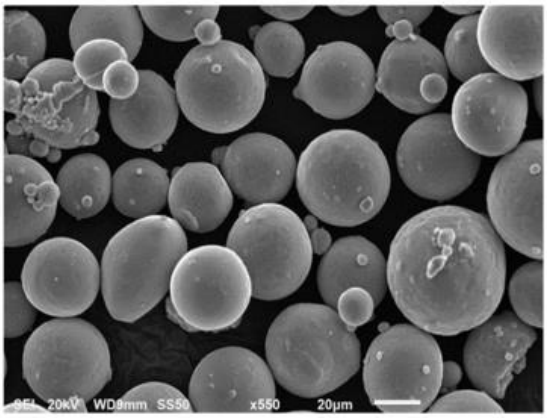


Figure 1. SEM image of the pre-alloyed Ti6Al4V Powder.

Figure 1 shows that the powder particles were spherical in shape, with no porosity and surface roughness observed. The samples were printed on an acetone rinsed Ti6Al4V base plate, which was used as a substrate.

2.2. Methods

All test samples were manufactured from the Aeroswift 3D printing SLM machine that is available in Pretoria, South Africa. The Aeroswift machine was equipped with a high power 5 kW single Ytteribium laser, with a wavelength of 1076 nm, and a build platform with a volume of 2000 mm × 600 mm × 600 mm. The powder was dried at 120 °C for 2 h in order to remove the moisture before it was processed. Moreover, before the actual printing of the samples could commence, the oxygen content inside the building chamber was reduced to 300 ppm by purging with inert argon gas with purity of 99.99%, and the base plate was pre-heated to a temperature of 200 °C. It is understood that this temperature could help with the reduction of thermal stresses build-up during printing. Post-sample manufacturing, a wire cutter was used to remove the samples from the base plate.

Samples were cut into smaller specimens using a Struers Labotom-5 cutting machine (manufactured by Struers Company, Cleveland, TN, USA) with a high-quality titanium cut-off wheel (20 S25) for metallurgic preparations and heat treatment. All test samples were heat-treated in a horizontal Lenton LFT model furnace (manufactured by Lenton Company, Randburg, South Africa) with an internal tube diameter of 1 m. The image of the heat treatment furnace is shown in Figure 2.

During heat treatment, oxygen concentration inside the furnace was reduced to 200 ppm by purging with argon gas. Gas was kept flowing continuously at a gas rate of 0.8 litres per minute during heat treatment so to avoid oxidation of the Ti6Al4V samples. The furnace is equipped with a K-type thermocouple that was used to measure the temperature inside the furnace during heat treatment. To evaluate the influence of heat treatment temperature, the samples were heat treated to temperatures of 700 °C, 950 °C and 1000 °C, respectively, at the heating rate of 4 °C/min for 2 h and cooled using furnace cooled (FC) method. During heat treatment, samples were placed on a hanging wire, which served as a sample holder.



Figure 2. Heat treatment furnace available at the University of Pretoria, South Africa.

To evaluate the influence of cooling method, all the test samples were heat-treated to a temperature of 1000 °C at a heating rate of 4 °C/min and held for 2 h and cooled using three different methods, which are water quenching (WQ), air cooling (AC), and furnace cooling (FC). The WQ samples were immersed in a beaker full of tap water, while AC were left-out in an open to cool at room temperature. For the evaluation of residence time, samples were heat treated to 1000 °C, while holding time was varied from 2 h, 4 h, and 8 h, respectively, followed with FC.

The as-built and heat-treated samples were then mounted using an AMP 50 automatic mounting press machine (Beijing, China). AKA Resin Phenolic SEM black conductive resin was used to mount all specimens. Mount specimens were mechanically ground with Struers Tetrapol-25 grinding and polishing machine (manufactured by Struers Company, Cleveland, TN, USA). Silicon carbide (SiC) grinding papers with grit sizes of 80, 320, 1200, and 4000 were used for grinding the specimens, which were later surface finished by polishing to a mirror finish using Diapro MD-Mol 3 µm diamond suspension and colloidal silica 0.04 µm OP-S suspension for 3 min. The specimens were etched with Kroll's reagents, a solution containing 100 mL H_2O, 1–3 mL HF, and 2–6 mL HNO_3. Samples were immersed in the etchant for about 10–15 s.

The metallographically prepared and etched specimens were observed for microstructure using an Olympus BX51M Optical microscope (manufactured by Olympus, Melville, NY, USA). To observe full view of the microstructure, microstructural images were taken using various magnifications of 5×, 10×, 20×, and 50×. Hardness measurements were performed using Matsuzawa Seiko Vickers model MHT−1 micro-hardness machine (manufactured in Kawabe, Japan). All measurements were done using a diamond type of indenter and applying a force of 0.3 kgf and dwell time of 10 s. For all samples, three hardness patterns were measured, and the average was calculated as the hardness of the material.

3. Results

Obtained result, for both as-built and heat treated samples, are reported in this section.

3.1. Microstructures

3.1.1. Influence of Temperature

The samples were heat treated to 750 °C, 950 °C, and 1000 °C for 2 h, followed with FC. The microstructures of the as-built and heat-treated samples are shown in Figure 3. For clear microstructural observation, the zoom in areas (on the microstructure) are indicated by red circles on all the microstructures.

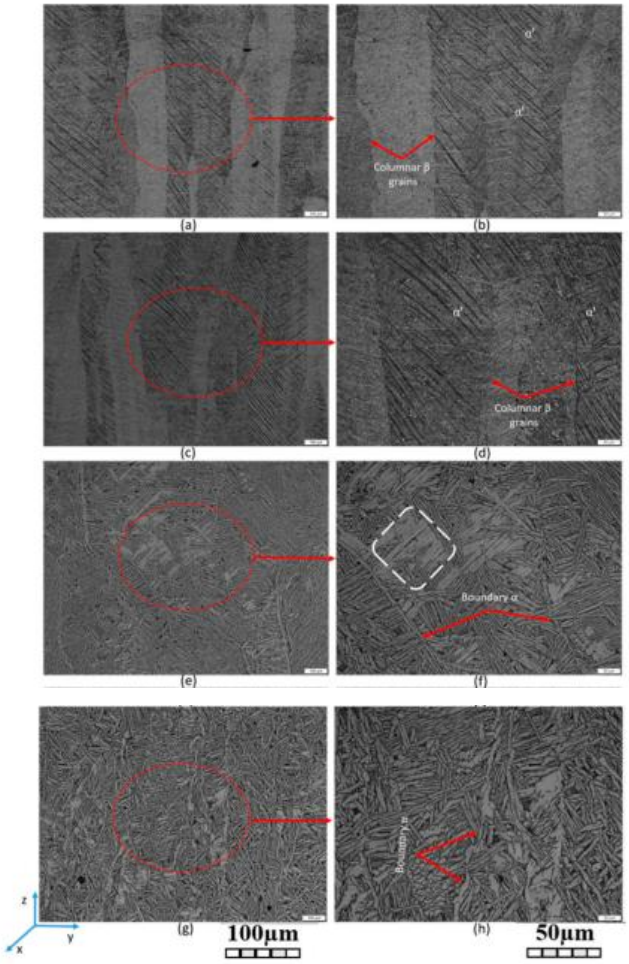


Figure 3. Optical microstructures of the samples: (**a**) As-built; (**b**) as-built zoom in; (**c**) 700 °C; (**d**) 700 °C zoom in; (**e**) 950 °C; (**f**) 950 °C zoom in; (**g**) 1000 °C; (**h**) 1000 °C zoom in.

The as-built sample revealed large columnar β grain that were in parallel to the built direction (z-axis), as shown in Figure 3a. These columnar grains are common on the microstructure of SLM processed Ti6Al4V [12,15] because they result from partial re-melting of the previously built layers as a new layer is scanned by the laser beam [1,17]. Inside these large columnar β grains, a fine needle-like martensite α′ phase was observed, as shown in Figure 3b. This martensite α′ phase is metastable and is formed by high heating and cooling rates experienced by the built samples during the SLM process [9,18].

Heat treatment at 700 °C did not initiate any observable microstructural change, as can be seen in Figure 3c. This was because the microstructure of as-built and 700 °C heat treated samples were observed to be similar in terms of phases and grain orientation. Temperature

of 700 °C is considered a low temperature that can be used to relieve residual thermal stress [8,14,19]. Ter Haar and Becker [11] categorized 700 °C as temperature in the low heat treatment strategy and further recommended it for stress relief purposes. The columnar β grains, together with the martensite α′ phase, were clearly visible after heat treatment at 700 °C, as shown in Figure 3d.

A clear microstructural transformation was observed after heat treatment at 950 °C. The metastable martensite α′ structure was fully transformed into more stable lamella α + β morphology. The observed phase transformation resulted in the changing of the columnar β grains into equiaxed shape, as can be seen in Figure 4e. This implies that 950 °C was able to fully transform the metastable martensite α′ phase. This observation was expected because 950 °C is a temperature slightly below the β-transus temperature for Ti6Al4V. Figure 3f shows that a process of grains growth (area marked in white in Figure 3f) was taking place, with more α-phase growing on the boundaries of the β grain. A similar observation of large amount of grain growth was observed after heat treatment of Ti6Al4V at 950 °C for 1 h [20].

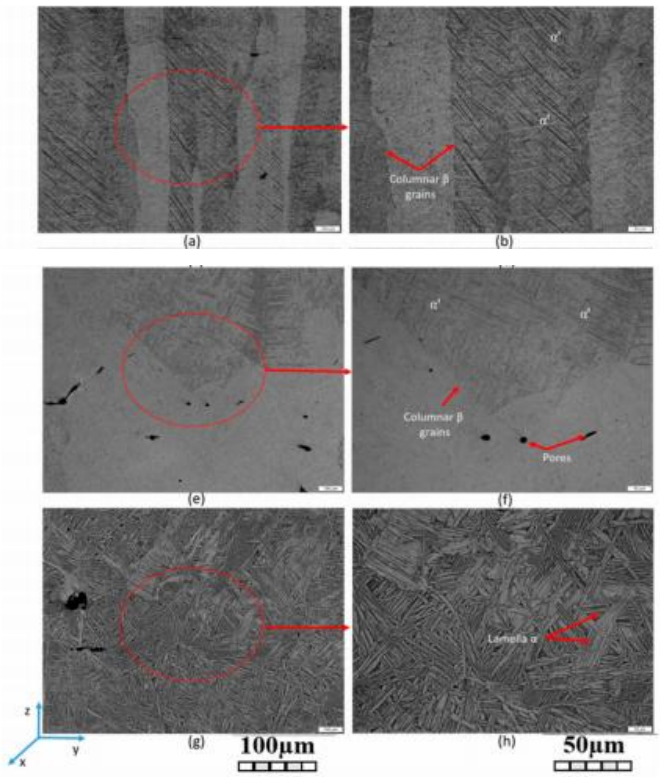


Figure 4. Optical microstructures of the samples: (**a**) As-built; (**b**) as-built zoom in; (**c**) water quenching (WQ); (**d**) WQ zoom in; (**e**) air cooling (AC); (**f**) AC zoom in; (**g**) furnace cooling (FC); (**h**) FC zoom in.

Heat treatment at 1000 °C resulted in growth of the lamella α + β phases, as can be seen in Figure 3g. This is emphasized more by growth of the α-phase on the grain boundaries of the β grain, as shown in Figure 3h. The grain growth was associated with the 1000 °C because it is a temperature above β-transus of Ti6Al4V. According to the phase diagram of Ti6Al4V, heat treating above β-transus transforms all the phases into β-phase, which results in growth of the β-phase. Since 1000 °C is above 950 °C, heat treatment at 1000 °C also resulted in complete transformation of the martensite α′ phase into stable lamella α + β phases. The same reason accounted for the disappearance of the large columnar β grains on the microstructure of the 1000 °C heat-treated sample (Figure 3g).

3.1.2. Influence of Cooling Method

The samples were heat treated to 1000 °C for 2 h, followed by cooling with water quenching (WQ), air cooling (AC), and furnace cooling (FC). Figure 4 shows the microstructure of the as-built and heat-treated samples. For clear microstructural observation, the zoom in areas are indicated by red circles on all the microstructures.

Cooling with WQ resulted in the introduction of a newly formed martensite α′ phase, which was distributed throughout the entire sample, as shown in Figure 4c. In other word, WQ resulted in the formation of a fully martensitic α′ microstructure. Obviously, this was due to the high cooling rate linked with the WQ method [21]. The large columnar β grains were observed on the microstructure of the sample that was WQ. Similarly, the microstructure of the sample that was AC also showed a fully martensitic α′ structure as presented in Figure 4d. However, the type of martensite α′ phase introduced by the AC was finer compared to the one on the as-built and WQ samples. A similar type of finer microstructure was obtained by Matthys [20], after WQ from 870 °C. This martensite α′ phase resulted from the high cooling rate associated with the AC method [21].

The microstructure of the FC sample showed different characteristics compared to the as-built, WQ and AC samples. The FC method resulted in the elimination of the undesired metastable martensite α′ phase, with the microstructure taking a fully lamella α + β morphology as shown in Figure 4h. Most importantly, FC leads to grain growth. The grain growth was due to the slow cooling rates offered by the FC method [21]. A basket weave type of α + β morphology was observed on the microstructure of this sample.

3.1.3. Influence of Residence Time

The study of residence time was conducted by heat treating the sample to 1000 °C for various residence times of 2 h, 4 h, and 8 h. The microstructures of the sample before and after heat treatment are represented in Figure 5. For clear microstructural observation, the zoom in areas are indicated by red circles on all the microstructures.

The large columnar β grains were no longer visible after heat treatment for 2 h, as can be seen in Figure 5c. In addition, heat treatment for 4 h transformed the microstructure into fully α + β. This implies that 4 h residence time was sufficient to allow full transformation of the martensite α′ phase to occur, while allowing the lamella α + β grains to grow. The evidence of grain growth was observed more on grain boundaries of the β grains as shown in Figure 5d. Heat treatment for 4 h resulted in more grain growth, with formation of large α-colonies in a basket weave morphology as presented in Figure 5e.

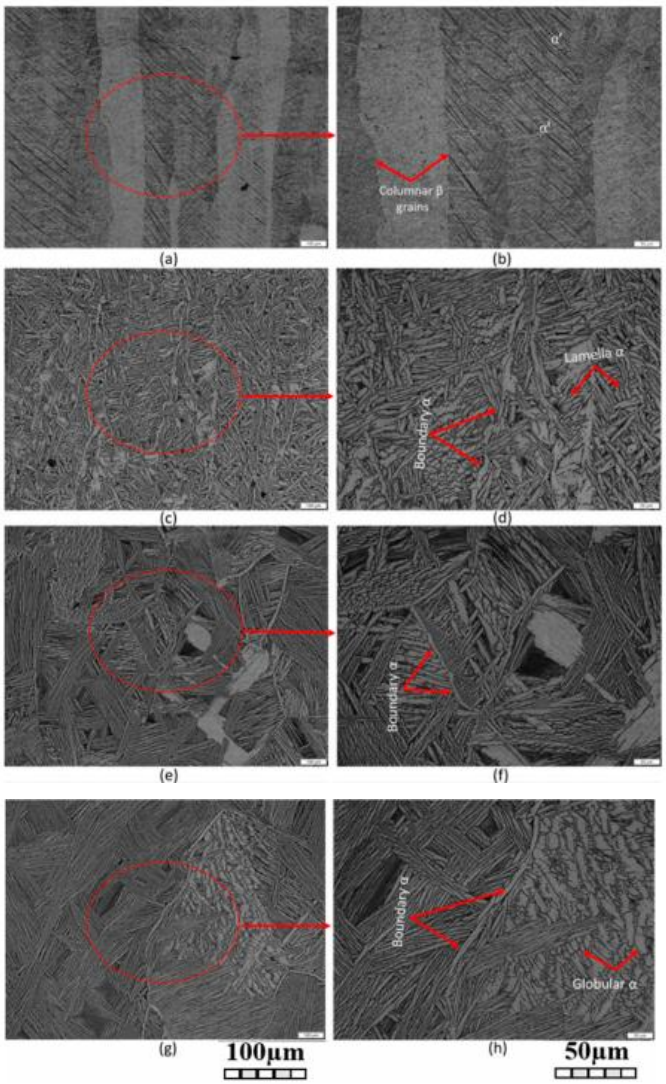


Figure 5. Optical microstructures of the samples: (**a**) As-built; (**b**) as-built zoom in; (**c**) 2 h; (**d**) 2 h zoom in; (**e**) 4 h; (**f**) 4 h zoom in; (**g**) 8 h; (**h**) 8 h zoom in.

Heat treatment for 8 h resulted in the thickening of the α-phase at the grain boundaries, as shown in Figure 5h. Furthermore, heat treatment for 8 h initiated the process of α-phase globularization, as depicted in Figure 5h. Since 8 h is regarded as longer residence time [16], globularization of the α-phases formed due to boundary splitting of the α-phase through thickening of the lamella α-phase [22]. In addition, the globularization of the phases originated at the boundaries of the β grains, as can be seen in Figure 5h. This was because of the α-phases at the grain boundaries, which are shorter than the other lamella α-phases, and, therefore, tend to globularize quicker. The α-colonies were clearly visible after heat treatment for 8 h (Figure 5g).

3.2. *Hardness*

3.2.1. Influence of Temperature

Figure 6 and Table 1 present the graph showing hardness profiles and average hardness of the as-built and heat-treated samples, respectively.

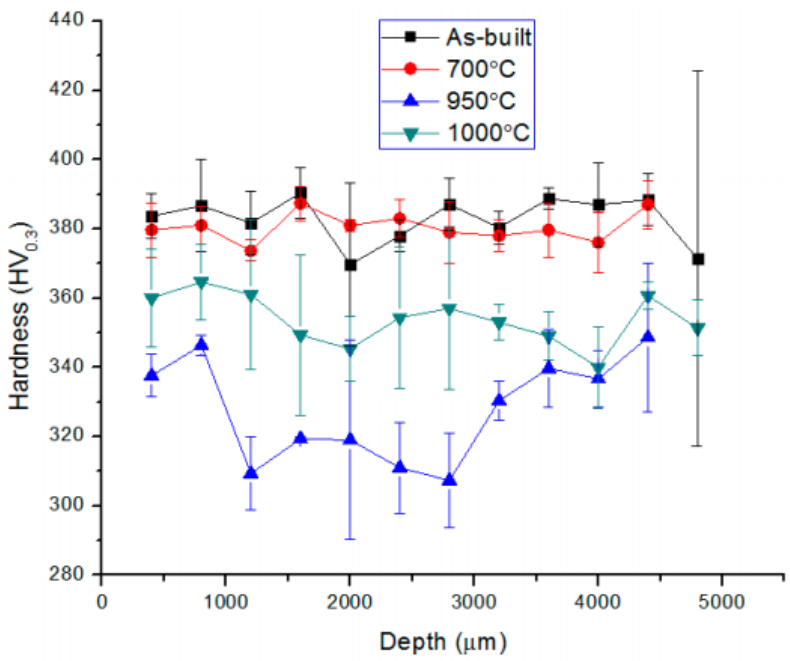


Figure 6. Hardness profiles of the as-built and heat-treated samples.

Table 1. Average hardness of the as-built and heat-treated samples.

Samples	As-Built	700 °C	950 °C	1000 °C
Hardness (HV)	383 ± 13	380 ± 6	327 ± 11	358 ± 14

The as-built and the 700 °C heat treated samples showed similar hardness profiles (Figure 6). In addition, these two samples gave the highest hardness profiles as can be seen in Figure 6. The similarity in hardness profiles of these samples was attributed to the similarity in their microstructures. Consequently, these two samples gave the highest similar average hardness values as presented in Table 1. The high hardness on these latter samples was attributed to the presence of the martensite α′ phase that was observed on microstructures of the samples (Figure 3b,c) [10,12].

Heat treatment at 950 °C and 1000 °C resulted in a visible reduction in hardness (Figure 6). However, 950 °C sample gave the lowest hardness profile and average hardness of 327 ± 11 HV, as can be seen in Figure 6 and Table 1. The decrease in hardness was associated with the transformation of the metastable martensite α′ phase into stable α + β phases. Even though 950 °C and 1000 °C reduced the hardness, an increase in hardness was observed after heat treatment at 1000 °C, as depicted in Table 1. According to the Hall-Petch relation, the harness of the material is expected to increase upon grain growth. Therefore, this observation was not expected since grain growth was observed on the microstructure of the 1000 °C heat treated sample (Figure 3h) [23].

3.2.2. Influence of Cooling Method

The graph showing hardness profiles and average hardness of the as-built and heat-treated samples are shown in Figure 7 and Table 2, respectively.

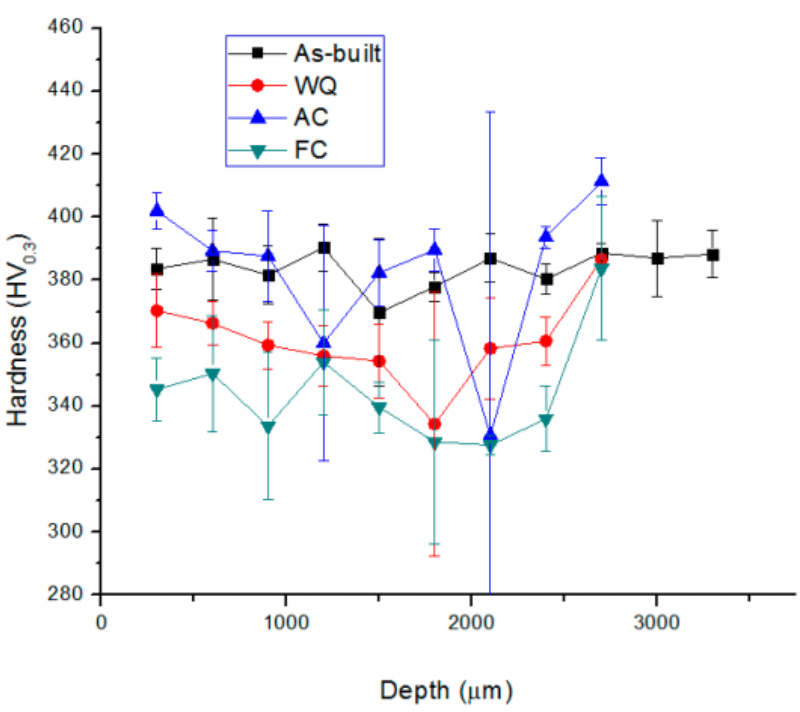


Figure 7. Hardness profiles of the as-built and heat-treated samples.

Table 2. Average hardness of the as-built and heat-treated samples.

Samples	As-built	WQ	AC	FC
Hardness (HV)	383 ± 13	361 ± 13	383 ± 23	344 ± 16

Figure 7 shows that as-built and AC samples gave the highest hardness profiles. Moreover, the as-built and AC sample gave the same average hardness value of 383 HV as can be seen in Table 2. This observation was expected since both cooling methods produced fully α′ structures. A decrease in hardness was observed on the WQ sample. The decrease hardness on this sample was not expected since this cooling method also produced a fully martensitic α′ structure, and there was no phase transformation that was observed. A major decrease in hardness was observed on the FC sample, as presented in Figure 7 and Table 2. The decrease in hardness was attributed to the transformation of the martensite α′ structure into lamella α + β structure.

3.2.3. Influence of Residence Time

Figure 8 and Table 2 shows the hardness profiles and average hardness of the as-built and heat-treated samples.

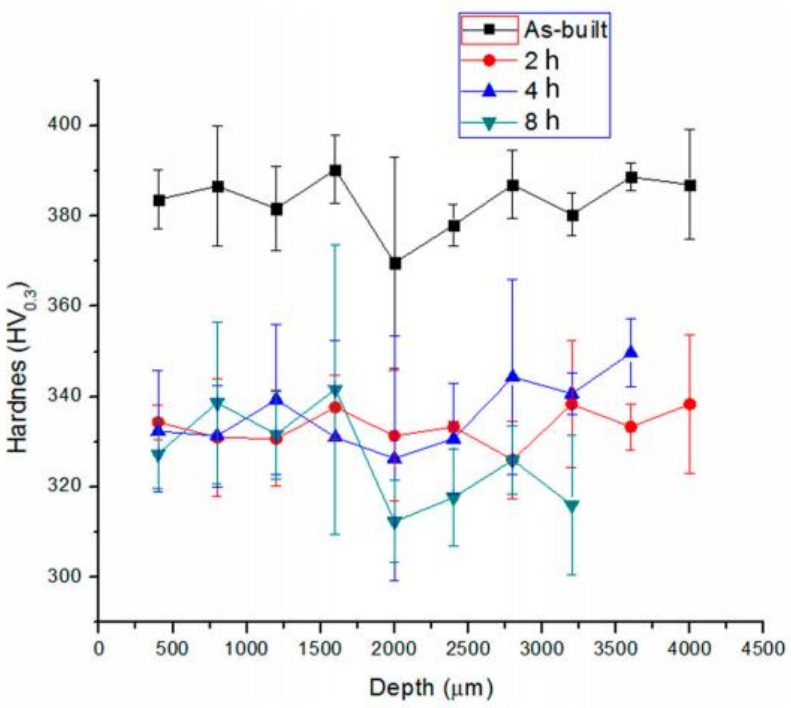

As-built
2 h
4 h
8 h
Hardnes ($HV_{0.3}$)
400
380
360
340
320
300
0
500
1000
1500
2000
2500
3000
3500
4000
4500
Depth (μm)

Figure 8. Hardness profiles of the as-built and heat-treated samples.

As anticipated, the as-built showed the highest hardness profile due to the martensitic α′ phase, as presented in Figure 8 and Table 3. It can be clearly seen from Figure 8 that all the heat treatment for all the residence times resulted in a major decrease in hardness with the 8 h heat treated sample showing the lowest hardness (Table 3). Obviously, this decrease in hardness was attributed to the transformation of the martensite α′ phase into stable α + β phases. Most importantly, Table 3 shows that heat treatment for all the residence times (2 h, 4 h, 8 h) resulted in similar average hardness results.

Table 3. Average hardness of the as-built and heat-treated samples.

Samples	As-built	2 h	4 h	8 h
Hardness (HV)	383 ± 13	333 ± 9	336 ± 15	327 ± 14

4. Discussion

Heat treatment was employed on SLM Ti6Al4V produced specimens in order to improve their microstructure and hardness properties. The effect of temperature, cooling method and residence time on microstructure and hardness was evaluated. The obtained results are reported in Section 3 and are now discussed in this section.

4.1. Temperature Analysis

It is well known that SLM Ti6Al4V is recognized by fully martensitic α′ structure due to rapid heating and cooling; hence, post-processing heat treatment is necessary to improve the microstructure and mechanical properties. This study has shown that heat treatment temperature plays an important role in improving the microstructure and hardness characteristics of SLM Ti6Al4V components. An improved microstructure will be characterized by improvement of other mechanical properties, such as strength and elongation (ductility). Both the microstructure of the as-built (Figure 3a) and 700 °C

(Figure 3c) samples showed similar microstructure, with the presence of martensitic α′ phase aligned within large columnar β grains. The similarity in the microstructure of these two samples was confirmed by similar high hardness of 383 ± 13 HV and 380 ± 6 HV for as built and 700 °C sample, respectively, due to the presence of the martensitic α′ phase. These results indicated that 700 °C does not have any observable microstructural change on high speed SLM produced Ti6Al4V components, and that the samples that underwent heat treatment at this temperature would have compromised mechanical properties. Intuitively, this temperature may be necessarily only for residual stress relieving. Similar observation was made by several other authors after heat treatment at temperatures below 730 °C [1,8,14,20,24].

At 950 °C and 1000 °C the samples showed a full transformation of the martensite α′ microstructure into lamella α + β microstructure (Figure 3e,f). This transformation was followed by a major decrease in hardness to 327 ± 11 HV and 358 ± 14 HV for the 950 °C and 1000 °C heat treated samples, respectively. This type of microstructural transformation is characterized by improved ductility of Ti6Al4V components [2,24]. According to Simonelli et al. [2], a lamella microstructure promotes slip transfers between α and β-phases which promote increased dislocation movement, this then result in a sample having an improved ductility. This implies that the transformation into lamella α + β structure and reduced hardness that resulted from heat treatment at 950 °C and 1000 °C improved the microstructure of high speed SLM produced Ti6Al4V components.

While 950 °C and 1000 °C had the same microstructure, it should be noted that the difference in hardness can be attributed to grain formation and size coarsening or refinement, which are known to affect properties, such as strength and hardness. Grain growth was observed to initiate at 950 °C (Figure 3f) and was sustained above this temperature as observed by the growth in the lamellar of the α + β phases reported in Figure 3g. This occurrence resulted in an increase in hardness. This observation did not follow the Hall-Petch relationship [23], which clearly indicate that the hardness of a material is inversely proportional to the size of the grain. Overall, it can be said that both temperatures (950 °C and 1000 °C) were significant in transforming the unwanted martensitic α′ phase into desired α + β phase microstructure.

Maybe the grain growth that was observed at 1000 °C was insignificant; hence, no variation in hardness was reported. This, therefore, prompted further investigation on the effects of 1000 °C on the properties of Ti6Al4V SLM built samples, as reported in Sections 4.2 and 4.3, on method of cooling and residence time, respectively.

4.2. Cooling Method Analysis

In view of cooling method, it has been already shown that the martensite α′ phase is unwanted and must be avoided due to the characteristics it possesses. WQ and AC methods resulted in the formation of a new martensite α′ structure. A study by Lamirand et al. [21] classified WQ and high cooling and AC as intermediate cooling. This newly formed phase is associated with high cooling rates as is with these two cooling methods. The newly formed martensite α′ phase is typically thinner and finer than the one on the as-built samples [1,25]. A similar type of microstructure was reported by Jovanovich et al. [26] after WQ Ti6Al4V samples from a temperature of 1010 °C. The WQ method produced a coarser type of martensite α′ phase (Figure 4d), while the AC method produced a finer type of martensite α′ phase (Figure 5f). Due to the newly formed martensite α′ phase, the as-built and AC samples gave similar hardness results of 383 ± 13 HV and 383 ± 23 HV, respectively. A decrease in hardness to 361 ± 13 HV was observed on the WQ sample because of the martensitic α′ structure that was observed on the microstructure of this sample (Figure 4c). The observed difference in hardness for AC and WQ can be attributed to grain type that formed. WQ was sustained with coarsening while AC had a finer newly formed martensite α′ phase.

The FC method was able to eliminate the unwanted martensite α′ phase and produced a fully lamella α + β structure that formed into a basket weave morphology (Figure 4g). The resulting lamella α + β microstructure was characterized by a decrease in hardness to

344 ± 16 HV. Since a fully lamella α + β structure is characterized by improved ductility [2,20], the above-mentioned observations implied that the FC method was the only cooling method that was able to improve the microstructure of high speed SLM Ti6Al4V parts and was tested further and the results are reported in Section 4.3.

4.3. Residence Time Analysis

As shown in Figure 5c,e,g, all samples that were heat-treated to 1000 °C at different residence time (2 h, 4 h, and 8 h) were able to dissolve and eliminate the formed martensitic α′ phase. The samples that were heat-treated at 1000 °C for 2 h and 4 h produced similar lamella α + β microstructures. These formed lamella α + β microstructures had similar hardness decrease, which was 333 ± 9 HV and 336 ± 15 HV for 2 h and 4 h samples, respectively.

A sample that was heat treated at 1000 °C for 8 h showed different microstructural from that of 2 h and 4 h. The microstructure of the 8 h sample showed a mixture of lamella and globular α + β phases. The globular α + β phases formed on the boundaries of the β grain. Obviously, this was due to prolonged residence time (8 h) [22,27]. This observation was a clear indication that the globularization process occurred. The globularization was attributed to the elongated residence time, which resulted in the thickening of the lamella α + β phases, that initiated α-phase boundary splitting [22]. Heat treatment for 8 h gave a hardness value of 327 ± 14 HV, which was similar to the 2 h and 4 h samples. From the above-mentioned results, it can be said that all the residence time studied improved the microstructure of high speed SLM produced Ti6Al4V components, but 8 h would not be an ideal residence time since a grain thickening occurred in the process during heating.

5. Conclusions

- In summary, this study undertook to understand the effect of heat treatment temperature on the microstructure and hardness of the SLM built Ti6Al4V samples. Several temperatures were used, and only 1000 °C seemed interesting enough to further characterized how long should a sample be held at temperature during heat treatment and which cooling method would be suitable to obtain an improved microstructure and mechanical properties for better performance. The results conclusively arrive at an indication 4 h should be the optimum residence time when heat-treating Ti6Al4V at 1000 °C since 8 h led to globalization. Moreover, FC should be the preferred method of cooling since WQ and AC led to formation of the new martensite α′ phase which is undesirable. These observations led to the following conclusion: Heat treatment at 950 °C and 1000 °C produce a lamella α + β microstructure.
- WQ and AC methods led to the formation of new martensite α phase.
- 2 h and 4 h should be taken as best residence time when heat treating Ti6Al4V at 1000 °C since a homogeneous improved lamellar α + β microstructure can be obtained without any grain refinement, coarsening, globalization, or formation of an undesirable new phases.

Author Contributions: Conceptualization, P.L., B.M. and M.T.; methodology, P.L., B.M., M.T. and K.A.; validation, B.M. and M.T.; investigation, P.L.; data curation, P.L.; writing original draft preparation, P.L., B.M. and M.T.; review and editing, P.L. and M.T.; supervision, B.M., M.T., K.A. and N.M.; project administration, B.M.; funding acquisition, B.M. All authors have read and agreed to the published version of the manuscript.

Funding: This research was funded by the Department of Science and Innovation (DSI) of South Africa (SA) through the Collaborative Program in Additive Manufacturing (CPAM), grant number LHEBBDL.

Informed Consent Statement: Not applicable.

Acknowledgments: Laboratory and equipment support from CSIR National Laser Centre and the University of Pretoria is acknowledged.

Conflicts of Interest: The authors declare no conflict of interest.

References

1. Vilaro, T.; Colin, C.; Bartout, J.D. As-fabricated and heat-treated microstructures of the Ti6Al4V alloy processed by selective laser melting. *Metall. Mater. Trans.* **2011**, *42*, 3190–3199. [CrossRef]
2. Simonelli, M.; Tse, Y.Y.; Tuck, C. On the texture formation of selective laser melted Ti6Al4V. *Metall. Mater. Trans.* **2014**, *45*, 2863–2872. [CrossRef]
3. Lekoadi, P.; Maledi, N.; Tlotleng, M.; Masina, B. Investigation of microstructural characteristics of heat treated high speed selective laser melted Ti6Al4V components. In Proceedings of the 19th Annual International RAPDASA Conference, Johannesburg, South Africa, 6–9 November 2018.
4. Yu, W.H.; Sing, S.L.; Chua, C.K.; Kuo, C.N.; Tian, X.L. Particle-reinforced metal matrix nanocomposites fabricated by selective laser melting: A state of the art review. *Prog. Mater. Sci.* **2019**, *101*, 330–379. [CrossRef]
5. Kruth, J.P.; Levy, G.; Klocke, F.; Childs, T.H.C. Consolidation phenomena in laser and powder-bed based layered manufacturing. *Manufac. Tech.* **2007**, *56*, 730–759. [CrossRef]
6. Dong, E.; Yu, W.; Cai, Q. Alpha-case kinetics and high temperature plasticity of Ti6Al4V alloy oxidized in different regions. *Proc. Eng.* **2017**, *207*, 2149–2154. [CrossRef]
7. Chang, K.; Liang, E.; Huang, W.; Zhang, X.; Chen, Y.; Dong, J.; Zhang, R. Microstructural features and mechanical property in different directions of additive manufactured Ti6Al4V alloy. *Mater. Lett.* **2020**, *267*, 1–5. [CrossRef]
8. Shipley, H.; McDonnell, D.; Culleton, R.; Coull, R.; Lupoi, G.; Odonell, D.; Trimble, D. Optimization of process parameters to address fundamental challenges during selective laser melting of Ti6Al4V: A review. *Int. J. Mach. Tool Manufac.* **2018**, *128*, 1–20. [CrossRef]
9. He, J.; Li, D.; Jiang, W.; Ke, L.; Qin, G.; Ye, Y.; Qin, Q.; Qui, D. The martensitic transformation and mechanical properties of Ti6Al4V prepared via selective laser melting. *Materials* **2019**, *12*, 321. [CrossRef]
10. Gupta, A.; Khatirkar, R.K.; Kumar, A.; Parihar, M.S. Investigations on the effect of heating temperature and cooling rate on evolution of microstructure in $\alpha + \beta$ titanium alloy. J. *Mater. Res. Soc.* **2018**, *54*, 1–12. [CrossRef]
11. Ter Haar, G.M.; Becker, T.H. Selective laser melting produced Ti6Al4V: Post-process heat treatments to achieve superior tensile properties. *Materials* **2018**, *11*, 1–15.
12. Zhang, X.; Fang, G.; Leeflang, S.; Bottger, A.J.; Zadpoor, A.A.; Zhou, J. Effect of subtransus heat treatment on the microstructure and mechanical properties of additively manufactured Ti6Al4V alloy. *J. Alloys Compd.* **2018**, *735*, 1562–1575. [CrossRef]
13. Yan, M.; Yu, P. An overview of densification, microstructure and mechanical properties of additively manufactured Ti6Al4V-comparison among selective laser melting, electron beam melting, laser metal deposition and selective laser sintering, and with conventional powder. *Sinter. Technol. Mater.* **2015**, *23*, 374–386. [CrossRef]
14. Wu, S.Q.; Lu, Y.J.; Gan, Y.L.; Huang, T.T.; Zhao, C.Q.; Lin, J.J.; Guo, S.; Lin, J.X. Microstructural evolution and microhardness of selective-laser-melted Ti6Al4V alloy after post heat treatments. *J. Alloys Compd.* **2016**, *672*, 643–652. [CrossRef]
15. Chicos, L.A.; Zaharia, S.M.; Lancea, C.; Pop, M.A.; Canadas, I.; Rodriguez, J.; Galindo, J. Concentrated solar energy used for heat treatment of Ti6Al4V alloy manufactured by selective laser melting. *Sol. Energy* **2018**, *173*, 76–88. [CrossRef]
16. Lekoadi, P.; Maledi, N.; Tlotleng, M.; Masina, B. Improving the microstructure of high-speed selective laser melted Ti6Al4V components by varying residence time during heat treatment. In Proceedings of the 20th Annual RAPDASA Conference, Bloemfontein, South Africa, 6–8 November 2019.
17. Algius, D.; Kourousis, K.I.; Wallbrink, C. A review of the as-built SLM Ti6Al4V mechanical properties towards achieving fatigue resistance designs. *Metals* **2018**, *8*, 1–24.
18. Qiu, C.; Ravi, G.A.; Dance, C.; Ranson, A.; Dilworth, S.; Attar, M.M. Fabrication of large Ti6Al4V structures by direct laser deposition. *J. Alloys Compd.* **2015**, *269*, 351–361. [CrossRef]
19. Alcisto, J.; Enriquez, A.; Garcia, H.; Hinkson, S.; Steelman, T.; Silverman, E.; Valdovino, P.; Gigerenzer, H.; Foyos, J.; Ogren, J.; et al. Tensile properties and microstructure of laser formed Ti6Al4V. *J Mater. Eng. Performance* **2011**, *20*, 203–212. [CrossRef]
20. Matthys Ter Haar, G. Selective laser melting produced Ti6Al4V: Influence of annealing strategy on crystallographic microstructure and tensile. Ph.D. Thesis, Stellenbosch University, Stellenbosch, South Africa, December 2017.
21. Lamirand, M.; Bonnentien, J.L.; Ferrierre, G.; Guerin, S.; Chevalier, J.P. Effect of interstitial oxygen on microstructure and mechanical properties of Ti-48Al-2Cr-2Nb with fully lamella and duplex microstructure. *Metall. Mater. Trans. A* **2006**, *37*, 2369–2378. [CrossRef]
22. Semiatin, S.L.; Seetharaman, V.; Weiss, I. The thermomechanical processing of alpha/beta titanium alloys. *Metals* **1997**, *49*, 33. [CrossRef]
23. Zuback, J.S.; Debroy, T. The hardness of additively manufactured alloys. *Materials* **2018**, *11*, 2070. [CrossRef]
24. Gong, X.; Anderson, K.; Chou, K. Review on powder-based electron beam additive manufacturing technology. *Manufac. Rev.* **2012**, *1*, 507–515.
25. Vrancken, B.; Thijs, L.; Kruth, P.J.; Van Humbeeck, J. Heat treatment of Ti6Al4V produced by selective laser melting: Microstructure and mechanical properties. *J. Alloys Compd.* **2012**, *541*, 177–185. [CrossRef]

26. Jovanovic, M.T.; Tadic, S.; Zec, S.; Miskovic, Z.; Bobic, I. The effect of annealing temperatures and cooling rates on the microstructure and mechanical properties of invest cast Ti6Al4V alloy. *Mater. Des.* **2006**, *27*, 192–199. [CrossRef]
27. Sabban, R.; Bahl, S.; Chatterjee, K.; Suwan, S. Globularization using heat treatment in additively manufactured Ti6Al4V. *Acta Mater.* **2019**, *162*, 239–254. [CrossRef]

Appendix B: 149th annual TMS conference paper 2020:

Investigation of Martensite α' Phase Transformation During Heat Treatment of High-Speed Selective Laser Melted Ti6Al4V Components

P. M. Lekoadi, N. Maledi, M. Tlotleng and B. N. Masina

Abstract This study presents the investigation of microstructural and hardness properties of high-speed selective laser melted (SLM) produced Ti6Al4V coupons after various heat treatments. Heat treatment was performed in order to homogenize and improve the microstructure of the as-built Ti6Al4V by transforming the acicular martensitic α' phase. Optimized heat treatment parameters were selected based on their impact on the transformation of the acicular martensite α' phase and the phase morphology produced after heat treatment. It was found that sub-transus heat treatments do not completely transform the martensite α' phase, but result in the decrease in hardness. Heat treatment at 1000 °C, for 2 h followed by furnace cooling, transformed the martensitic α' phase into a lamella $\alpha + \beta$ phase. A relationship of hardness, as a function of heat treatment temperature, is also reported.

Keywords Heat treatment · Ti6Al4V · Martensite

P. M. Lekoadi (✉) · M. Tlotleng · B. N. Masina
CSIR National Laser Centre, Laser Enabled Manufacturing Group, 395, Pretoria 0001, South Africa
e-mail: PLekoadi@csir.co.za

M. Tlotleng
e-mail: MTlotleng@csir.co.za

B. N. Masina
e-mail: BMasina@csir.co.za

N. Maledi
School of Chemical & Metallurgical Engineering, University of the Witwatersrand, Private Bag 3, Wits, 2050 Johannesburg, South Africa
e-mail: Nthabiseng.maledi@wits.ac.za

M. Tlotleng
Department of Mechanical Engineering Science, University of Johannesburg, Auckland Park Campus, Johannesburg 2012, South Africa

© The Minerals, Metals & Materials Society 2020

The Minerals, Metals & Materials Society (ed.), *TMS 2020 149th Annual Meeting & Exhibition Supplemental Proceedings*, The Minerals, Metals & Materials Series, https://doi.org/10.1007/978-3-030-36296-6_36

UNCORRECTED PROOF

Introduction

Selective laser melting (SLM) is a type of powder-bed-based additive manufacturing (AM) technology, whereby parts are produced layer by layer from metal powders using a laser beam as an energy source to promote fusion according to a previously defined computer-aided design (CAD) [1–3]. During SLM process, a layer of powder, which is in few tens of microns thick, is distributed from feed container into the build platform. A focused laser beam scans each layer of the powder, based on the CAD data, and the scanning result in a localized melting and solidification of the powder to form a layer of the part. Subsequent layers are built one over the other by lowering the build platform and depositing a layer of the powder which is equivalent to the layer thickness. The process repeats itself until the 3D part is completed [4, 5]. Some of the advantages offered by SLM over conventional manufacturing techniques include the ability to produce complex geometrical structures, reduction of material waste, production of near-net-shapes, saving time, and high level of flexibility [2].

SLM process has been extensively investigated for the processing of Ti6Al4V. Ti6Al4V is the most widely used titanium alloy, accounting for more than 50% of all titanium usage worldwide [6, 7]. The microstructure of Ti6Al4V consists of hexagonal closed packed (hcp) α phase and body-centered cubic (bcc) β phase at lower temperatures. These two phases constitute very important group of microstructural and mechanical properties since their microstructures can be manipulated to obtain balanced mechanical properties [8]. Ti6Al4V is preferred over other alloys because of its good stability at high operating temperatures, high specific strength, and good corrosion resistance properties. A combination of strength and low density makes it more attractive for AM [3, 9].

Although SLM offers various advantages, there are challenges associated with the techniques. Firstly, the microstructure and mechanical properties of SLM produced Ti6Al4V components are different to those produced by conventional techniques. The microstructure of SLM produced Ti6Al4V components, in the as-built state, is characterised by an acicular martensitic α' phase, high hardness, and low ductility [10, 11]. The second challenge is the built-up of residual stresses due to the high cooling rates during manufacturing. Heat treatment is used to relieve these residual stresses while transforming the acicular martensitic α' phase into a more desirable phase depending on the intended application [3, 12, 13].

It is important to understand the transformation of martensite α' phase during heat treatment. Selecting appropriate heat treatment and cooling method can likely give desired properties. Hence, this study aimed at investigating the behaviour of martensite α' phase transformation during heat treatment of Ti6Al4V parts that were produced using high speed and high power. In addition, the hardness as a function of heat treatment temperature and cooling method was investigated and reported.

UNCORRECTED PROOF

Methodology

Materials

Spherical grade 5 titanium alloy (Ti6Al4V) powder with a particle size distribution in the range of 20–60 μm was used as deposition material during the production of the samples. The powder was supplied by TLS Technik GmbH & Co and was used as received. Ti6Al4V base plate of dimension 320 × 340 × 30 mm^3 was used as a substrate.

Methods

Sample Manufacturing

All samples were produced on a high-speed SLM machine known as the Aeroswift that is available at the Council for Scientific and Industrial Research (CSIR), Pretoria Campus. The platform uses a single-mode fibre laser with a wavelength of 1073 nm was used during the production of the test samples.

Heat Treatment

All samples were heat treated in column tube furnace under argon environment to prevent oxidation on the produced component. The furnace was flooded by a continuous flow of argon until oxygen content was lower and then maintained by continuous argon flow before production of the samples. All samples were heat treated to various temperatures of 750, 800, 900, and 1000 °C at a heating rate of approximately 10 °C/min for 2 h before they were furnace cooled.

Sample Preparation and Characterisation

After heat treatment, the samples were mounted and mechanically ground using SiC papers up to a grit 4000 and then polished for surface finish. Kroll's reagent was used as an etchant to reveal the microstructure of the samples. Samples were analyzed for microstructural evolution using Joel JSM-6010PLUS/LA scanning electron microscope (SEM) and hardness using Matsuzawa Seiko Vickers model MHT-1 microhardness machine. An X-ray diffraction (XRD) machine was used to study the phases that were present. (XRD) determinations were executed on X-ray diffractometer (XPERT PRO PaNalytical, Netherlands) for phase identification. The patterns were run with CuKα radiation with a secondary monochromator ($\lambda = 0.1545$) AT 45 kV and 40 mA. The diffraction measurements were conducted at room temperature in a

UNCORRECTED PROOF

Bragg–Brenton geometry with a scan range of $2\theta = 5$–$90°$ using continuous scanning at a rate of 0.02°/s.

Results

Microstructures

The microstructures of the as-built and heat-treated samples are shown in Fig. 1. The size of the samples was 10 mm, and the microstructures were taken at the centre of the samples.

The microstructure of the as-built sample (Fig. 1a) showed sharp acicular martensite α' phase which is mostly common with the microstructure of SLM produced Ti6Al4V components. This martensitic α' phase is due to high heating and cooling rates that are associated with SLM process [1, 2]. It was discussed by Rafi et al. [4] that SLM produced components undergo very high cooling rates in order to obtain maximum density on the produced component. The martensitic α' phase lath grows inside large columnar prior β grains that grow epitaxial throughout the sample in a direction parallel to the built direction. Microstructural porosity was also observed on the microstructure of the as-built and all the heat-treated samples.

Heat treated at 750 °C resulted in the formation of β phase precipitates. Although the sharp acicular martensite α' phase was still observed after heat treatment at 750 °C, a β phase precipitate was also faintly observed. This implies that the martensite α' phase was starting to transform into β phase. According to Yan et al. [14], martensite α' phase starts to transform approximately at 650 °C upon heating.

Intense β phase was observed on the microstructure at heat treatment of 800 °C (Fig. 1c). It is known that the volume fraction of the martensite α' phase tends to decreases as the temperature is increased until it transforms into full β phase when the β transus temperature is reached [3, 9]. This is why the volume fraction of the β phase was increased as temperature was increased to 800 °C. The acicular martensitic α' phase was no longer observed after heat treatment at 800 °C. Again the acicular martensitic α' phase was no longer observed on the microstructure of the sample that was heat treated at 900 °C (Fig. 1d). This implies that the martensite α' phase was fully transformed into lamella $\alpha + \beta$ phases. The lamella $\alpha + \beta$ morphology in this case is due to the temperature (900 °C) and cooling method that was used (furnace cooling). Heat treatment temperature of 900 °C is known to be a temperature below the β transus temperature of Ti6Al4V. Qian et al. [15] defined the β transus temperature of Ti6Al4V as 996 ± 14 °C.

The microstructure of the sample that was heat treated at 1000 °C showed lamella $\alpha + \beta$ phases that were thicker than the ones on the microstructure of the 900 °C heat-treated sample. The increase in thickness was attributed to grain growth. Evidence of fully martensite α' phase transformation was observed again since there was no martensite α' phase on the microstructure of the 1000 °C heat-treated sample.

UNCORRECTED PROOF

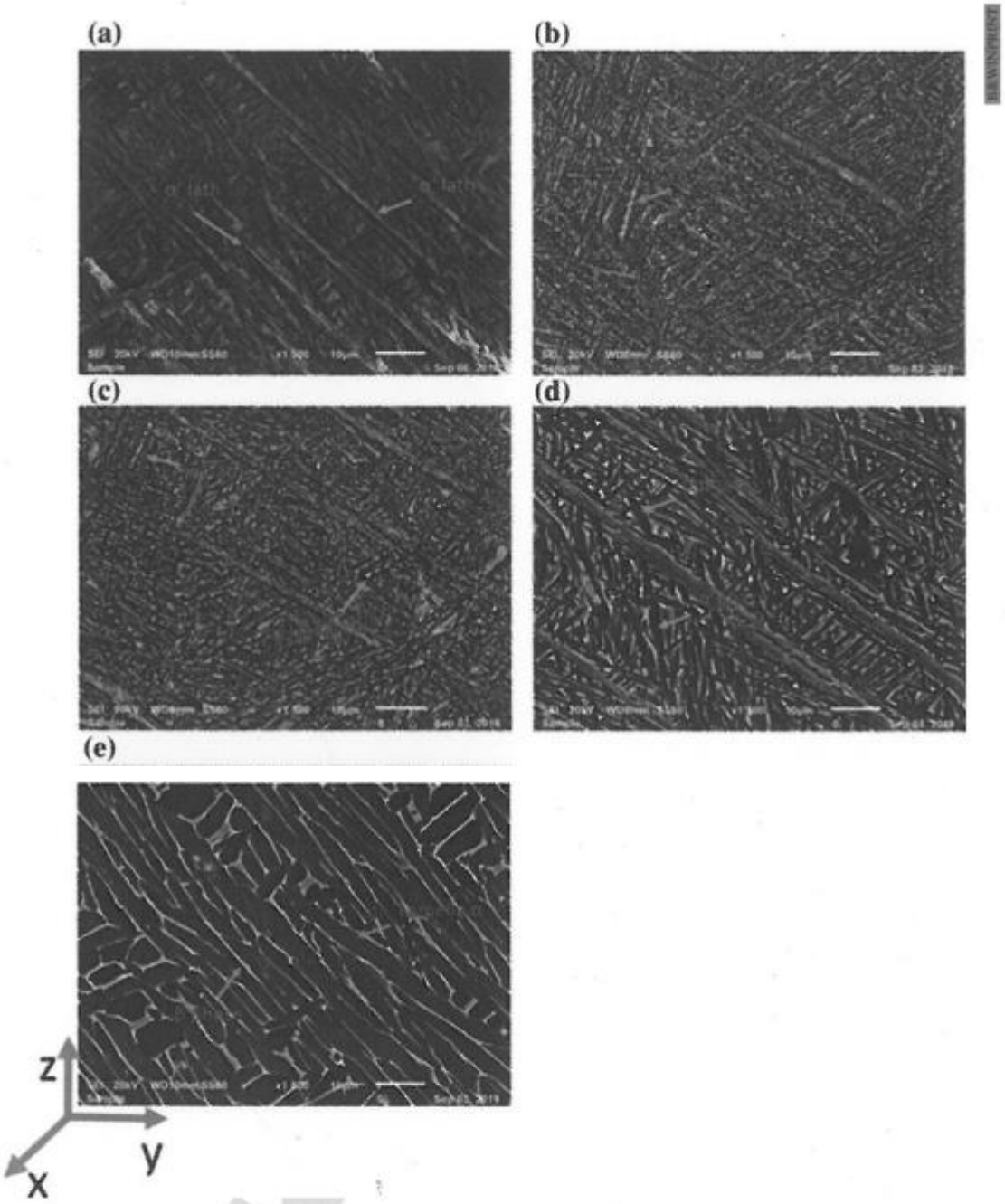


Fig. 1 SEM images of the samples **a** as-built, **b** 750 °C, **c** 800 °C, **d** 900 °C, and **e** 1000 °C

XRD

XRD analysis was performed to complement the observations that were made on the microstructures of the samples. XRD results of the as-built and heat-treated samples are shown in Fig. 2.

The peaks on the XRD graphs were labelled α'/α because martensite α' and α phases have the same hexagonal close packed (hcp) crystalline structure and produce XRD peaks at same angular positions[17]. The diffractogram pattern of the as-built

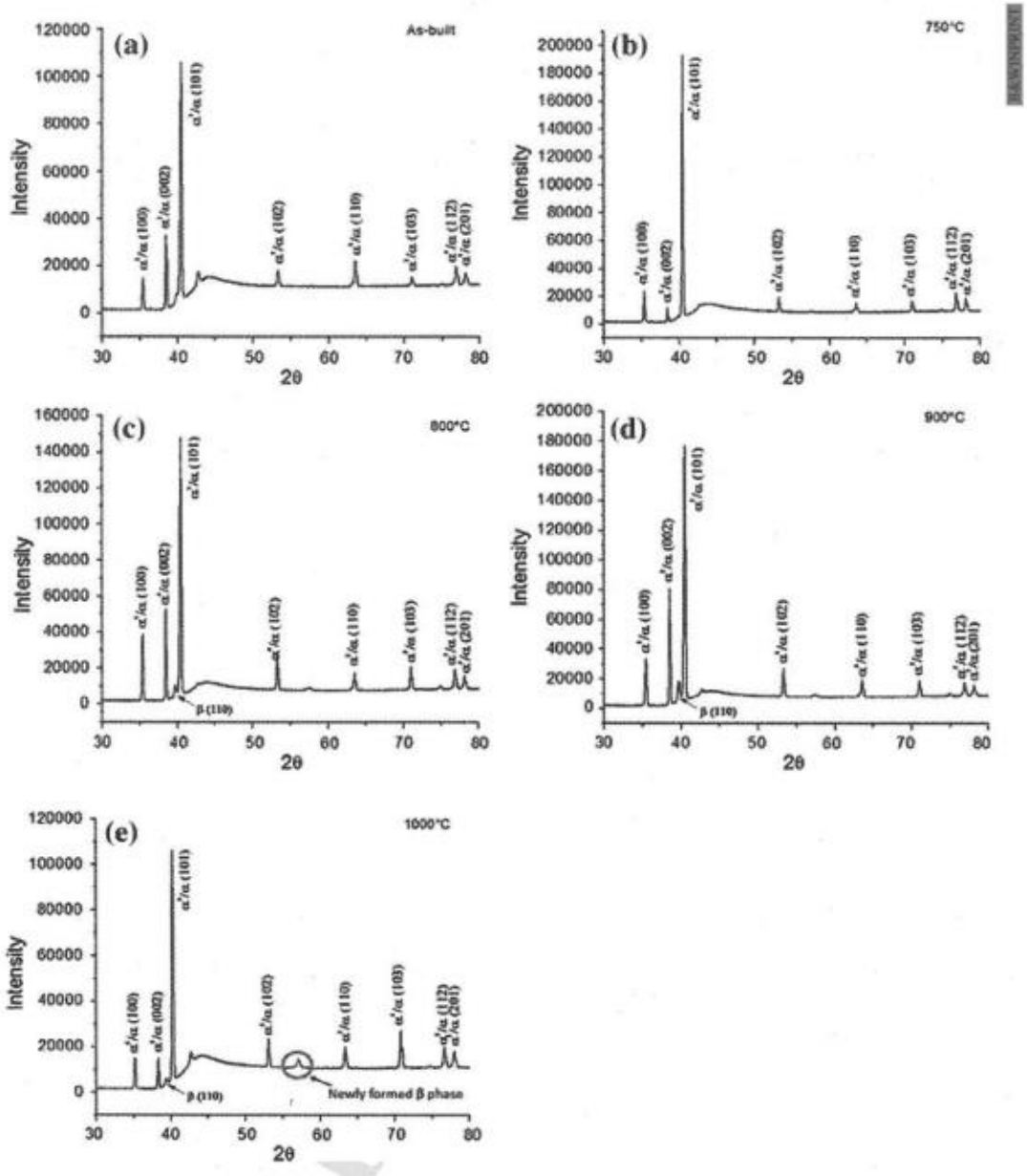


Fig. 2 XRD graphs of the as-built and heat-treated samples

sample (Fig. 2a) and that of the 750 °C heat-treated samples (Fig. 2b) showed α'/α peaks only, implying that the microstructure composed only of martensitic α' and α phases. This observation supports the one that was made with the microstructure of the as-built sample (Fig. 1a) where a martensitic α' microstructure was obtained. Concerning ~~the to~~ the 750 °C sample, the observation differed with the one that was made on its microstructure (Fig. 1b) since there was no β phase peak that was observed on the XRD results. Although there was a difference between the microstructure of the as-built and 750 °C heat-treated samples, their XRD patterns are similar except for a single peak on the as-built sample. The difference that was observed between the XRD patterns of these samples was the peak intensities, where

a high intensity was observed for sample that heat treated at 700 °C to that of the as-built sample.

β phase peak was observed on the XRD pattern of the 800 °C (Fig. 2c), 900 °C (Fig. 2d), and 1000 °C (Fig. 2e) heat-treated samples. Again this observation is in agreement with the microstructures of these samples where the β phase volume fraction increased. This observation also confirms that phase transformation from martensite α' to $\alpha + \beta$ took place. The XRD spectra of the 800 and 900 °C were similar beside the intensity of the peaks. A new β phase peak (highlighted in red in Fig. (2e) was observed on XRD pattern of the sample that was heat treated at 1000 °C. This might be due to the fact that 1000 °C is a temperature above the β transus of Ti6Al4V. During heating all the phases transformed into β phase before they transformed into lamella $\alpha + \beta$ during furnace cooling.

Hardness

The harness profiles and summarised average hardness of the as-built and heat-treated samples are shown by Fig. 3 and Table 1, respectively. The hardness was measured in a vertical direction at the centre of the samples.

The hardness profile of the as-built sample showed a linear pattern, while the ones of the 750, 800, 900, and 1000 °C showed wavy patterns. The sample that was heat treated at 750 °C showed the highest hardness profile hardness than all the other

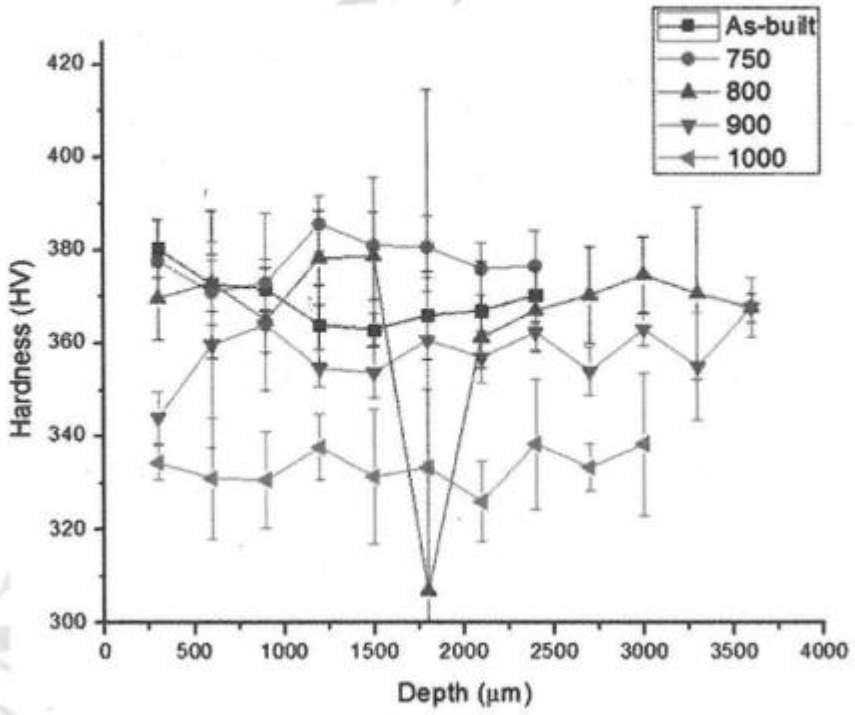


Fig. 3 Hardness profile of the as-built and heat-treated samples

UNCORRECTED PROOF

Table 1 Summary of the hardness profiles of the as-built and heat-treated samples

Sample	Hardness
As-built	369 ± 8
750 °C	378 ± 16
800 °C	365 ± 8
900 °C	358 ± 9
1000 °C	333 ± 9

samples then followed by the as-built sample (Table 1). Heat treatment at 750 °C led to hardening effect as this sample is harder than all the samples including the as-built sample, while the sample heat treated at 1000 °C showed softening effect. This high hardness is due to the martensitic α' phase that was observed on the microstructures of the samples. A study by He et al. [15] discussed that the martensite α' phase is harder than α phase, even though these two phases have the same hcp structure and lattice parameters. The as-built and 800 °C heat-treated sample showed similar hardness results, while a decrease in hardness was observed on the 900 °C heat-treated sample. The sample that was heat treated at 800 °C showed one point that was an outlier. This outlined point resulted on the microhardness indent hitting at a pore, resulting in a decreased hardness value.

Conclusion

Different heat treatment temperatures were performed on the SLM built Ti6Al4V in order to investigate the transformation of martensite phase. It was found that martensite transformation occurred linearly with heat treatment temperature. SEM and XRD showed full transformation of martensite to $\alpha + \beta$ lamella structure at 900 and 1000 °C. High hardness was measured on the sample that was heat treated at 700 °C, while low hardness was measured on the sample that was heat treated at 1000 °C. This corresponded very well with the microstructure for both samples. It can be concluded that only 1000 °C can improve the microstructure.

References

1. Thijs L, Verhaeghe F, Craeghs T, Van Humbeech J, Kruth J (2010) A study of microstructural evolution during selective laser melting of Ti6Al4V. Acta Mater 50:3303–3312
2. Vilaro T, Colin C, Bartout JD (2011) As-fabricated and heat-treated microstructures of the Ti6Al4V alloy processed by selective laser melting. Metall Mater Trans 42A:3190–3199
3. Sallica-Leva E, Caram R, Jardini AL, Fogagnolo JB (2016) Ductility improvement due to martensitic α' decomposition in porous Ti6Al4V parts produced by selective laser melting for orthopaedic implants. J Mech Behav Biomed Mater 54:149–158

UNCORRECTED PROOF

4. Rafi HK, Karthi NV, Gong H, Starr TL, Stucker BE (2013) Microstructure and mechanical properties of Ti6Al4V parts fabricated by selective laser melting and electron beam melting. J Mater Eng Perform 22:3872–3883
5. Simonelli M, Tse YY, Tuck C (2014) On the texture formation of selective laser melted Ti6Al4V. Metallugical Mater Trans A 45A:2863–2872
6. Semiatin SL, Seetharaman V, Weiss I (1997) The thermomechanical processing of alpha/beta titanium alloys. Metals 49(6):33
7. Alcisto J, Enriquez H, Garcia S, Hinkson T, Steelman E, Silverman P, Valdovino H, Gigerenzer J, Foyos J, Ogren J, Dorey K, Karg T, McDonald OS (2011) Es-said, tensile properties and microstructure of laser-formed Ti6Al4V. J Mater Eng Perform 20(2):203–212
8. William JC, Starke EA (2003) Progress in structural materials for aerospace systems. Acta Mater 51:5575–5799
9. Shipley H, McDonnell D, Culleton R, Coull R, Lupoi G, Odonell D, Trimble D (2018) Optimization of process parameters to address fundamental challenges during selective laser melting of Ti6Al4V: a review. Int J Mach Tool Manuf 128:1–20
10. Wysocki B, Maj P, Krawczynska A, Rozniatowski K, Zdunek J, Kurzydlowski KJ, Swieszkowiski W (2017) Microstructure and mechanical properties investigation of CP titanium processed by selective laser melting (SLM). J Mater Process Technol 241:13–23
11. Xu W, Brandt M, Sun S, Elambasseril J, Liu Q, Latham K, Xia K, Qian M (2015) Additive manufacturing of strong and ductile Ti6Al4V by selective laser melting via in situ martensite decomposition. Acta Mater 85:74–84
12. Dong E, Yu W, Cai Q (2017) Alpha-case kinetics and high temperature plasticity of Ti6Al4V alloy oxidized in different regions. Procedia Eng 207:2149–2154
13. Vrancken B, Thijs L, Kruth PJ, Van Humbeeck J (2012) Heat treatment of Ti6Al4V produced by selective laser melting: microstructure and mechanical properties. J Alloy Compd 541:177–185
14. Yan M, Yu P (2015) An overview of densification, microstructure and mechanical properties of additively manufactured Ti6Al4V-comparison among selective laser melting, electron beam melting, laser metal deposition and selective laser sintering, and with conventional powder. Sintered Technol Mater 26:23–37
15. He J, Li D, Jiang W, Ke L, Qin G, Ye Y, Qin Q, Qiu D (2019) The martensitic transformation and mechanical properties of Ti6Al4V prepared via selective laser melting. Materials 12:2–14

PROOF

Appendix C: 20th annual RAPDASA conference paper 2019:

IMPROVING THE MICROSTRUCTURE OF HIGH SPEED SELECTIVE LASER MELTED Ti6Al4V COMPONENTS BY VARYING RESIDENCE TIME DURING HEAT TREATMENT

P. Lekoadi[1*], M. Tlotleng[2, 3], N. Maledi[1] & B.N. Masina[2]

[1] University of the Witwatersrand, School of Chemical & Metallurgical Engineering, Private Bag 3, Wits 2050, Johannesburg, South Africa, Plekoadi@csir.co.za, nthabiseng.maledi@wits.ac.za

[2] CSIR National Laser Centre, Laser Enabled Manufacturing Group, PO BOX 395, Pretoria, 0001, South Africa , Bmasina@csir.co.za, Mtlotleng@csir.co.za

[3] University of Johannesburg, Department of Mechanical Engineering Science, Auckland Park Campus, Johannesburg, 2012, South Africa, daopase@gmail.com

ABSTRACT

Selective laser melting (SLM) is a powder bed additive manufacturing technique that produces components layer-by-layer from computer aided designs as opposed to conventional manufacturing methods. Although this manufacturing technique offers various advantages, the microstructure of the produced components exhibits an acicular martensitic α' phase which exhibits low ductility and high hardness on the produced components. Heat treatment is known to improve the microstructure and ductility and hardness of SLM produced Ti6Al4V components. This study reports on the effect of residence time during heat treatment of Ti6Al4V samples that were built with Aeroswift 3D printing SLM machine. Samples were heat treated to a temperature of 1000°C and held for 2hrs, 4hrs, 8hrs, 10hrs and 12hrs before furnace cooling. It was found that the microstructure transformed from martensitic to lamella α+β, then to globular α+β as residence time was increased. Furthermore, grain growth was observed with an increase in residence time.

[1*] University of the Witwatersrand, School of Chemical & Metallurgical Engineering, Private Bag 3, Wits 2050, Johannesburg, South Africa
[2] CSIR National Laser Centre, Laser Enabled Manufacturing Group, PO BOX 395, Pretoria, 0001, South Africa
[3]University of Johannesburg, Department of Mechanical Engineering Science, Auckland Park Campus, Johannesburg, 2012, South Africa

1. INTRODUCTION

Selective Laser Melting (SLM) is a type of powder bed fusion additive manufacturing (AM) technique whereby parts are produced from a metal powder, layer-by-layer, using the laser beam as an energy source to selectively melt powder and promote fusion according to a previously defined computer aided design (CAD) model [1, 2, 3]. SLM products, such as aircraft turbines, pressure vessels, and surgical implants, are used in various industries including aerospace, automotive, electronic, chemical, biomedical and other high technology areas [4, 5]. The success of SLM is linked with its ability to produce complex geometrical structures, reduction of material waste, reduced production time, production of near net shapes and high level of flexibility [4].

Ti6Al4V also known as Ti64 is an α+β titanium alloy with 6 wt% aluminum stabilizing the α phase and 4 wt% vanadium stabilizing the β phase. Ti6Al4V is the most commonly used titanium alloy, accounting for more than 50% of all titanium usage worldwide [6, 7, 8]. The advantages of Ti6Al4V, over other alloys, include good stability at high operating temperatures, high specific strength, and good corrosion resistance properties [15]. Ti6Al4V is widely used in aerospace applications such as components in aero-engine and space shuttles because of their superior strength to weight ratio [13]. The microstructure of Ti6Al4V consists of hexagonally closed packed (hcp) α phase and some retained body centered cubic (bcc) β phase at room temperature [9]. The microstructure of Ti6Al4V can be varied significantly in the process of heat treatment [10].

SLM produced Ti6Al4V parts, in the as-built state, are unable to achieve high material performance compared to their wrought counterparts [11, 12, 13]. This is because the starting microstructure of SLM produced Ti6Al4V is significantly different from that of its wrought alloys of the same composition. A study by **Kasperovich et al.** [14] compared the microstructures of SLM produced Ti6Al4V to that of wrought counterparts. The microstructures are shown in Figure 1.

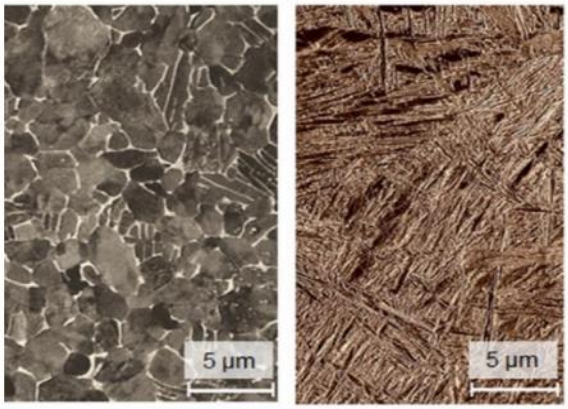


Figure 1: Microstructures of Ti6Al4V (a) Wrought, (b) SLM [14].

The microstructure of the wrought components consists of α globular phase in a matrix of α+β (Figure 1a) [14]. This type of microstructure is characterized by a good balance of strength and ductility [14]. SLM produced samples consist of acicular martensitic α' phase which is characterized by low ductility and high residual stresses [15]. In order for the microstructure of SLM produced components to match that of wrought components, heat treatment must be performed on the SLM produced Ti6Al4V components [15, 18]. It is well known from literature that a bimodal microstructure achieves good balance of ductility and strength [19, 20].

Heat treatment is used to transform the martensitic α' phase, improve the microstructure and reduce residual stresses of SLM produced Ti6Al4V components [3, 16, 17]. Heat treatment temperature, residence time and cooling method are the three parameters that play an important role during heat treatment. In this study, residence time was varied during heat treatment above β transus temperature (at 1000°C) to allow grain growth. This was done in order to improve the microstructure in an attempt to produce globular α+β phases.

2. METHODOLOGY AND RESULTS

2.1 Methodology

2.1.1 Materials

Spherical Grade 5, titanium alloy (Ti6Al4V) powder with a particle size distribution in the range of 20-60µm was used as deposition material during the production of the samples. The powder was supplied by TLS Technik GmbH & Co and was used as received. Ti6Al4V base plate of dimension 320 x 340 x 30mm^3 was used as a substrate.

2.1.2 Powder Characterization

Powder characterization of the Ti6Al4V was conducted at North West University (Potchefstroom Campus). A Malvern PANalytical G3 advanced particle characterization machine (RAMANXRN System) was used for the measurement of powder shape from 0,5µm to several millimetres. Joel JSM-6010PLUS/LA Scanning Electron Microscope (SEM) was used to study particle morphology and to get images of the powder.

Figure 2 shows the morphology and shape distribution curve of the Ti6Al4V powder. The powder particles were spherical in shape (Figure 2a). The same observation was complemented by the high sensitive (HS) circularity curve in Figure 2b which shows a high percentage peak at approximately 1.0 (a perfect circle has a HS circularity of 1).

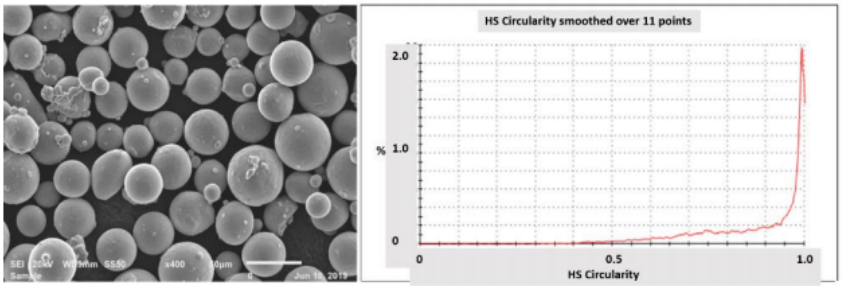


Figure 2: Powder morphology of the Ti6Al4V powder.

2.1.3 Methods

A high speed SLM 3D printing machine (Aeroswift), with a single mode fibre laser of wavelength of 1073 nm available at CSIR NLC, was used to produce the samples. The samples were received and heat treated at a temperature of 1000°C. The samples were heat treated in a columnar tube furnace under an argon protected environment at a gas flow rate of 2l/min and heating rate of 10°C/min. The residence times during heating were varied from 2hrs, 4hrs, 8hrs, 10hrs, and 12hrs before furnace cooling. It should be noted that most literature uses 2hrs as their residence time and not much work has been done on residence times above 2hrs [16, 17]. This study aimed at evaluating other residence times above 2hrs.

After heat treatment, the samples were mounted and mechanically ground using SiC papers up to a grit 4000 and then polished for surface finish. Kroll's reagent was used as an etchant to reveal the microstructure of the samples. Samples were analyzed for microstructural evolution using Joel JSM-6010PLUS/LA Scanning Electron Microscope (SEM) and hardness using Matsuzawa Seiko Vickers model MHT-1 micro-hardness machine.

2.2 Results

2.2.1 Microstructures

All the microstructures were taken on the top left corner of the samples and it should be noted that the microstructural features across the samples were homogeneous. Figure 3 shows the microstructure of the as-built and a corresponding 2hrs heat treated sample.

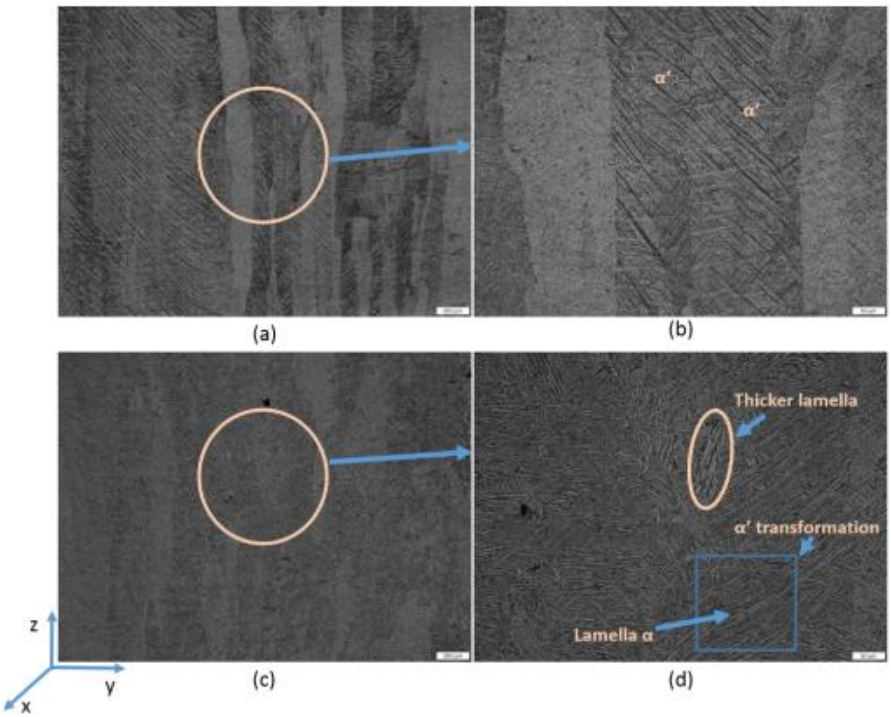


Figure 3: Microstructures of the As-built sample (a) and 2hrs heat treated sample (c) and their specific zoom in (b and d)

As expected, large columnar prior ß grains microstructure was observed along the build direction for the as-built sample (Figures 3a, 3b). According to **Vilaro et al.** [11] these prior ß grains grow epitaxially along the direction of the heat conduction in a columnar way and are due to partial remelting of the previous layer during SLM processing. An acicular sharp martensitic α' phase (Figure 3b) was observed inside the formed columnar prior ß grains of the as-built sample. SLM process is associated with high heating and cooling rates which are the cause of these martensite phase [2, 4, 10, 13]. **Kasperovich et al.** [14] discussed that these martensite α' phase contributes to the low ductility of SLM produced Ti6Al4V components and suggested that heat treatment can be used to transform the martensite α' phase and improve the ductility of the components.

The columnar prior ß grains were still observed after heat treatment for 2hrs (Figure 3c) and evidence of phase transformation was also observed. The martensitic α' phase transformed into lamella α+ß phases of different sizes and thickness (Figure 3d) and this might be due to the temperature used. It was shown that the lamella structure is preferred in applications where fracture toughness and fatigue crack propagation are a priority [14].

The microstructure of the 4hrs and 8hrs are shown in Figure 4.

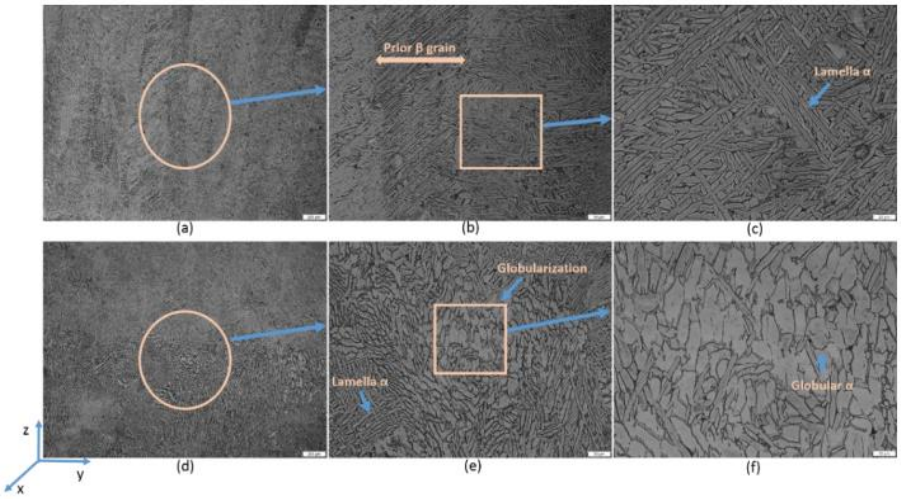


Figure 4: Microstructures of the heat treated samples (a, b & c) 4hrs, (d, e & f) 8hrs.

The large columnar prior ß grains were still observed after heat treatments at 4hrs (Figure 4a) but were no longer observed after heat treatment for 8hrs (Figure 4d). It should be noted that as the residence time increases, the large columnar grains tend to be fading until the disappeared at 8hrs heat treatment.

Lamella α+ß growth was evidenced after 8hrs heat treatment. The lamella α+ß changed shape and size to globular α+ß, a process known as globularization (Figure 4e). **Kasperovich et al.** [14] showed that the globular structure is preferred because of better strength, ductility and crack initiation properties. Heat treatment for 8hrs was sufficient to allow the grains to change from lamella to globular.

More evidence of grain lamella α+ß transformation into globular α+ß was observed as the residence time was increased. Figure 5 shows the microstructures of the samples that were heat treated for 10hrs and 12hrs, respectively.

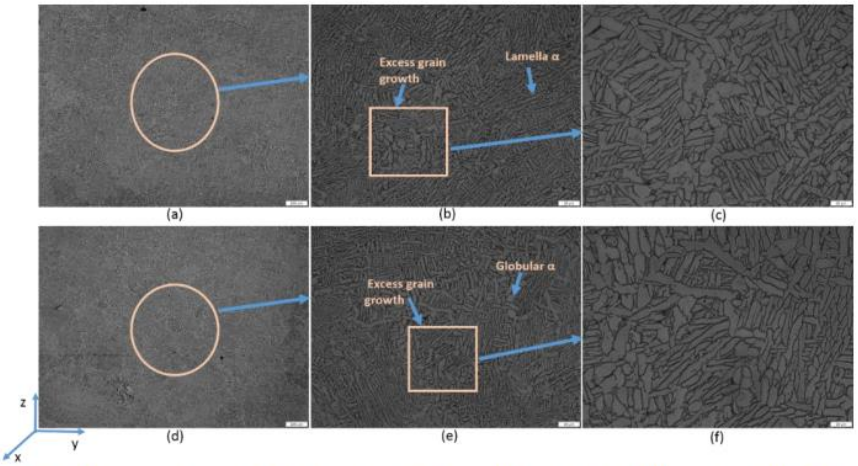


Figure 5: Microstructures of the heat treated samples (a. b & c) 10hrs, (d, e & f) 12 hrs.

The large columnar prior ß grains were no longer visible on the microstructure of both samples (Figure 5a, 5d). More of thicker globular α+ß grains were observed on the microstructure of the sample that was heat treated for 10hrs (Figure 5b) but with some of the phases starting to show an irregular shape. Figure 5c demonstrates well the irregular grains. As the residence time was increased to 12hrs, excess grain growth was observed (Figure 5e). Some of the globular α+ß phases were growing thicker and others were showing more of the irregular shape (Figure 5f). This implies that an increase in the residence allows the lamella α+ß phases enough time to grow to different shapes. Furthermore, lamella growth was also observed on the sample that was heat treated for 12hrs.

2.2.2 Hardness

The hardness profiles of the as-built and its heat treated samples is shown in Figure 6.

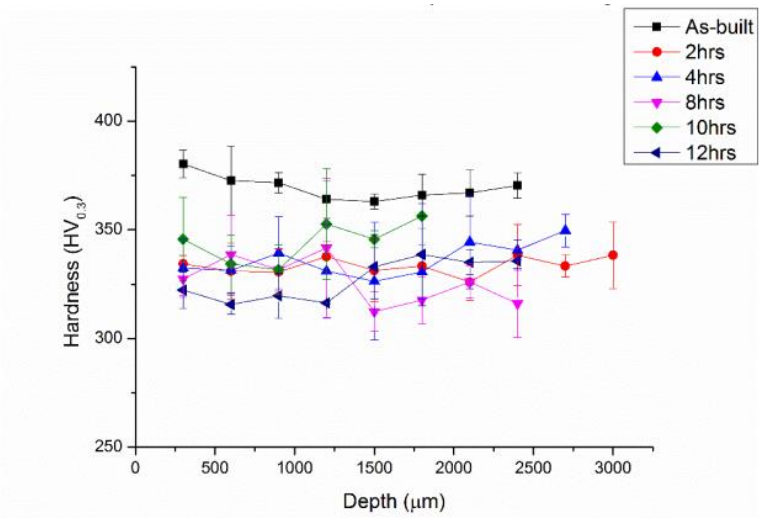


Figure 6: Average hardness profiles of the as-built and heat treated samples.

The as-built sample together with the samples that were heat treated for 2hrs and 4hrs displayed a linear pattern. The sample that was heat treated for 8hrs, 10hrs and 12hrs showed wavy patterns. The as-built sample showed the highest hardness profile with a decrease in hardness observed after heat treatment at different residence times. This decrease in hardness profiles was associated with the transformation of the martensitic α' phase and grain growth. From this observation, it can be discussed that the martensite α' phase is harder and brittle than the lamella α+β and globular α+β phases. This means that heat treatment at 1000°C softened the components.

The hardness profiles in Figure 6 are summarized in Table 1.

Table 1: Summarized hardness of the as-built and heat treated samples.

Sample	As-built	2hrs	4hrs	8hrs	10hrs	12hrs
Hardness (HV)	369±8	333±9	336±15	327±14	342±12	327±9

The as-built sample showed the highest hardness value as compared to the heat treated samples. This high hardness was associated with the martensitic α' phase that was observed on the microstructure of the as-built sample. There was no much variation between the hardness values of the heat treated samples.

3. CONCLUSION

High Speed SLM process was used to produce Ti6Al4V samples. The effect of residence time during heat treatment on Ti6Al4V microstructure and hardness were investigated. It was observed that the martensite α' phase transformed into lamella α+β after heat treatment for 2hrs and 4hrs and further transformed into globular α+β after heat treatment for 8hrs, 10hrs and 12 hrs with lamella phases still observed. The large columnar prior β grains were observed on the as-built, 2hrs and 4hrs heat treated samples were no longer observed after heat treatment at 8hrs, 10hrs and 12 hrs. It was also observed that residence time influence grain growth. Furthermore, it was found that hardness remained the same as residence time was increased.

REFERENCES

[1] Sallica-Leva, E. Caram, R. Jardini, A.L. Fogagnolo, J.B. 2016, Ductility improvement due to martensitic α'decomposition in porous Ti6Al4V parts produced by selective laser melting for orthopaedic implants, *Journal of the Mechanical Behavior of Biomedical Materials*, 54, pp 149-158.

[2] Wysocki, B. Maj, P. Krawczynska, A. Rozniatowski, K. Zdunek, J. Kurzydlowski, K.J. Swieszkowiski,W. 2017, Microstructure and mechanical properties investigation of CP titanium processed by selective laser melting (SLM), *Journal of Material Processing Technology*, 241, pp 13-23.

[3] Xu, W. Brandt, M. Sun, S. Elambasseril, J. Liu, Q. Latham, K. Xia, K. Qian, M. 2015, Additive manufacturing of strong and ductile Ti6Al4V by selective laser melting via in situ martensite decomposition, *Acta Material*, 85, pp 74-84.

[4] Yadroitsev, I. Krakhmalev, P. Yadroitsava, I. 2014, Selective laser melting of Ti6Al4V alloy for biomedical application: Temperature monitoring and microstructural evolution, *Journal of Alloys and Compounds*, 53, pp 404-409.

[5] Tong, J. Bowen, C.R. Persson, J. Plummer, A. 2017, Mechanical properties of titanium based Ti6Al4V alloy manufactured by powder bed additive manufacture, *Material Science and Technology*, 33, pp 138-148.

[6] Semiatin, S.L. Seetharaman, V. Weiss, I. 1997, The Thermomechanical Processing of Alpha/Beta Titanium alloys, *Metals*, 49, pp 33.

[7] Alcisto, J. Enriquez, H. Garcia, S. Hinkson, T. Steelman, E. Silverman, P. Valdovino, H. Gigerenzer, J. Foyos, J. Ogren, J. Dorey, K. Karg, T. McDonald, O.S. 2011, Es-said, Tensile properties and microstructure of laser-formed Ti6Al4V, *Journal of Material Engineering Performance*, 20, pp 203-212.

[8] Lutjering, G. 1998, Influence of processing on the Microstructure and Mechanical Properties of α+β Titanium Alloys, *Materials Science Engineering*, A243, pp 32-45.

[9] Pederson, R. Babushkin, O. Skystedt, F. Warren, R. 2003, Use of high temperature X-ray diffractometer to study phase transitions and thermal expansion properties in Ti6Al4V, *Material Science and Technology*, 19, pp 1533-1538.

[10]] Markovskya, P.E. Semiatin, S.L. 2011, Tailoring of microstructure and mechanical properties of Ti6Al4V with local rapid heat treatment, *Material Science and Engineering*, A528, pp 3079-3089.

[11] Khorasani, A. Gibson, I. Golberg, M. Littlefait, G. 2017, On the role of different annealing heat treatments on mechanical properties and microstructure of selective laser melted and conventional wrought Ti6Al4V, *Rapid Prototyping Journal*, 23, pp 295-304.

[12] Joshi, VA. 2006, An Atlas of Structures and Fracture Features, *Titanium Alloys*, ISBN-9781420006063, 1st edition, CRC Press: Boca Raton, FL, USA.

[13] Ter Haar, G.M. Becker, T.H. 2018, Selective Laser Melting Produced Ti6Al4V: Post-Process Heat Treatments to achieve Superior Tensile Properties, *Materials*, 11, pp 1-15.

[14] Kasperovich, G. Hausmann, J. 2015, Improvement of fatigue resistance and ductility of Ti6Al4V processed by selective laser melting, *Journal of Materials Processing Technology*, 220, pp 202-214.

[15] Shipley, H. McDonnell, D. Culleton, R. Coull, R. Lupoi, G. Odonell, D. Trimble, D. 2018, Optimization of process parameters to address fundamental challenges during selective laser melting of Ti6Al4V: A review, *International Journal of Machine Tool and Manufacture*, 128, pp 1-20.

[16] Villaro, T. Colin, C. Bartout, J.D. 2011, As-Fabricated and Heat-Treated Microstructures of the Ti6Al4V Alloy Processed by Selective Laser Melting, *Metallurgical and Materials transactions*, 42A, pp 3190-3199.

[17] Vrancken, B. Thijs, L. Kruth, P.J. Van Humbeeck, J. 2012, Heat treatment of Ti6Al4V produced by Selective Laser Melting: Microstructure and mechanical properties, *Journal of Alloys and Compounds*, 541, pp 177-185.

[18] Yan, M. Yu, P. 2015, An overview of densification, microstructure and mechanical properties of additively manufactured Ti6Al4V-comparison among selective laser melting, electron beam melting, laser metal deposition and selective laser sintering, and with conventional powder, *Sintered Technology Material*, 23, pp 374-386.

[19] Ter Haar, M. Becker, H. 2018, Selective laser melting produced Ti6Al4V: Post process heat treatment to achieve superior tensile properties, *Materials*, 11, pp 5-15.

[20] Nalla, R.K. Boyce, B.L. Cambell, J.P. Peters, J.O. Ritchie, R.O. 2002, Influence of Microstructure on high cycle fatigue Ti6Al4V: Bimidal vs lamella structure, Metallurgical and Materials Transection, 33A, pp 202- 218.

Appendix D: 19th annual RAPDASA conference paper 2018:

INVESTIGATION OF MICROSTRUCTURAL CHARACTERISTICS OF HEAT TREATED HIGH SPEED SELECTIVE LASER MELTING FABRICATED TI6AL4V COMPONENTS

P. Lekoadi[1, 2], N. Maledi[2], M. Tlotleng[1, 3*], & B.N. Masina[1*]

[1]CSIR National Laser Centre, Laser Enabled Manufacturing Group, PO BOX 395, Pretoria, 0001, South Africa
PLekoadi@csir.co.za and BMasina@csir.co.za

[2]University of the Witwatersrand, School of Chemical and Metallurgical Engineering, Private Bag 3, Wits, 2050, Johannesburg, South Africa
Nthabiseng.maledi@wits.ac.za

[3]University of Johannesburg, Faculty of Engineering and the Built Environment, Auckland Park Campus, Johannesburg, 2012, South Africa
MTlotleng@csir.co.za

ABSTRACT

This study presents an investigation of the effect of different heat treatments on the microstructure of Ti6Al4V fabricated components produced by high speed selective laser melting. 10 mm x 10 mm x 10 mm cubes were heat treated in an inert oven at temperatures of 700 °C and 950 °C. The samples were heat treated at their respective temperatures for 2 hours before air cooling to room temperature. Subsequent to heat treatment, the microstructures of the heat treated samples and the as-built were studied. The as-built sample showed a martensitic alpha phase which was also observed on the 700 °C sample. Elongated columnar grains were observed on the as-built and the 700 °C heat treated sample. Furthermore, a fully transformed lamella α+β microstructure was observed for the 950 °C heat treated sample.

1. INTRODUCTION

Additive manufacturing (AM) is currently a topic of interest in the aerospace industry due to its various advantages over conventional methods. These advantages include possibility of manufacturing parts of any geometric complexity, great design freedom and reduced production time, **Galti et.al** [1]. There are various types of AM techniques/platforms which are currently being used. These platforms include powder beds, direct energy deposition, material extraction and sheet laminating, **Gockel et.al** [2]. This study focus on selective laser melting (SLM), a powder bed AM technique which build components by selectively melting powder layer-by-layer with focused laser beam, **Vrancken et.al** [3]. The advantages of SLM include high level of flexibility (able to change easily according to situation), material efficiency, near net shape production and the build-up of complex geometries in a very short period of time, **Vrancken et.al & Eylon et.al** [3-4]. Various materials can be used in AM processes including Titanium alloys [2].

Titanium alloy grade 5 (Ti6Al4V) is an attractive material for aerospace industry because of its light weight, high strength properties and excellent corrosion resistance at high temperatures, **Eylon et.al & Wanying et.al** [4-5].

Ti6Al4V was developed in early 1950s for aerospace application and it is now qualified and widely used. Ti6Al4V is widely used in the aerospace industry because it possesses high specific strength and high corrosion resistance at temperatures up to 500°C, **Yaidroitsev et.al & Vilaro et.al** [6-7]. It has a crystal structure of α+β, which allows full transformation to beta phase during heat treatment and transform back to α+β when cooling [5].

[1] CSIR National Laser Centre, Laser Enabled Manufacturing Group, PO BOX 395, Pretoria, 0001, South Africa (Corresponding authors: BMasina@csir.co.za and MTlotleng@csir.co.za)
[2] University of the Witwatersrand, School of Chemical & Metallurgical Engineering, Private Bag 3, Wits 2050, Johannesburg, South Africa.
[3] University of Johannesburg, Department of Mechanical Engineering Science, Auckland Park Campus, Johannesburg, 2012, South Africa.

Another interesting feature of Ti6Al4V powder is that it has an excellent combination of ductility and low weight ratio which makes it a suitable alloy for aerospace industry, **He et.al** [8]. Ti6Al4V is used for high performance engineering solutions in aerospace motor cases, aircraft turbines, pressure vessels and marine components, **Imam et.al** [9-10].

Ti6Al4V component produced from SLM, in the as-built state, are unable to achieve high material performance to wrought counterparts (**Ter-Haar et.al** [11]) for aerospace application. This is because Ti6Al4V component produced from SLM exhibit α' phase which is associated with residual stresses that are generated during processing, **Zaeh et.al** [12]. These stresses are as a result of high temperature gradients which form during fabrication. **Kong et.al** [13] investigated the microstructure of Ti6Al4V samples produced by SLM and found that it exhibited fine martensitic α' phase with tensile strength of about 1.45 GPa and elongation of 4,4%. **Thijs et.al** [14] found that Ti6Al4V materials processed by SLM shows a very fine, non-equilibrium microstructure due to high temperature gradients. Post production heat treatment is one of the methods that can be used to relieve these residual stresses that result in a part post production.

Several studies [3, 5, 7, 11, 15] showed that heat treatment can improve the microstructure and mechanical properties of SLM Ti6Al4V components. The Ti6Al4V microstructures of the produced components were complex and differed within a built. The types of microstructures depend largely on the heat treatment temperature and the cooling rate. It is possible to achieve a highly desirable microstructural features such as a highly refined precipitate, **Collins et.al** [16]. The aim of this paper was to investigate the effect of heat treatment on the microstructure of Ti6Al4V produced by a high speed SLM system.

2. METHODOLOGY AND RESULTS

2.1 Methodology

Gas atomized Ti6Al4V powder with a particle distribution of 20-60 µm was used in this study. The powder was supplied by TLS and used as received. Ti6Al4V samples were produced with energy densities of 42.41 J/mm^3 and

78.46 J/mm^3 using the high speed SLM system available at CSIR (NLC). The energy densities were calculated using this formula $E=\frac{P}{hvt}$ where P is the laser power, h is the hatch spacing, v is the speed and t is the layer thickness. A schematic diagram of the SLM process is shown in Figure 1. During processing, a CAD model of the part is loaded onto the machine working station where a pre-processing software slices the model into layer of finite thickness. A powder is deposited onto a plate above the built platform then a focused laser beam scans over the powder bed based on the sliced CAD data. The scanning results in localised melting and solidification of the powder form layer of the part. Subsequent layers are built one over the other by lowering the platform equivalent to the layer thickness until a part is completed.

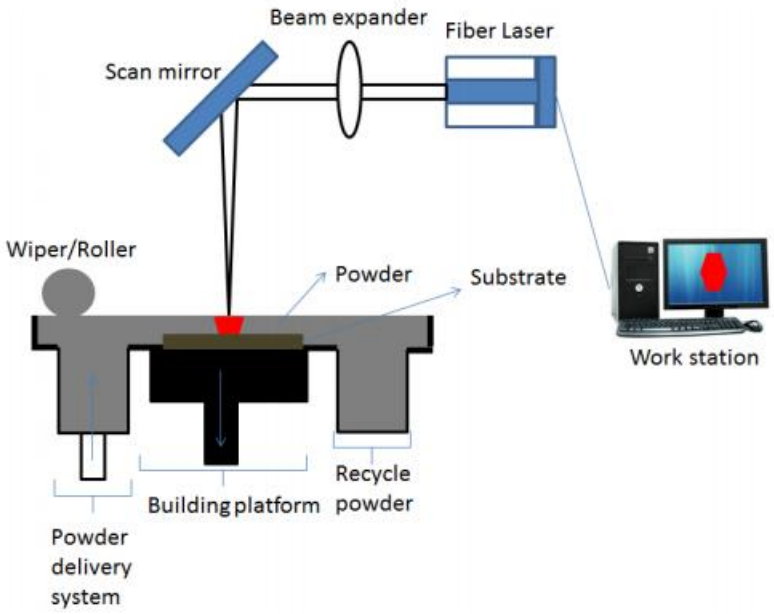


Figure 1: A schematic diagram of SLM process.

During the printing process 10 mm x 10 mm x 10 mm cubes of Ti6Al4V samples were produced by scanning very fast the focused high power fibre laser beam with wavelength of 1073 nm over the pre-placed powder bed. Post manufacturing, the produced samples were then heat treated in an air rich oven at temperatures of 700 °C and 950 °C, respectively. The temperatures were chosen on the context that 700 °C is a stress relieving temperature and 950 °C is the β-transus temperature, **Vracken et.al** & **Dong et.al** [3, 17]. During heat treatment the condition was such that the set temperature was held for 2 hours. The samples were allowed to air cool to room temperature.

The as-built and heat treated samples were mechanically prepared and polished for microstructural analyses. The samples were cross sectioned in direction perpendicular to the built direction. The samples were then etched with Kroll's reagent before metallographic examination. Metallurgical samples (as-built and heat treated) were analysed for microstructural evolution using Joel JSM-6010PLUS/LA Scanning Electron Microscope (SEM) with an accelerating voltage of 20 kV.

2.2 Results

2.2.1 Microstructures

Figure 2 below shows microstructures of the as-built samples.

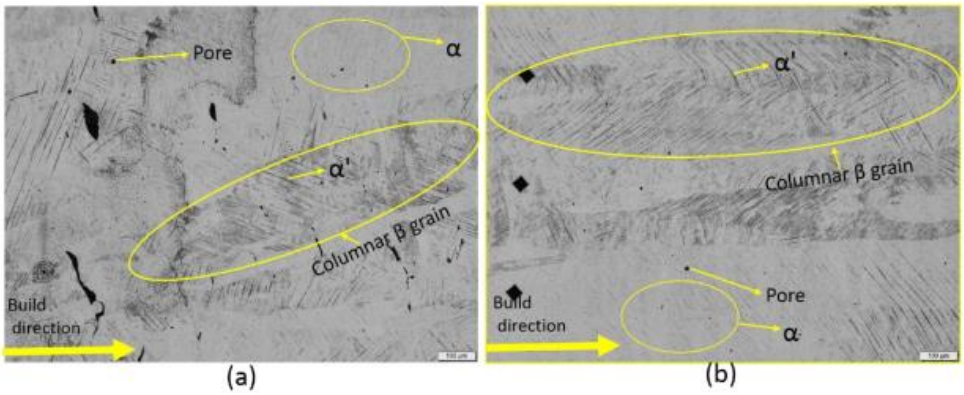


Figure 2: Microstructures of the as-built samples: (a) 42.41 J/mm³ and (b) 78.46 J/mm³.

Both samples show large columnar grains as highlighted on the optical images. These grains are orientated along the build direction. Additionally, both samples show an acicular martensitic α' phase which forms as a result of high cooling rates. Figure 2a shows regions where there are sharp crack-like pores which are attributed to the low energy density that was used. The crack-like pores are not observed on the microstructure sample in Figure 2b which was manufactured a high energy density. Both of the samples show the presence of three phases (α, β and α'), but β phase is present in small quantity. These observations are detailed in the high magnification SEM microstructures that are presented in Figure 3.

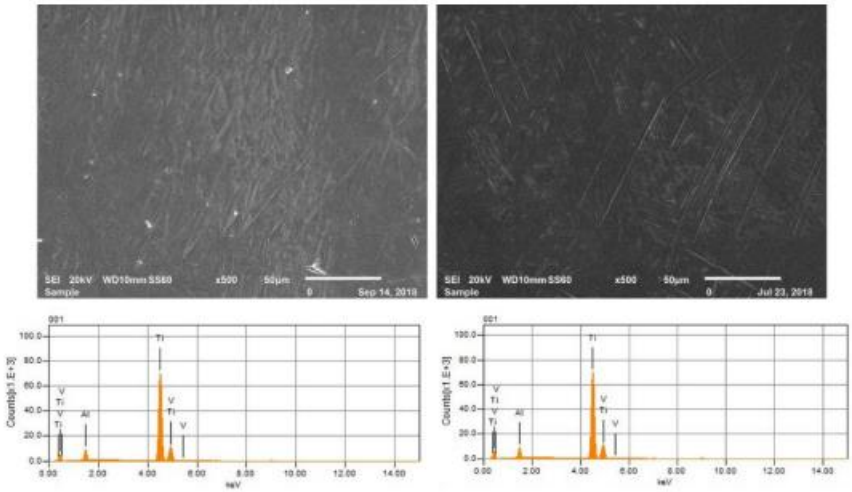


Figure 3: EDS graphs (a) 42.41 J/mm³ and 78.46 J/mm³.

From Figure 3, α' martensitic structure are rods or needle like structures that are seen on the image. This phase is somewhat precipitated with higher energy density (Figure 3b). The bright-white particles on the image are β-

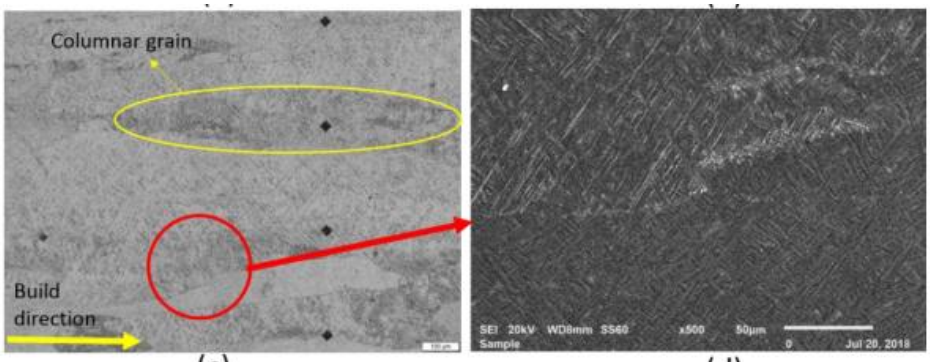


Figure 4: Micrographs of the samples after heat treated at 700 °C: (a and b) 42.41 J/mm^3 and (c and d) 78.46 J/mm^3.

Heat treatment at 700 °C, for 2 hours followed by air cooling, resulted in no phase transformation, however the grain sizes of the sample that was manufactured with energy density of 42.41 J/mm^3 (Figure 4a) were refined to smaller size and became more equiaxed as compared to the as-built (Figure 2a). This is due to nucleation when ß columnar grain changed to ß equiaxed grains. The sample that was built at 78.46 J/mm^3 and heat treated to 700 °C seem to remain the same since no grain growth or nucleation can be reported, however, the SEM microstructure clearly depict that at this heat treatment temperature ß phase was highly precipitated and the α'martensitic phase grew longer in the rich ß-precipitated columnar grain (top of the b-image) and shorter on the α grain (bottom part of image b). In both samples all three phases can still be identified. The microstructures of the sample after heat treatment at 950 °C are shown in Figure 5.

phase while α is the overall darker matrix of the sample. The microstructures of the heat treated samples are given in Figures 4 and 5 for 700 °C and 950 °C, respectively.

The microstructures of the samples that were heat treated at 700 °C.

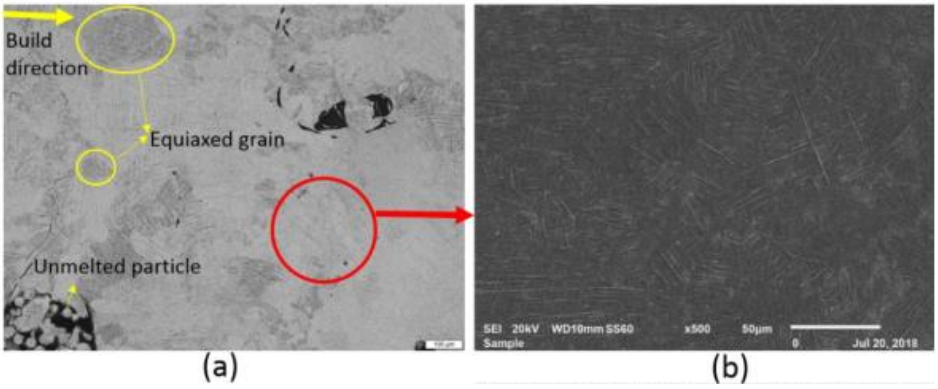


Figure 5 below shows the microstructures samples after heat treatment at 950 °C.

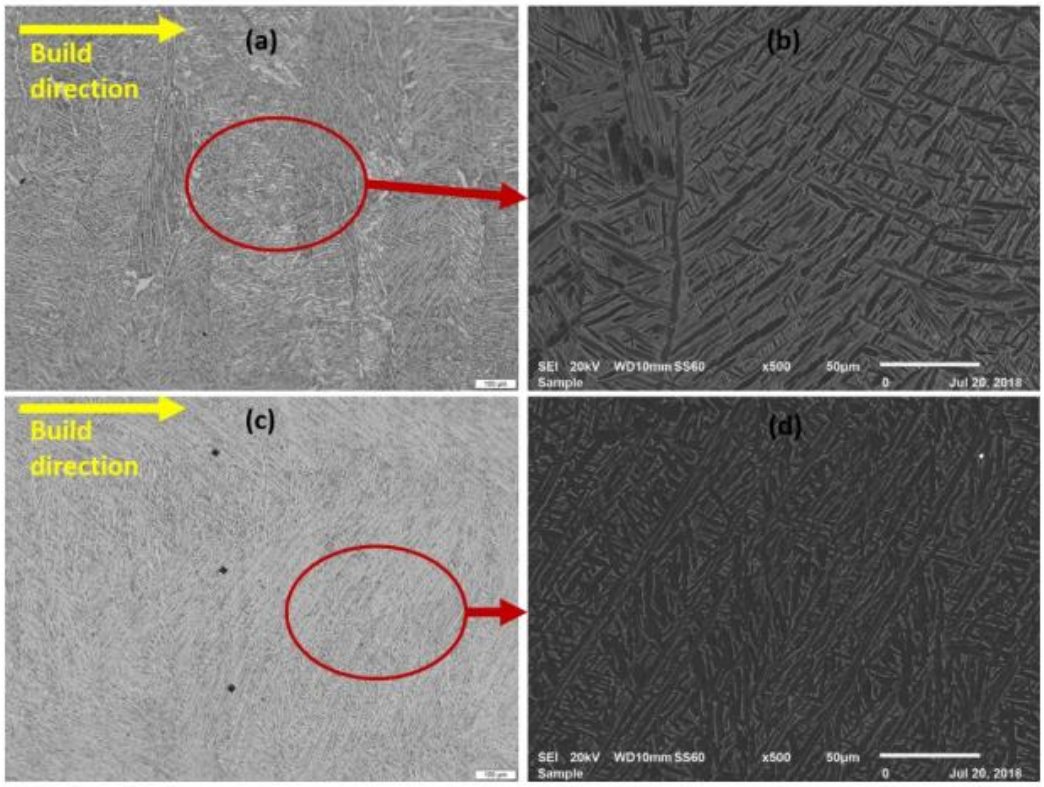


Figure 5: Micrographs of the samples after heat treated at 950 °C: (a and b) 42.41 J/mm^3 and (c and d) 78.46 J/mm^3.

Heat treatment at 950°C altered the grain sizes and phases for both samples. Full phase transformation was observed on the microstructures of the two samples. α' martensitic phase present in both the as-built samples (Figure 2a & 2b) and samples that were heat treated at 700 °C (Figure 4a & 4c) can no longer be observed after heat treatment at 950 °C as shown on Figures 5a & 5c. It has been cited that when Ti64 is heat treated at ß-transus temp or above α' martensitic phase will fully transform to ß phase. This transformation leads to a lamellar α+ß structure being formed (**Vracken et.al & Vilaro et.al** [3, 7]) as seen on Figures 5 (a and b). Study by **Vrancken et. al** [3] has shown that when Ti6Al4V is heat treated above the ß-transus temperature, it would homogenise, and all the beta phase present will transform to lamella α+ß during furnace cooling. They also observed grain growth with increase in heat treat temperature. Similar results [Figure 4d (700 °C) and Figure 5d (950 °C)] were observed in this study when temperature was increased.

2.2.2 Hardness

Hardness is the measure of strength of material and is influence main by material consolidation and homogeneity. Meanwhile a sample that underwent heat treatment will have its hardness influence by formed grains, precipitates and the resulting phases. The Hall-Petch relationship is the accepted relationship that explains the influence of mechanical] properties to the grains of the alloy (**Malheiros et.al & Ruan** [18-19]). This background is necessary for the interpretation of the hardness results presented in this study. Figures 6 and 7 show the hardness profiles of the samples in both as-built and heat treated conditions.

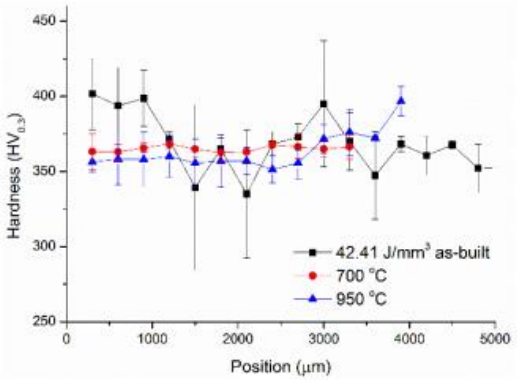


Figure 6: Average hardness profile of 42.41 J/mm³ sample.

Figure 6 presents the micro-hardness profile of the as-built sample and its corresponding heat treated samples. The sample was built using 42.41 J/mm³ energy density, and heat treated at 700 °C and 950 °C followed by air cooling, respectively. Hardness was measured across the sample perpendicular to the build direction. The hardness profile of the as-built sample is wavy. This observation can be attributed to the microstructural inhomogeneity, defects, and also might be due to the observed α' martensitic phase. The hardness profile of the heat treated samples remained constant. This might be due to a homogenised microstructure, and the refinement α' martensitic and its partial transformation to β-precipitate. It should be noted that the hardness profile of the sample that was heat treated at 950 °C is a bit lower than the sample that was heat treated at 700 °C. This can be attributed to the over refinement in the microstructure and full transformation of α' to β leading to a lamellar α+ β microstructure.

The micro-hardness profiles of the sample that was built at 78.46 J/mm³ energy density and its corresponding heat treated samples are reported in Figure 7.

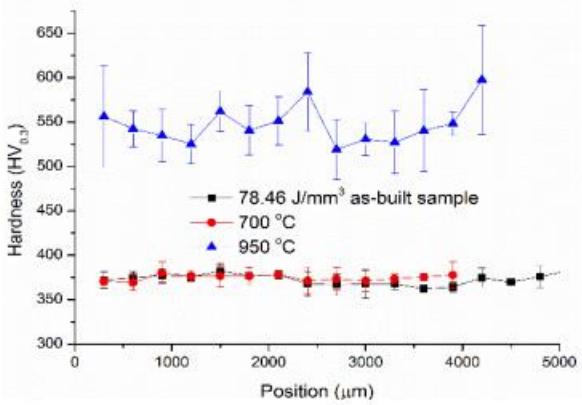


Figure 7: Average hardness profile of 78.46 J/mm³ sample.

It can be said from Figure 7 that the hardness profile of the as-built sample and its heat treated sample (700 °C) are the same. Both samples had similar microstructure. The hardness profile of the sample that was heat treated at 950 °C is wavy and significantly increased when compared to the hardness of the as-built sample and the sample that was heat treated at 700 °C. The increase in hardness cannot be attributed to the presence of α' phase as it was fully transformed. **Dong et. al** [17] reported a similar jump in hardness and attributed it to the thermal oxidation. This study would investigate the effects of thermal oxidation and its impact on the hardness of the Ti64 alloy as a future study. The overall hardness values of the samples are summarised in Table 1 with the error.

Table 1: Overall hardness ($HV_{0.3}$) values.

Sample ID	As-built	700 °C	950 °C
42.41 J/mm^3	367±30	365 ±30	363±30
78.21 J/mm^3	377±30	375 ±30	547±30

Table 1 summarises that there was no significant difference in the as-built and heat treated sample for the sample that was built at 42.41 J/mm^3, but a significant jump was observed in the sample that was heat treated at 950 °C for the sample that was built at 78.21 J/mm^3.

3. CONCLUSION

High Speed SLM process was used to produce 10 mm x 10 mm x 10 mm cubes Ti6Al4V samples. The effect of heat treatment on Ti6Al4V microstructure was investigated. It was observed that the resulting Ti6Al4V microstructure after annealing depend mainly on the heat treatment temperature. It was also observed that grain size increases with heat treatment temperature for the same cooling method. It was also observed that heat treatment at 700 °C does not allow full α' transformation but 950 °C allow full phase transformation to lamella α+β.

REFERENCES

[1] **Galti, M, Luliano, L**, 2018, A literature review of powder-based electron beam melting focusing on numerical simulations, *Additive Manufacturing*, 19, pp 1-20.
[2] **Gockel, J, Beuth, J**, 2012, Understanding Ti6Al4V Microstructure Control in additive Manufacturing via Process Maps, *Department of Mechanical Engineering*, Carnegie Mellon University, PA15213, pp 666-674.
[3] **Vrancken, B, Thijs, L, Kruth, J, Humbeeck, J**, 2012, Heat treatment of Ti6Al4V produced by Selective Laser Melting: Microstructure and mechanical properties, *Journal of Alloys and Compounds*, 541, pp 177-185.
[4] **Eylon, D, Newman, JR, Thorne, JK**, 1990, Metal Handbook, 10th ed. Material Park, OH: ASM Int, vol 2.
[5] **Wanying, L, Yuanhau, L, Yuhai, C, Taihe, S, Singh A**, 2017. Effect of different heat treatment on microstructure and mechanical properties of Ti6Al4V titanium alloy, *Rare metal Materials and engineering*, 46(3), pp 0034-0039.
[6] **Yaidroitsev, J, Krakhmalev, P, Yaidroitsava, I**, 2014, Selective Laser Melting of Ti6Al4V alloy for biomedical application: Temperature monitoring and microstructural evolution, *Journal of Alloys and Compounds*, 583, pp 404-409.
[7] **Vilaro, T, Collin, C, Bartout, JD**, 2011, As-Fabricated and Heat- Treated Microstructures of the Ti6Al4V Alloy Processed by Selective Laser Melting, *Metallurgical and Materials Transactions*, 24A, PP 3190-3199.
[8] **He, B, Wu, W, Liang, Z, Lu, L, Yang, Q, Long, Q, Chang, K**, 2018, Microstructure characteristic and mechanical property of Ti6Al4V alloy fabricated by selective laser melting, *Vacuum*, 150, pp 79-83.
[9] International Titanium Association, <www.titanium.org.>
[10] **Imam, MA, Franker, AC, Brown, SA, Lemons, JE**, 1996, Medical applications of Titanium and its Alloy, *ASTM Special Technical Publication*, pp 3-16.
[11] **Ter-Haar, GM, Becker, TH**, Selective Laser Melting Produced Ti6Al4V: Post-Process Heat Treatment to Achieve Superior Tensile Properties, *Materials*, 2018, 146, pp 1-15.
[12] **Zaeh, MF, Btanner, G**, 2009, Investigation on residual stresses and deformations in selective laser melting, *German Academic Society for Production Engineering*, 4, pp35-45.

[13] **Kong, CJ, Tuck, CJ, Ashcroft, A, Wildman, RD, Hauge, R**, 2011, High density Ti6Al4V via SLM processing: microstructure and mechanical properties, *proc. Of Solid Freeform Fabricated Symposium*, pp 337-483.
[14] **Thijs, L, Verhaeghe, F, Craeghs, T, Van Humbeeck, J, Kruth, J**, 2010, A study of the microstructural evolution during selective laser melting of Ti6Al4V, *Acta Materialia*, 58, pp-3303-3312.
[15] **Semiatin, S, Knisley, SL, Fagin, PN, Zhang, F, Barker, DR**, 2003. Microstructural Evolution during Alpha-Beta Heat Treatment of Ti6Al4V, *Metallurgical and Materials transections*, 34A, pp 2377-2386.
[16] **Collins, PC, Brice, DA, Samini, P, Ghamarian, I, Fraser HL**, 2016, Microstructural control of Additive Manufactured Metallic Materials, *Annual Review of Materials Research*, 46, pp 63-91.

[17] **Dong, E, Yu, W, Cai, Q**, 2017, Alpha-case kinetics and high temperature plasticity of Ti6Al4V alloy oxidized in different phase regions, *Procedia Engineering*, 207, pp 2149-2154.
[18] **Malheiros, LR, Figueredo, RB, Langdon, TG**, 2015, Grain size and microhardness evolution during annealing of a magnesium alloy processed by high-pressure torsion, *Journal of Material Research and Technology*, 4(1), pp 14-17.
[19] **Ruan, Y, Mohajerani, A, Dao, M**, 2016, Microstructural and Mechanical property Manipulation through Rapid Dendrite Growth and Undercooling in an Fe-based Multinary alloy, *Scientific report*, 6:1038, pp 1-11.